Department of AERONAUTICS and ASTRONAUTICS
STANFORD UNIVERSITY

JAMES KALLIS

DEDUCTION OF STATIC TEMPERATURE IN NITROGEN BY MEANS OF SPARK SPECTROSCOPY - A FEASIBILITY STUDY

NOVEMBER
1968

The research was sponsored by the
National Aeronautics and Space Administration
under Research Grant NGR 05-020-116

SUDAAR
NO. 364

Department of Aeronautics and Astronautics
Stanford University
Stanford, California

DEDUCTION OF STATIC TEMPERATURE IN NITROGEN BY MEANS OF SPARK SPECTROSCOPY – A FEASIBILITY STUDY

by

James Kallis

SUDAAR No. 364
November 1968

The research was sponsored by the
National Aeronautics and Space Administration
under Research Grant NGR 05-020-116

ABSTRACT

This is the analytical part of an analytical and experimental study of the feasibility ultimately of measuring the static temperature of flowing nitrogen in a hypersonic wind tunnel by means of spark spectroscopy. The intention is to deduce the effective rotational temperature of the spark, and hence the static temperature, from the relative line intensities within an emission band. The spark would be struck perpendicular to the flow in the tunnel test section.

The experiments, from a non-flow study by J. B. Kyser (NASA CR-760, May 1967), used the N_2 second-positive band system. The measured temperatures were higher than ambient. Because of this discrepancy, a method for calculating the ambient temperature as a function of the measured rotational temperature is required. This method must relate the relative line intensities to the quantities characteristic of the ambient gas (temperature and pressure) and the spark (voltage, current, etc.). The objective of the present research is the development of such a method.

For the conditions of Kyser's tests, order-of-magnitude calculations and referenced experiments show the following simplified model to be valid:

Population of the excited electronic state occurs

entirely by direct electron-impact excitation from the ground electronic state. The ground-electronic-state molecules remain at ambient conditions during the spark duration; collisions with slow electrons have a negligible effect on the translational and rotational temperatures and on the distribution of rotational states. The molecules undergo no collisions between the time at which they are excited and the time at which they radiate.

There are then three steps as follows in developing the relative line intensities:

1) Calculation of the rotational excitation accompanying the electronic excitation produced by electron impact - For this purpose we devise a "quantized-classical" analysis, in which we use the classical impact parameter but exploit the quantum nature of the rotational levels.

2) Calculation of the resulting populations of the rotational levels in the excited electronic state on the basis of statistics of these collisions - We extend the standard derivation for the collision frequency of point molecules to the case of point masses (electrons) colliding with rigid dumbbells (molecules). The resulting formula for the excitation rate to a given rotational level contains a complicated integral, which we evaluate by a Monte-Carlo method.

3) Derivation of a formula for the relative line

intensities as a function of the populations of the upper-state rotational levels (and thence of the measured temperature) - We improve the derivation of Kyser, who integrated over an assumed continuous distribution of intensity versus wavelength, by summing over the individual spectral lines. For an intensity ratio of 0.274, the present formula gives a temperature 13°K lower than Kyser's formula.

The predictions of our analysis are compared with the measurements from Kyser's no-flow tests. In those tests the ambient temperature was 295°K, the pressure 1 mm Hg, and the spark energy 0.5 joule. Our prediction disagrees with Kyser's measurement. We deduce a temperature 29°K below ambient, whereas the measured temperature was 47°K above ambient. The cause of the predicted temperature decrease is that few of the electron-molecule collisions causing electronic excitation change the rotational quantum number. The predicted temperature, as a result, equals the ambient temperature times the ratio of the B-values of the two electronic states. We can demonstrate that, with the exception of the assumption that the classical impact parameter is a valid concept for analyzing the electron-molecule collisions, the assumptions in the analysis either are undoubtedly valid or affect the predictions very little. We therefore conclude that the use of classical mechanics is the cause of the disagreement between theory and

experiment. Unfortunately, the current state of knowledge in collision theory precludes a full quantum-mechanical analysis.

ACKNOWLEDGEMENTS

The author learned much and received considerable help in the analysis from his supervisors, Dr. James Kyser (early part of the research) and Prof. Maurice Rasmussen (later part of the research). The dissertation was improved greatly by the criticism of these men and Professors Walter Vincenti and Daniel Bershader, all of whom read the manuscript. Mr. James Stein gave helpful advice on the computer programming involved in this research, including the suggestion that the phase-space integral be evaluated by the Monte-Carlo technique. Prof. Leonard Schiff and Dr. Russell Duff provided several stimulating discussions on the physics of the problem.

This research was supported by a National Aeronautics and Space Administration Grant, which enabled the author to devote full time to his graduate work.

TABLE OF CONTENTS

$$I_n = \int_{\ell}^{u} x^{n+2} e^{-ax^2} dx \quad (n = 0,1,\ldots, 5)$$

NOMENCLATURE

(If a section or chapter number is listed after a symbol, the notation is used only there.)

B_v	rotational constant (Chapter 6)
b_0	impact parameter (Section 4.3.2)
C_e, C_M	constants defined by Equations (4.3-14)
$\vec{D}$	distance between the electron and the center of mass of the molecule
E_e	electronic energy of molecule (Section 3.3)
E_r	rotational energy (Section 3.3)
E_v	vibrational energy (Section 3.3)
e	chemical symbol for a free electron
F	excitation function
f	velocity distribution function (Section 4.3)
$G(g_0)$	defined by Equation (5.2-8)
$\vec{g}$	relative velocity
h	Planck's constant (6.625×10^{-27} erg-sec)
$\hbar$	$h/2\pi$ (1.054×10^{-27} erg-sec)
$h\nu$	chemical symbol for a photon
I	molecular moment of inertia; also, line intensity
I_{K_0,K_1}	phase-space integral, defined by Equation (5.2-5)
$\vec{J}$	resultant molecular angular momentum (Section 2.6)
J	rotational quantum number corresponding to J
$\vec{K}$	total molecular angular momentum apart from spin

K	rotational quantum number corresponding to $\vec{K}$
k	Boltzmann's constant (1.38054×10^{-16} erg/^{o}K)
m	mass of an electron (9.108×10^{-28} gm)
$\vec{N}$	angular momentum of nuclear rotation (Section 2.6)
N	number density; also, quantum number corresponding to $\vec{N}$ (Section 2.6)
$P(\phi_{g_0})$	defined by Equations (5.2-9)
$p(K_0)$	number of collisions with a given value of K_0 in which no integer value of K_1 is possible (Chapter 5)
Q	relative instrument response (Section 6.2.5)
$q(K_0,K_1)$	number of times each value of K_1 occurs, with a given value of K_0 (Chapter 5)
r	intensity ratio
r_{em,K_1}	rate at which molecules undergo radiative transitions from the K_1 rotational level (Section 4.2)
r_{ex,K_1}	rate at which molecules are excited to the K_1 rotational level (Chapter 4)
r_0	half the internuclear distance in $N_2(X^1\Sigma_g^+)$, i.e., the radius of a nitrogen molecule (0.547×10^{-8} cm)
$\vec{S}$	angular momentum due to electron spin (Section 2.6)
S	line strength; also, quantum number corresponding to $\vec{S}$ (Section 2.6)
$s(K_0)$	number of collisions computed with a given value of K_0 (Chapter 5)
T	temperature

T_0	ambient temperature
T_1	rotational temperature of portion of gas affected by spark
t	time
$\vec{V}$	molecular translational velocity
$\vec{v}$	electron velocity
v	electron speed; also, vibrational quantum number (Chapter 6)
$\vec{W}$	center-of-mass velocity
w	width of molecule (Section 4.3)
α_{K_0,K_1}	defined by Equation (4.3-1)
$\beta(g_0,D_0)$	defined in Section 4.3.1
γ	angle between $\vec{g}_0$ and the internuclear axis (see Figure 4-2)
$\Delta( )$	change in ( ) during the time interval Δt (Chapter 2)
Δt	defined by Equation (2.2-2)
δ	angle between the internuclear axis and an arbitrary line in the plane perpendicular to $\vec{K}_0$ (Section 4.3)
ε	mean electron energy (Chapter 2)
θ	polar angle (see Figure 3-1)
$\vec{\Lambda}$	orbital angular momentum of the molecular electrons (Section 2.6)
Λ	quantum number corresponding to $\vec{\Lambda}$ (Section 2.6)

λ fraction of the electron's energy that is transferred to the molecule in a collision (Chapter 2); also, wavelength (Chapter 6)

μ reduced mass

ν wave number (Chapter 6)

$\nu(g_0,D_0)$ defined in Section 4.3.1

σ population-alternation factor; also, collision cross section (Chapter 2)

τ_{K_0,K_1} volume in phase space

ϕ polar angle (see Figure 3-1)

ψ angle between $\vec{g}_0$ and $\vec{W}$ (Section 4.3)

Ω solid angle (Section 4.3)

Subscripts:

$( )_e$ electron

$( )_{eM}$ electron-molecule collision

$( )_g$ refers to direction of $\vec{g}$

$( )_J$ rotational level J of a given electronic and vibrational state

$( )_K$ rotational level K of a given electronic and vibrational state

$( )_M$ molecule

$( )_{max}$ maximum

$( )_{min}$ minimum

$( )_r$ rotational

$( )_t$ translational

$( )_v$ vibrational level v

$( )_W$ refers to direction of $\vec{W}$

$( )_x$, $( )_y$, $( )_z$ component in x, y, z direction, respectively (see Figure 3-1)

$( )_0$ before the electron-molecule collision that causes the $C^3\Pi_u \leftarrow X^1\Sigma_g^+$ electronic excitation, i.e., refers to the incoming electron and the $X^1\Sigma_g^+$ molecule

$( )_1$ after the electron-molecule collision that causes the $C^3\Pi_u \leftarrow X^1\Sigma_g^+$ electronic excitation, i.e., refers to the outgoing electron and the $C^3\Pi_u$ molecule.

Superscripts:

$( )'$ $C^3\Pi_u$ state

$( )''$ $B^3\Pi_g$ state

Electronic States of N_2:

$B^3\Pi_g$ lower state of the second-positive band system

$C^3\Pi_u$ upper state of the second-positive band system

$X^1\Sigma_g^+$ ground state

LIST OF TABLES

LIST OF FIGURES

CHAPTER 1

INTRODUCTION

1.1 Objective of the Present Research

The present research, on the feasibility of deducing the static temperature of flowing nitrogen in a hypersonic wind tunnel by means of spark spectroscopy, is suggested by a study carried out by Kyser (1966) on the structure of spark columns for velocity measurement in a hypersonic stream. Kyser performed experiments which indicated that the spark disturbs the gas in such a way that the measured temperature is higher than the ambient temperature. Because of this discrepancy, a theoretical method for calculating the ambient temperature as a function of the measured temperature is required for the spark technique to be a reliable means of deducing static temperature. No such method was available to Kyser. The objective of the present research is the development of such a method.

1.2 Kyser's Tracer-Spark Experiments

Kyser (1964) developed a tracer-spark technique for measuring the gas velocity in a hypersonic wind tunnel that uses nitrogen as the working fluid. Later Kyser (1966) suggested the feasibility of using the tracer spark to measure static temperature. In the test section of a

hypersonic wind tunnel, the rotational and translational temperatures are for all practical purposes equal to each other. Hence, a measurement of the undisturbed rotational temperature would yield the static (i.e., translational) temperature. The rotational temperature can be deduced from band spectra emitted by the nitrogen. In the test section, however, the nitrogen is too cold (about $50^{\circ}K$) to radiate spontaneously. Kyser's idea was to deduce the rotational temperature from the emission excited by the spark.

In some exploratory experiments whose main purpose was to understand the structure of the spark column, Kyser applied this technique to the simplest possible situation - nonflowing nitrogen of known temperature and pressure. The ambient temperature in all the experiments was $295^{\circ}K$. The pressure varied between 0.1 mm Hg and 10 mm Hg and the spark energy between 0.05 joule and 5 joules, the most extensive group of tests being conducted at 1 mm Hg and 0.5 joule. These are the only pertinent experiments that have been performed. The result of Kyser's experiments was that the spectroscopically deduced rotational temperature was higher than the known ambient temperature. For the tests at 1 mm Hg and 0.5 joule, the spectroscopically deduced temperature was $355^{\circ}K$, which was $60^{\circ}K$ higher than the ambient temperature.

To understand the cause of this difference, we must consider how the rotational temperature is deduced. We discuss this in the following sections.

1.3 Spectroscopic Measurement of Rotational Temperature

The technique for deducing rotational temperature from band spectra, which is based on the microscopic definition of temperature, is well known (Herzberg 1950). If the gas is in rotational equilibrium at a temperature T_r, the number of molecules N_J in the rotational level J of a given electronic and vibrational state is given by the Boltzmann distribution

$$N_J = F_1(J) \exp[-F_2(J)/T_r], \qquad (1.3\text{-}1)$$

where F_1 and F_2 are functions of the rotational quantum number J as will be specified later. The rotational temperature T_r is thus intimately related to the equilibrium distribution of the populations of the rotational levels.

The intensity I_J of a spectral line caused by a transition from a rotational level J is proportional to the population N_J and the transition probability. Hence, the line intensities at equilibrium are given by

$$I_J = F_3(J) \exp[-F_2(J)/T_r], \qquad (1.3\text{-}2)$$

where F_3 is a function that will be specified later. By plotting the measured line intensities in a given band in the form $\ln[I_J/F_3(J)]$ versus $F_2(J)$, we obtain a straight line of slope $(-1/T_r)$. Thus we can find the rotational temperature of the emitting molecules from the slope of the

straight line.* This is known as the "log-slope method."

1.4 Cause of the Change in Rotational Temperature

The source of the discrepancy between the deduced and ambient temperatures is that the emission must be excited artificially. We must disturb the gas in order to measure its rotational temperature, and it is the disturbed gas whose properties we measure.

At the ambient temperatures of interest, almost all the N_2 molecules are in the ground vibrational level of the ground electronic state $X^1\Sigma_g^+$. The static temperature that we wish to deduce is the translational temperature of these $X^1\Sigma_g^+$ molecules, which, as we said above, is for all practical purposes equal to the rotational temperature of the $X^1\Sigma_g^+$ molecules.

One can use any of the many spectral bands excited by the spark to measure the rotational temperature of the spark. Kyser used the (0,2) band of the second-positive band system, which is in the blue edge of the visible spectrum. Although the (0,0) and (0,1) bands are probably more prominent than the (0,2) band, they lie too far toward the

*For light to be emitted spontaneously, the molecules must be in an excited electronic state. The temperature computed from the slope of the line is what we mean by the temperature of the excited state.

violet for ease in instrumentation. The second-positive band system arises from spontaneous transitions from the excited electronic state $C^3\Pi_u$ to the excited electronic state $B^3\Pi_g$. Excitation from the $X^1\Sigma_g^+$ state to the $C^3\Pi_u$ state results from impact between an N_2 molecule and a high-speed electron in the spark. Thus, the excitation-emission process is as follows:

$$\text{Excitation:} \quad N_2(X^1\Sigma_g^+) + e \rightarrow N_2(C^3\Pi_u) + e. \qquad (1.4\text{-}1a)$$

$$\text{Emission:} \quad (N_2(C^3\Pi_u) \rightarrow N_2(B^3\Pi_g) + h\nu. \qquad (1.4\text{-}1b)$$

In Equation (1.4-1a), the kinetic energy of the outgoing electron is lower than that of the incoming electron by the amount of the excitation energy of the $C^3\Pi_u$ electronic state. We illustrate the process in Figure 1-1 and show a schematic energy-level diagram in Figure 1-2. The many vibrational and rotational levels that occur within each electronic level have been omitted from this diagram. A more complete energy-level diagram is shown in Figure 6-1.

We would like to find the rotational temperature of the $X^1\Sigma_g^+$ molecules. The emission spectrum, however, is characteristic of the populations of the $C^3\Pi_u$ rotational states. The distributions of the $X^1\Sigma_g^+$ and $C^3\Pi_u$ rotational levels may differ, because rotational excitation can accompany the electronic excitation.

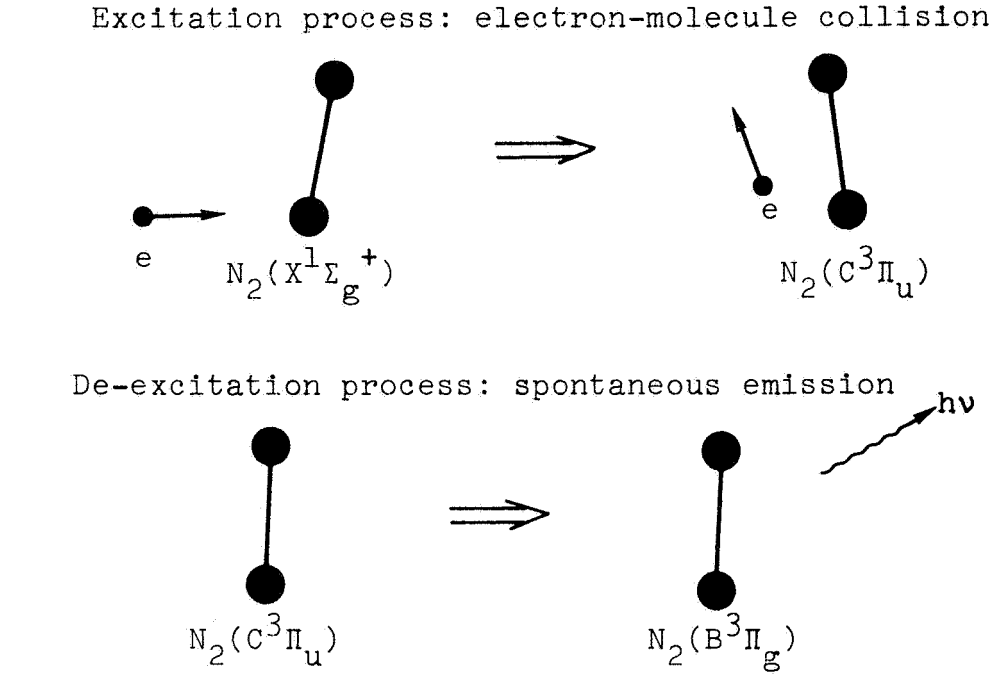

Figure 1-1: Excitation of the Second-Positive Band System of N_2

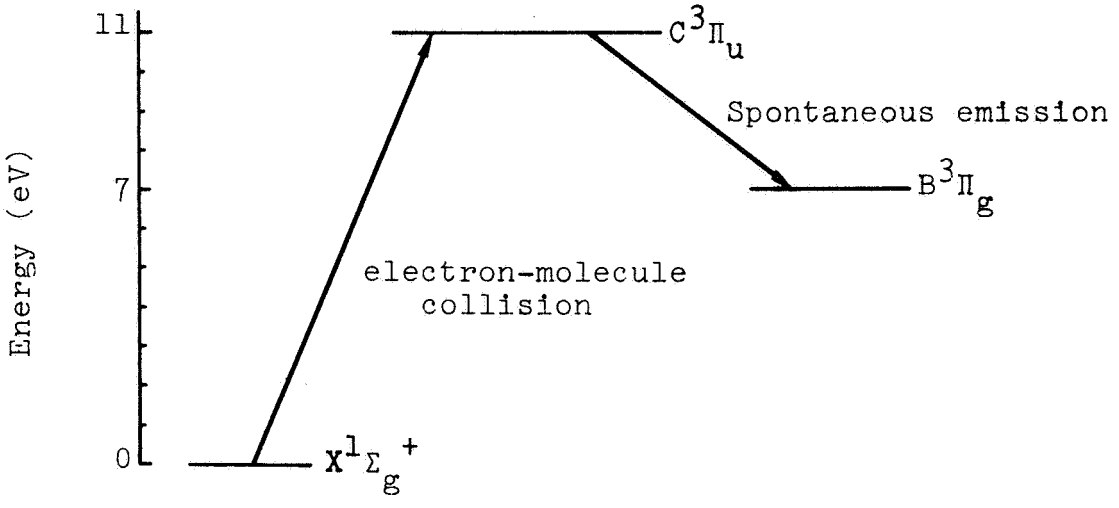

Figure 1-2: Schematic Energy-Level Diagram of the Excitation-Emission Process

1.5 Outline of the Present Research

The relative intensities of the lines in the (0,2) band of the second-positive band system are what Kyser actually measured in his tests. Our specific objective therefore is to develop a method for predicting these relative line intensities as functions of the quantities that characterize the ambient gas (temperature and pressure) and the spark (voltage, current, etc.).

We begin by ascertaining which of the complicated, transient phenomena that occur in a spark can be neglected for our purpose. This will enable simplifications to be made in the analysis. In Chapter 2, we discuss this preliminary work. There are then three steps in developing the relative line intensities. These are discussed in Chapters 3 through 6. In Chapter 3 a method is developed for calculating the rotational excitation that accompanies the electronic excitation $C^3\Pi_u \leftarrow X^1\Sigma_g^+$ produced by electron impact. In Chapters 4 and 5 the statistics of these collisions are used to calculate the resulting populations of the $C^3\Pi_u$ rotational levels. In Chapter 6 a formula is obtained for the relative line intensities as a function of the populations of the $C^3\Pi_u$ rotational levels. This last step was necessary because Kyser used a variation of the log-slope method in his experiments and modified Equation (1.3-2) for his case. The present investigation indicates the need for

modifying Kyser's derivation.

In Chapter 7, the predicted relative line intensities resulting from the present analysis are compared with those measured by Kyser. For this purpose all the numerical computations are based on Kyser's tests at 1 mm Hg and 0.5 joule (Section 1.2). Kyser's experiments are in fact the only ones available for comparison with the theory.

1.6 Differences between the Tracer-Spark Method and Muntz's Electron-Beam Method

Muntz (1962) has also studied the spectroscopic measurement of rotational temperature, exciting the emission with an electron beam, rather than a spark. (For a survey of more recent work on Muntz's method, see Marrone 1967.) Such a beam has much lower current than the spark, and the light output is correspondingly lower. As a result, milliseconds are required for a readily measurable amount of light to be emitted from the gas. With the spark, on the other hand, temperature measurements could be made in less than a microsecond. Furthermore, the spark equipment is cheaper and easier to set up than the beam equipment. Another advantage of the spark is that the flow velocity and static temperature could be measured with the same equipment.

The electrons in Muntz's beam had energies of the order of 50,000 eV, compared with 18 eV for those in Kyser's

spark. The excitation energy of the upper excited state is of the order of 10 eV. The electrons in the beam thus lost only a small fraction of their energy in the electronic-excitation collisions, so that Muntz could use the Born approximation of quantum mechanics in analyzing the collisions. In fact, at these energies the electrons act like photons in interacting with the molecules. Hence, Muntz used the standard formulas (Herzberg 1950) for molecular transitions caused by absorption of light to calculate the populations of the rotational levels in the upper excited state. The electrons in Kyser's spark, on the other hand, have energies of the same order as the excitation energy of the $C^3\Pi_u$ state, so that the Born approximation is not valid.

In summary, the tracer spark would have practical advantages over the electron beam. The tracer-spark technique for deducing static temperature is therefore worth developing. On the other hand, the tracer-spark excitation process is considerably more difficult to analyze than the electron-beam process.

CHAPTER 2

SIMPLIFICATION OF THE ANALYTICAL MODEL

2.1 Simplified Analytical Model

Although the collisional phenomena in the spark are inherently complicated, we can make several useful simplifications. Some of these can be made because of the nature of the spectroscopic method for deducing rotational temperature; others can be made because of the low nitrogen pressure and the short duration of the spark used by Kyser.

First, by the basic nature of the technique the rotational temperature depends only on the relative, not the absolute, line intensities. Hence, we need not know the absolute excitation cross section for each rotational transition, but only the relative cross sections. In other words, we do not have to answer the question, "What is the probability that excitation will occur to the ground vibrational level of $C^3\Pi_u$ with a given rotational excitation?". Rather, we have only to answer the much simpler question, "If excitation to the ground vibrational level of $C^3\Pi_u$ occurs, what is the probable accompanying rotational excitation?". To answer the latter question, we must examine the collision statistics. This requires knowledge of the

excitation function, i.e., the relative variation of the excitation cross section with electron energy. Again, this is easier to obtain (Section 3.2) than the absolute cross section.

Second, certain phenomena that one might expect in a spark did not have time to occur in Kyser's tests, because of the low pressure and short duration of the spark. (The spark parameters are listed in Section 2.2.) In particular, no process other than direct excitation by electron impact (Equation 1.4-1a) was significant in populating the $C^3\Pi_u$ state. In Section 2.3, we shall discuss the experimental results and order-of-magnitude calculations that lead to this conclusion. Furthermore, the translational and rotational distributions of the $X^1\Sigma_g^+$ molecules are not significantly disturbed from the ambient conditions during the time interval of interest. This statement will be justified in Section 2.4. Finally, the molecules can be assumed to undergo no collisions between the time at which they are excited to the $C^3\Pi_u$ state and the time at which they radiate. This is substantiated in Section 2.5. Another simplification is possible because of the low ambient temperature - that is, nearly all the molecules are in the ground vibrational level of $X^1\Sigma_g^+$ prior to excitation.

Our simplified model of the spark process is thus as follows. The ground vibrational level of $C^3\Pi_u$ is populated

solely by direct excitation caused by impact of electrons with ambient molecules in the ground vibrational level of $X^1\Sigma_g^+$. The resulting $C^3\Pi_u$ molecules then radiate before they collide with other particles in the spark. The radiation is thus characteristic of the excitation, which in turn is characteristic of the ambient conditions (temperature and pressure) and the spark parameters (voltage, current, etc.)

2.2 Order of Magnitude of the Spark Parameters

The following data were obtained by Kyser (1966), some by measurement in a no-flow chamber and others through computation by a semi-empirical method.

The total spark duration τ was

$$\tau \approx 0.8 \text{ μsec.} \qquad (2.2\text{-}1)$$

Within the first 0.2 μsec of the spark duration, the spark had begun to emit a measurable amount of light. Kyser made the temperature measurements at this earliest possible time, because the gas was then disturbed the least by the spark. We are therefore interested in what occurs in the initial time interval

$$\Delta t \approx 0.2 \text{ μsec.} \qquad (2.2\text{-}2)$$

The electron and molecule parameters were as follows:

Mean electron energy $\varepsilon \approx 7$ eV, (2.2-3)

Mean electron speed $v_e \approx 10^8$ cm/sec , (2.2-4)

Electron density $N_e \approx 10^{12}$ cm^{-3} , (2.2-5)

Molecule density $N_M \approx 10^{16}$ cm^{-3} . (2.2-6)

After the spark was initiated, these quantities attained nearly the values listed above within a time small compared with Δt. They remained constant to within an order of magnitude during the rest of the interval Δt.

2.3 Processes for Populating the $C^3\Pi_u$ State

Various investigators have suggested that processes other than direct excitation by electron impact (Equation 1.4-1a) may contribute to the population of the $C^3\Pi_u$ state and thus to the second-positive emission. Bates (1949) suggested electronic recombination with the ground-state N_2^+ ion as indicated by

$$N_2^+\left(X^2\Sigma_g^+\right) + e \rightarrow N_2\left(C^3\Pi_u\right) + h\nu . \qquad (2.3\text{-}1)$$

To estimate the relative importance of this process, we make the following order-of-magnitude calculation. Using a cross section σ_D of 10^{-17} cm^2 for direct excitation (which is the order of magnitude measured by Jobe, Sharpton, and St. John 1967, and Stewart and Gabathuler 1958 for electron energies between 10 and 25 eV), we find that

$$\text{Rate of direct electron-impact excitation to } C^3\Pi_u = \sigma_D\, v_e\, N_M\, N_e \approx (10^{-17}\ \text{cm}^2)(10^8\ \tfrac{\text{cm}}{\text{sec}})(10^{16}\ \text{cm}^{-3})(10^{12}\ \text{cm}^{-3}) = 10^{19}\ \text{excitations per sec per cm}^3. \tag{2.3-2}$$

From Kyser (1966), Equation 19, we obtain

$$\text{Recombination rate} = 0.9 \times 10^{-7}\, N_e^{\,2}/\varepsilon^{1/2} \approx (0.9 \times 10^{-7})(10^{12}\ \text{cm}^{-3})^2/(7\ \text{eV})^{1/2} \cong 3 \times 10^{16}\ \text{recombinations per sec per cm}^3. \tag{2.3-3}$$

Since the direct-excitation rate is 300 times larger than the recombination rate, the process (2.3-1) makes a negligible contribution to the population of $C^3\Pi_u$.

Tyte (1962), who performed experiments with a pure-nitrogen discharge tube at 0.2 mm Hg, considered electronic excitation of the metastable $A^3\Sigma$ state according to

$$N_2(A^3\Sigma_u^{\,+}) + e \rightarrow N_2(C^3\Pi_u) + e. \tag{2.3-3}$$

Tyte's data showed no evidence that this was an important population process in his discharge, which has similarities to Kyser's spark.

Bauer and Bartky (1965), who calculated the direct-excitation cross section, suggested the cascade process

$$\left.\begin{aligned} N_2(X^1\Sigma_g^{\,+}) + e &\rightarrow N_2(E^3\Sigma_g^{\,+}) + e \\ N_2(E^3\Sigma_g^{\,+}) &\rightarrow N_2(C^3\Pi_u) + h\nu \end{aligned}\right\}. \tag{2.3-4}$$

The transition $N_2(E) \rightarrow N_2(C)$, however, has never been observed. Furthermore, the magnitude of Bauer and Bartky's predicted cross sections agrees better with Stewart and Gabathuler's (1958) experimental data when only the direct excitation is considered than when the cascade process is included.

There is also experimental evidence that the process given in Equation (1.4-1a) makes the only significant contribution to populating the $C^3\Pi_u$ state. An apparatus similar to Kyser's spark was studied by Leonard (1965), who observed laser action in the second-positive band system of N_2 during a fast-rising, high-current, high-voltage discharge. With pressures ranging from 1 mm Hg to several tens of mm Hg, Leonard produced laser pulses of 0.02 μsec duration. Gerry (1965) devised a corresponding theory based on direct electron-impact excitation as the only excitation mechanism of $C^3\Pi_u$. Gerry's predicted laser-power density as a function of time agrees well both qualitatively and quantitatively with Leonard's data.*

*Gerry's theory predicts only the rate of electronic excitation to $C^3\Pi_u$, not the relative rates of excitation to the various rotational levels, and thus is not applicable to the calculation of the relative line intensities.

Further evidence in this regard was obtained in Tyte's (1962) experiments. Tyte concluded that the direct-excitation process (Equation 1.4-1a) accounted for at least 90% of his measured intensity, with the other 10% coming from the recombination process (Equation 2.3-1). As indicated above, the recombination contribution to the $C^3\Pi_u$ population was negligible in Kyser's tracer spark.

Several experimenters who excited the second-positive band system with electron beams in pure nitrogen also have concluded that the only significant population process is direct excitation. These include Langstroth (1934), Stewart and Gabathuler (1958), Kishko and Kuchinka (1959), and Jobe, Sharpton, and St. John (1967). These experiments, however, were conducted at pressures less than 0.1 mm Hg; the importance of secondary processes grows as the pressure increases.

We conclude that the direct-excitation process (1.4-1a) is the only significant process for populating the $C^3\Pi_u$ state. Although the supporting experiments are not identical to Kyser's, we feel that they are close enough to justify this conclusion.

2.4 Effects of Collisions Between Molecules and Slow Electrons

2.4.1 Increase of Translational Temperature

The increase ΔT_t in translational temperature caused by elastic electron-molecule collisions during the interval

Δt is given by

$$\frac{3}{2} k \Delta T_t = \text{(mean translational energy transferred to each molecule by collisions during } \Delta t\text{)}$$
$$= \text{(mean number of collisions per molecule during } \Delta t\text{)}$$
$$\times \text{(mean translational energy transferred per collision)}, \qquad (2.4\text{-}1)$$

where k is Boltzmann's constant (1.38054×10^{-16} erg/^{o}K). The mean number of collisions per molecule is given by

$$v_e N_e \sigma_{eM} \Delta t, \qquad (2.4\text{-}2)$$

where σ_{eM} is the cross section for elastic electron-molecule collisions.

The mean translational energy transferred per collision is given by

$$\varepsilon \lambda_t, \qquad (2.4\text{-}3)$$

where the mean electron energy ε is given in Equation (2.2-3) and λ_t is the mean fraction of the electron's energy that is transferred to molecular translational energy in a collision. Substituting Equations (2.4-2) and (2.4-3) into Equation (2.4-1), we obtain

$$\frac{3}{2} k \Delta T_t = v_e N_e \sigma_{eM} \Delta t \, \varepsilon \lambda_t. \qquad (2.4\text{-}4)$$

Since σ_{eM} is roughly the area of a circle whose diameter is the internuclear distance, which is 1.094 Å

for $N_2(X^1\Sigma_g^+)$, we take

$$\sigma_{eM} \approx 10^{-16} \text{ cm}^2. \qquad (2.4\text{-}5)$$

To make the calculation conservative, we use the maximum possible value of λ_t. From the laws of conservation of energy and momentum in a collision this is

$$\lambda_t = m/M = 0.39 \times 10^{-4}, \qquad (2.4\text{-}6)$$

where m is the mass of an electron and M is the mass of a nitrogen atom.

The numerical value of ΔT_t is

$$\Delta T_t \approx 10^{-3} \text{ }^{\circ}\text{K}, \qquad (2.4\text{-}7)$$

which is negligible compared with the ambient temperature of 295 $^{\circ}$K.

We conclude that the translational temperature of the $N_2(X^1\Sigma_g^+)$ molecules remains practically constant and equal to the ambient temperature during the interval Δt.

2.4.2 Increase of Rotational Temperature

The increase ΔT_r in rotational temperature caused by electron-molecule collisions during the interval Δt is similarly given by

$$k \, \Delta T_r = v_e \, N_e \, \sigma_r \, \Delta t \, \varepsilon \, \lambda_r, \qquad (2.4.8)$$

where σ_r is the cross section for rotational excitation by means of electron impact and λ_r is the mean fraction of the electron's energy that is transferred to rotational energy in a collision.

The value of λ_r, which is deduced from experimental data (Kyser 1966), is

$$\lambda_r \quad 2.72 \times 10^{-4} \quad . \tag{2.4-9}$$

Oksyuk (1966) has made the only calculation of σ_r that is valid for electron energies of the order of 7 eV. The other available analyses, e.g., Gerjuoy and Stein (1955), Sampson and Mjolsness (1965), and Takayanagi and Geltman (1965), are valid only for electrons of much lower energy (about 0.5 eV). Oksyuk's predicted total cross sections (elastic + inelastic) agree with the measured values. At 7 eV his predicted value of σ_r is

$$\sigma_r \quad 2 \times 10^{-16} \text{cm}^2 \; . \tag{2.4-10}$$

The value of ΔT_r is

$$\Delta T_r \approx 10^{-2} \; ^{\circ}\text{K} \tag{2.4-11}$$

which is again negligible compared with the ambient temperature. Hence, the rotational temperature of the $N_2(X^1\Sigma_g^+)$ molecules also remains practically constant and equal to the ambient temperature during the interval Δt.

2.4.3 Change in the Distribution of Rotational States

Experiments on electrons drifting through nitrogen, which led to the value of λ_r, indicate that the actual mean energy loss per collision is an order of magnitude higher than the value for purely elastic collisions. Since this is observed even for electron energies well below the

vibrational threshold, the result must be caused by rotational excitation. It follows that upward rotational transitions occur more often than downward ones. Indeed, Oksyuk's (1966) analysis predicts that

$$\sigma_{J_A \to J_B} = \frac{2J_B+1}{2J_A+1} \sigma_{J_B \to J_A} , \qquad (2.4\text{-}12)$$

where $\sigma_{J_A \to J_B}$ is the cross section for the electron-impact excitation from the rotational state J_A to the rotational state J_B without vibrational or electronic excitation occurring. Hence,

$$\sigma_{J_A \to J_B} > \sigma_{J_B \to J_A} \text{ if } J_B > J_A \quad . \qquad (2.4\text{-}13)$$

As a result of this imbalance between upward and downward rotational transitions, the distribution of the rotational states of the $X^1\Sigma_g^+$ molecules may be changed from a Boltzmann distribution. (This is distinct from the change in rotational temperature analyzed in the preceding section.)

We now estimate the order of magnitude of the change that occurs during the interval Δt. According to Oksyuk's theory, rotational transitions can occur only if J changes by an even number: 0, $\pm$ 2, $\pm$ 4, ... The cross section is negligible for $|J_B - J_A| > 4$. Hence, for a given J, the fractional change $\Delta N_J / N_J$ during the interval Δt is given by

$$\Delta N_J/N_J = v_e\, N_e\, \Delta t \left[N_{J-2}\, \sigma_{J-2\to J} + N_{J+2}\, \sigma_{J+2\to J} - N_J \left(\sigma_{J\to J+2} + \sigma_{J\to J-2} \right) + N_{J-4}\, \sigma_{J-4\to J} + N_{J+4}\, \sigma_{J+4\to J} - N_J \left(\sigma_{J\to J+4} + \sigma_{J\to J-4} \right) \right] / N_J \,. \tag{2.4-14}$$

The third term in Equation (2.4-14) is

$$(\Delta N_J/N_J)_{\text{third term}} = - v_e\, N_e\, \Delta t\, (\sigma_{J\to J+2} + \sigma_{J\to J-2}). \tag{2.4-15}$$

We point out that N_J appears in both the numerator and denominator of this equation and thus cancels. Using Equation (2.4-10) for the order of magnitude of the cross section, we obtain

$$(\Delta N_J/N_J)_{\text{third term}} \approx - 8 \times 10^{-3}. \tag{2.4-16}$$

None of the other terms in Equation (2.4-14) is of a larger order of magnitude than the third term. Hence we have

$$\Delta N_J << N_J \,, \tag{2.4-17}$$

that is, the $X^1\Sigma_g^+$ molecules remain effectively in rotational equilibrium during the interval Δt.

2.5 Lifetime of the $C^3\Pi_u$ State Compared with the Time Between Collisions of the $C^3\Pi_u$ Molecules

If the radiative lifetime τ_R (i.e., the inverse of the radiative transition probability) of the $C^3\Pi_u$ state is much less than the mean time τ_C between collisions, we can assume that the $C^3\Pi_u$ molecules will radiate before they collide with another particle. From Kyser (1966), we obtain

$$\left.\begin{aligned} \tau_R &\approx 0.045 \text{ μsec} \\ \tau_C &\approx 0.140 \text{ μsec} \end{aligned}\right\} . \qquad (2.5\text{-}1)$$

The value of τ_R is the inverse of the sum of the transition probabilities of all transitions from the zeroth vibrational level of $C^3\Pi_u$. The value of τ_C is the inverse of the molecular collision rate at a temperature of 295°K and a pressure of 1.0 mm Hg. Kyser does not mention the uncertainties on either of these values, both of which come from experiments referenced by him. Hence we obtain

$$\tau_C/\tau_R \approx 3. \qquad (2.5\text{-}2)$$

Although this number (3) is a bit borderline to justify the stated assumption, we have used this assumption in our analysis.

2.6 Labelling of the Rotational Levels

The resultant molecular angular momentum $\vec{J}$ (disregarding nuclear spin) is the vector sum of the contributions from nuclear rotation, electronic orbiting about the nuclei, and electron spin (Herzberg 1950). These contributions add in different ways, depending on the coupling between them. The $C^3\Pi_u$ and $B^3\Pi_g$ states are intermediate between Hund's coupling cases (a) and (b) (Herzberg 1950), but both go over to case (b) with increasing rotation. Since we are interested primarily in large rotational quantum numbers and since we wish to simplify the analysis, we assume that the $C^3\Pi_u$ and $B^3\Pi_g$ states are both case (b). There is no need to distinguish which case $X^1\Sigma_g^+$ belongs to, because it is a singlet state.

For singlet states and for states belonging to case (b), we can write $\vec{J}$ as

$$\vec{J} = \vec{K} + \vec{S}, \qquad (2.6\text{-}1)$$

where $\vec{S}$ is the angular momentum due to electron spin and $\vec{K}$ is the total angular momentum apart from spin. We have

$$\vec{K} = \vec{\Lambda} + \vec{N}, \qquad (2.6\text{-}2)$$

where $\vec{\Lambda}$ is the orbital angular momentum of the electrons, which is essentially along the internuclear axis, and $\vec{N}$ is the angular momentum of nuclear rotation, which is

essentially perpendicular to the internuclear axis. Since J, K, and S are all quantized, J can have the following 2S+1 possible values for a given value of K:

$$J = (K+S), (K+S-1), (K+S-2), \ldots, |K-S|. \quad (2.6\text{-}3)$$

The numerical superscript in the symbol of the electronic state is the value of 2S+1. For the singlet state $X^1\Sigma_g^+$, we have

$$S = 0, \quad (2.6\text{-}4)$$

whereas for the triplet states $C^3\Pi_u$ and $B^3\Pi_u$, we have

$$S = 1. \quad (2.6\text{-}5)$$

Since $\vec{\Lambda}$ is perpendicular to $\vec{N}$, K is given by

$$K = (\Lambda^2 + N^2)^{1/2}. \quad (2.6\text{-}6)$$

Whereas K and Λ are quantized, N is not quantized but must be such that K has one of the values

$$K = \Lambda, \Lambda+1, \Lambda+2, \ldots. \quad (2.6\text{-}7)$$

The Greek letter in the symbol of the electronic state denotes the value of Λ. For the Σ state $X^1\Sigma_g^+$, we have

$$\Lambda = 0, \quad (2.6\text{-}8)$$

whereas for the Π states $C^3\Pi_u$ and $B^3\Pi_g$, we have

$$\Lambda = 1. \quad (2.6\text{-}9)$$

For the $X^1\Sigma_g^+$ state we have accordingly

$$\vec{J} = \vec{K} = \vec{N}, \qquad (2.6\text{-}10)$$

so that there is no ambiguity in labelling the rotational levels. This is why the distinction between case (a) and case (b) is pointless for this state.

The situation is complicated, however, for the $C^3\Pi_u$ and $B^3\Pi_g$ states. Each rotational level is split into two levels, one for each direction of $\vec{\Lambda}$ (Λ-type doubling). Furthermore, for a given value of K, there are three possible values of J, one for each direction of $\vec{S}$ (triplet splitting):

$$J = K+1,\ K,\ K-1. \qquad (2.6\text{-}11)$$

For a given value of K, the energy difference produced between the levels by Λ-type doubling and triplet splitting is small compared with the energy difference between the levels for different value of K. Corresponding to the splitting of the rotational levels, each line of the second-positive band system, which is produced by a transition from a rotational level K' in the $C^3\Pi_u$ state to a rotational level K" in the $B^3\Pi_g$ state, is split into several lines of slightly different wavelength. Since the resolution of the spectrometer used in Kyser's experiments was not great enough to resolve the Λ-type doubling and triplet splitting, we will neglect them here. This will simplify the analysis by allowing us to treat the $C^3\Pi_u$ and $B^3\Pi_g$ states, for the purpose of calculating the populations of the rotational

levels and the line intensities, as singlet states with the rotational levels labelled by K instead of J.

For the $C^3\Pi_u$ and $B^3\Pi_g$ states, K is related to N by

$$K = (1 + N^2)^{1/2}. \qquad (2.6\text{-}12)$$

For large values of N, which are of interest here, the foregoing formula becomes

$$K \approx N. \qquad (2.6\text{-}13)$$

Hence, exactly for the $X^1\Sigma_g^+$ state and approximately for the $C^3\Pi_u$ and $B^3\Pi_g$ states, $\vec{K}$ is equal to $\vec{N}$.

Henceforth, we will write all our equations in terms of $\vec{K}$, rather than $\vec{J}$ or $\vec{N}$.

CHAPTER 3

DYNAMICS OF AN ELECTRON-MOLECULE COLLISION

3.1 Introduction

The objective in this chapter is to answer the question, "If, by electron impact, an N_2 molecule is excited from the ground vibrational level of the $X^1\Sigma_g^+$ state to the ground vibrational level of the $C^3\Pi_u$ state, what is the rotational quantum number K_1 of the $C^3\Pi_u$ molecule as a function of

(1) The rotational quantum number K_0 of the $X^1\Sigma_g$ molecule and

(2) The collision parameters (relative velocity, impact parameter, etc.)?"

To answer this question we had to develop our own analysis, because the experimental data and analytical methods available in the literature were of no help. This literature pertinent to the $C^3\Pi_u \leftarrow X^1\Sigma_g^+$ excitation is reviewed briefly in the following section.

3.2 Literature on Electron-Impact excitation of the Second-Positive Band System of N_2 and Related Collisions

The magnitude of the cross section for electron-impact excitation of the second=positive band system of N_2 has been measured by Stewart and Gabathuler (1958) and Jobe, Sharpton,

and St. John (1967). The excitation function has been measured by these workers and by Langstroth (1934) and Kishko and Kuchinka (1959). None of these experimenters, however, measured the relative cross sections of the various rotational transitions that accompany the electronic excitation.

Inelastic collisions can be treated theoretically from one of two standpoints - quantum mechanics or classical mechanics. Although the quantum approach is the more realistic on the atomic scale (Section 3.6.1), both approaches have been used to analyze electron-molecule collisions. The collision of interest here, however, has not been analyzed using either approach. In fact, no method for calculating the cross section for simultaneous excitation of two or more molecular energy modes by electron impact has been developed.

The first analysis of electron-impact excitation of rotation alone (no vibrational or electronic excitation) was that of Gerjuoy and Stein (1955). Since then, additional such analyses have been published, the most recent being those of Takayanagi and Geltman (1965), Sampson and Mjolsness (1965), and Oksyuk (1966). These are all quantum-mechanical analyses.

Electronic excitation by electron impact has been analyzed quantum-mechanically for hydrogen only (Khare 1966).

(This analysis treats "purely" electronic excitation, in the sense that the vibrational and rotational transitions are assumed to be unresolved.) Nitrogen is more difficult to handle because the electronic wave function becomes more complex as the atomic number increases. (Since this is not true of the rotational wave function, rotational excitation can be analyzed quantum-mechanically as easily for nitrogen as for hydrogen.) Bauer and Bartky (1965) used classical mechanics to calculate the cross section for excitation of the second-positive band system of nitrogen and obtained good agreement between theory and experiment. Neither Bauer and Bartky's nor Khare's analysis, however, can predict how much rotational excitation accompanies the electronic excitation.

3.3 Conservation Equations

We begin our analysis by writing the algebraic equations that govern the summational invariants of the collision - energy, linear momentum, and angular momentum. In general, the angular-momentum equation must include both orbital and spin momenta. For light molecules such as N_2, however, the spin-orbit interaction is much smaller than the coulombic interaction between the free electron and the orbital electrons. Hence the probability of the free electron's spin being transferred to $\vec{K}$ is much less than the probability of the free electron's orbital angular

momentum being transferred. We therefore have two separate angular-momentum equations, one for orbital angular momentum and another for spin. Since spin must be automatically conserved for electron exchange to occur (Section 3.4), we will not write the latter equation.

The conservation equations are as follows (see below for definition of symbols):

Energy:

$$(1/2)mv_0^2 + (1/2)\,MV_0^2 + E_{e_0} + E_{v_0} + E_{r_0} =$$

$$(1/2)mv_1^2 + (1/2)\,MV_1^2 + E_{e_1} + E_{v_1} + E_{r_1} \,. \qquad (3.3\text{-}1a)$$

Linear momentum:

$$m\vec{v}_0 + M\vec{V}_0 = m\vec{v}_1 + M\vec{V}_1, \qquad (3.3\text{-}1b)$$

Angular momentum:

$$\mu\vec{D}_0 \times (\vec{v}_0 - \vec{V}_0) + \vec{K}_0 = \mu\vec{D}_1 \times (\vec{v}_1 - \vec{V}_1) + \vec{K}_1. \qquad (3.3\text{-}1c)$$

In these equations, subscript 0 denotes quantities long before the collision, i.e., those of the incoming electron and the $X^1\Sigma_g^+$ molecule; subscript 1 denotes quantities long after the collision, i.e., those of the outgoing electron and the $C^3\Pi_u$ molecule; $\vec{v}$ is the velocity of the free electron; $\vec{V}$ is the molecular translational velocity; E_e is the molecular electronic energy; E_v is the molecular vibrational

energy; E_r is the molecular rotational energy; $\vec{D}$ is the distance between the electron and the center of mass of the molecule; and μ is the reduced mass, defined by

$$\mu = \frac{mM}{m + M} . \tag{3.3-2}$$

All velocities are relative to an inertial coordinate system. The interaction potential between the electron and the molecule does not appear in the energy equation because the equations are meant to apply outside the interaction region. In the angular-momentum equation, which is derived in Appendix A, we have anticipated Section 3.5 by writing the free electron's angular momentum classically. The excitation energy ΔE_e is

$$\Delta E_e = E_{e_1} - \Delta E_e = 11.05 \text{ eV}. \tag{3.3-3}$$

We now transform to relative and center-of-mass coordinates. The relative velocity $\vec{g}$ is defined by

$$\vec{g} = \vec{v} - \vec{V}, \tag{3.3-4}$$

and the center-of-mass velocity $\vec{W}$ is defined by

$$\vec{W} = \frac{m\vec{v} + M\vec{V}}{m + M} . \tag{3.3-5}$$

In terms of $\vec{g}$ and $\vec{W}$, the conservation equations are as follows:

Energy:

$$(1/2)\mu g_0^2 + E_{e_0} + E_{v_0} + E_{r_0} =$$

$$(1/2)\mu g_1^2 + E_{e_1} + E_{v_1} + E_{r_1} \ . \qquad (3.3\text{-}6a)$$

Linear momentum:

$$\vec{W}_0 = \vec{W}_1 . \qquad (3.3\text{-}6b)$$

Angular momentum:

$$\mu\vec{D}_0 \times \vec{g}_0 + \vec{K}_0 = \mu\vec{D}_1 \times \vec{g}_1 + \vec{K}_1 \ . \qquad (3.3\text{-}6c)$$

The foregoing equations are exact.

We can simplify the energy equation because rotational and vibrational quanta are much smaller than electronic quanta; that is,

$$\left|E_{r_1} - E_{r_0}\right| << \left|E_{v_1} - E_{v_0}\right| << \Delta E_e . \qquad (3.3\text{-}7)$$

Therefore, to a good approximation, the energy equation is simply a balance between the change in kinetic energy and the electronic-excitation energy:

$$(1/2)\mu g_1^2 = (1/2)\mu g_0^2 - \Delta E_e . \qquad (3.3\text{-}8)$$

Accordingly, the magnitude (but not the direction) of $\vec{g}_1$ is determined as a function of g_0.

The simplified energy equation (3.3-8) gives g_1 as an

explicit function of g_0. The linear-momentum equation (3.3-6b) simply states that the center-of-mass velocity is constant (which results because no external forces act on the system) and is not involved in the evaluation of K_1.

If we assume that the precollision quantities $\vec{g}_0$, $\vec{K}_0$, and the angular momentum of the incoming electron are given, then we have 6 scalar unknowns - the 2 components of $\vec{K}_1$, the 2 angles specifying the direction of $\vec{g}_1$, and the 2 components of the angular momentum of the outgoing electron (which are related to $\vec{D}_1$). Since the angular-momentum equation provides only 2 nontrivial scalar equations, the system of equations and unknowns is underdetermined.

3.4 Difficulties in Progressing Further

Further progress is made in both the classical and quantum-mechanical approaches by using the differential equation of motion (Chapman and Cowling 1952). This equation is Newton's law for the positions of the collision partners in the classical theory and Schrödinger's equation for the wave functions of the collision partners in the quantum theory. For the collision of interest, however, both approaches are difficult for the reasons given below.

(1) The interaction potential is unknown.

Whereas the conservation equations are algebraic, Newton's and Schrödinger's equations are differential. To solve either of them, we must know the electron-molecule

interaction potential throughout all space. For the interaction between an electron and a homonuclear diatomic molecule, however, the potential is known only at large separation distances (Takayanagi and Geltman 1965).

(2) The Born approximation is not valid.

The excitation cross section for the $C^3\Pi_u \leftarrow X^1\Sigma_g^+$ transition is large only near threshold. The excitation function is zero at threshold (11.05 eV), rises to a maximum at about 18 eV, and decreases monotonically with further increase in electron energy (see Figure 5-4). Hence, we cannot use for this collision the Born approximation of quantum mechanics, whose basis is the assumption that the bombarding particle loses only a small part of its energy to the target particle. Very few quantum-mechanical analyses of inelastic electron-molecule collisions have been developed using anything but the Born approximation.

(3) Two energy modes are excited simultaneously.

Since our interest is in the rotational excitation that accompanies the electronic excitation, we must consider both these excitations together. The difficulty of treating the excitation of more than one energy mode is indicated by the dearth of analyses of the problem (Section 3.2).

(4) The collision involves electron exchange.

The resultant spin of the molecular electrons is different in the triplet state $C^3\Pi_u$ than in the singlet

state $X^1\Sigma_g^+$. Hence, the $C^3\Pi_u \leftarrow X^1\Sigma_g^+$ transition is optically forbidden by the selection rule that spin must be conserved. The transition can actually occur by electron exchange. The incoming electron, which can have arbitrary spin, changes places with a molecular electron, which then becomes the outgoing electron, Exchange collisions are more complicated to analyze than collisions in which exchange does not occur. Although the $C^3\Pi_u \leftarrow X^1\Sigma_g^+$ transition has been observed in absorption* (Tilford, Vanderslice, and Wilkinson 1965), it seems to occur by electron exchange when it is excited by electron impact. The evidence for this is that the excitation function has the characteristic shape for electron-exchange collisions (Stewart and Gabathuler 1958).

3.5 Present Approach to the Problem

3.5.1 Introduction of the Classical Impact Parameter

In the present state of knowledge of quantum-mechanical collision theory, it appears hopeless to calculate accurately by quantum-mechanical methods the cross section for simultaneous electronic and rotational excitation for an

*Selection rules for optical transitions vary in "strictness". The rule that spin must be conserved is one of those most frequently violated in nature.

electron-exchange collision for which the Born approximation is not valid. We therefore turn our attention to a semiclassical approach.

The conservation equations for energy and linear momentum are valid in both the quantum and classical theories. The angular-momentum equation is not usually written in a quantum theory, but it is valid if the angular momentum is written in a quantum form. To make further progress, however, we write the angular momentum of the free electron as the vector product of distance and linear momentum. From this point on, the analysis is not purely quantum-mechanical, because the impact parameter is strictly a classical concept. We discuss the implications of this step in Section 3.6.

The coordinate system is shown in Figure 3-1. The origin is on the internuclear axis midway between the nitrogen atoms. The axes are chosen so that, before collision, the molecule is aligned with the z axis and has angular momentum $|\vec{K}_0|$ in the positive-x direction. Hence the components of $\vec{K}_0$ are as follows:

$$(\vec{K}_0)_x = \hbar[K_0(K_0+1)]^{1/2}. \qquad (3.5\text{-}1a)$$

$$(\vec{K}_0)_y = 0. \qquad (3.5\text{-}1b)$$

$$(\vec{K}_0)_z = 0. \qquad (3.5\text{-}1c)$$

In Equation (3.5-1a) $\hbar=1.054\times10^{-27}$ erg-sec is related to

Before collision
($X^1\Sigma_g^+$ state)

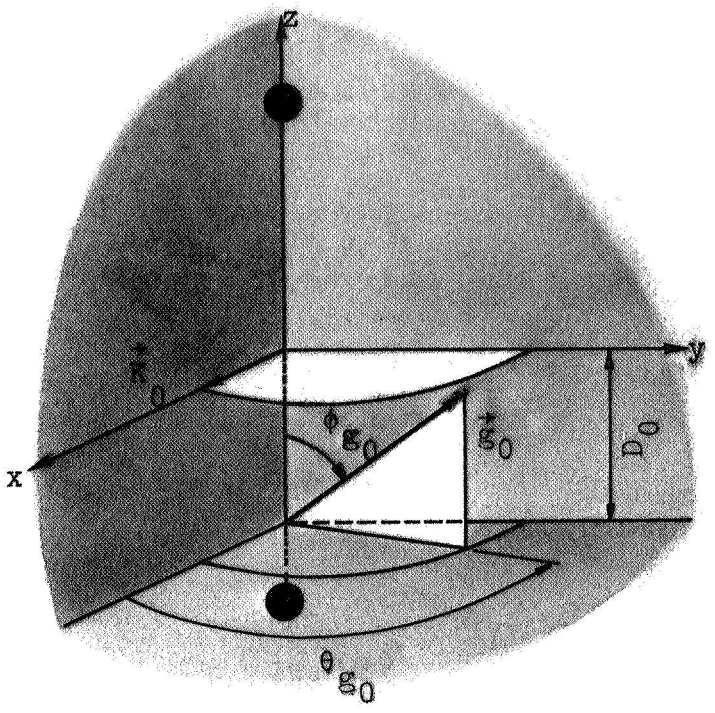

After collision
($C^3\Pi_u$ state)

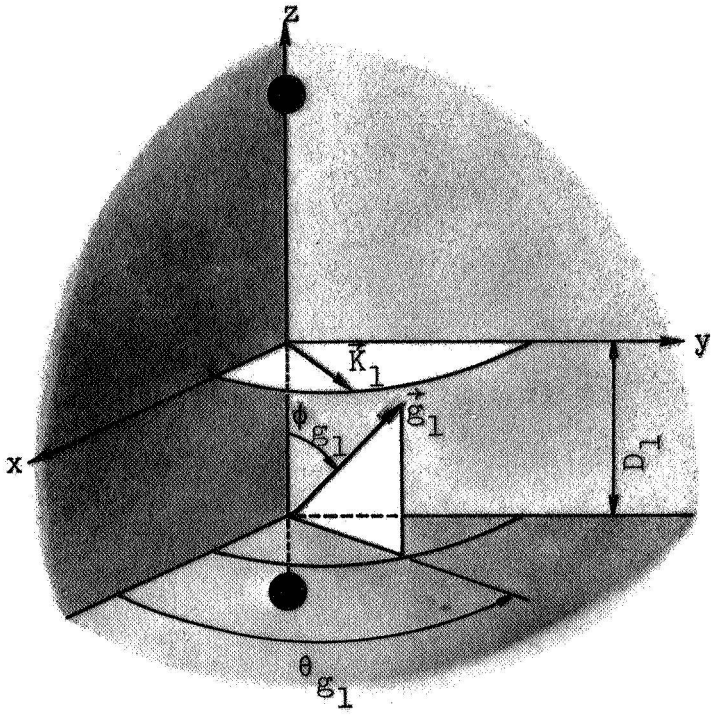

Figure 3-1: Coordinate System for Classical Collision Analysis

Planck's constant h by $\hbar = h/2\pi$. We put arrows over the components of $\vec{K}$ to avoid confusion with the quantum number K. We assume that a collision occurs only if the electron strikes the internuclear axis (which we assume has a finite width w), so that the components of $\vec{D}$ are as follows:

$$D_x = 0. \tag{3.5-2a}$$

$$D_y = 0. \tag{3.5-2b}$$

$$D_z = -D. \tag{3.5-2c}$$

The distance D is related to the impact parameter b for the collision. We emphasize that our coordinate axes are aligned with the initial directions of the internuclear axis and $\vec{K}$; they do not rotate with the molecule. The collision occurs in a time interval that is small compared with the period of rotation of the molecule, however, so that the molecule stays practically aligned with the z axis during the collision. Hence Equations (3.5-2) hold for both $\vec{D}_0$ and $\vec{D}_1$. The direction of $\vec{g}$ relative to the axes is specified by the polar angles ϕ_g and θ_g, so that we have

$$g_x = g \sin \phi_g \cos \theta_g. \tag{3.5-3a}$$

$$g_y = g \sin \phi_g \sin \theta_g. \tag{3.5-3b}$$

$$g_z = g \cos \phi_g . \qquad (3.5\text{-}3c)$$

With the foregoing notation, we can write the angular-momentum equations in component form as follows:

x component:

$$\mu D_0 \, g_0 \sin \phi_{g_0} \sin \theta_{g_0} + \hbar[K_0(K_0+1)]^{1/2} =$$

$$\mu D_1 \, g_1 \sin \phi_{g_1} \sin \theta_{g_1} + (\vec{K}_1)_x . \qquad (3.5\text{-}4a)$$

y component:

$$\mu D_0 \, g_0 \sin \phi_{g_0} \cos \theta_{g_0} =$$

$$\mu D_1 \, g_1 \sin \phi_{g_1} \cos \theta_{g_1} + (\vec{K}_1)_y . \qquad (3.5\text{-}4b)$$

z component:

$$(\vec{K}_1)_z = 0. \qquad (3.5\text{-}4c)$$

The unknowns in Equations (3.5-4) are the final impact distance D_1, the angles ϕ_{g_1} and θ_{g_1} that specify the direction of $\vec{g}_1$, and the two components of $\vec{K}_1$. By introducing the classical impact parameter, we have reduced the number of unknowns by one. Instead of the 2 components of the outgoing electron's angular momentum, we have the scalar quantity $\vec{D}_1$.

The magnitude of $\vec{K}_1$ is given in terms of its components by

$$|\vec{K}_1| = [(\vec{K}_1)_x^2 + (\vec{K}_1)_y^2 + (\vec{K}_1)_z^2]^{1/2} \qquad (3.5\text{-}5)$$

and in terms of the final rotational quantum number K_1 by

$|\vec{K}_1|^2 = \hbar^2[K_1(K_1+1)]$. Solving for K_1, we obtain

$$K_1 = \left\{-1 + [1 + (2|\vec{K}_1|/\hbar)^2]^{1/2}\right\} / 2. \qquad (3.5\text{-}6)$$

Thus, K_1 is a function of the precollision quantities as indicated by

$$K_1 = K_1(g_0, D_0, \phi_{g_0}, \theta_{g_0}; K_0). \qquad (3.5\text{-}7)$$

3.5.2 Exploitation of the Integer Nature of the Final Rotational Quantum Number

It is possible to make the system of equations and unknowns determinate by exploiting the quantum requirement that

$$K_1 = (\text{an integer}). \qquad (3.5\text{-}8)$$

For given values of the precollision quantities, only certain combinations of values of the postcollision quantities will yield an integer value for K_1. These postcollision quantities have the ranges (See Figure 3-1)

$$-r_0 \leq D_1 \leq r_0 . \qquad (3.5\text{-}9)$$

$$0 \leq \phi_{g_1} \leq \pi. \qquad (3.5\text{-}10)$$

$$0 \leq \theta_{g_1} \leq 2\pi. \qquad (3.5\text{-}11)$$

If we consider K_1 to be a continuous function of D_1, ϕ_{g_1}, and θ_{g_1}, then K_1 will in general have a minimum value $K_{1_{min}}$ and a maximum value $K_{1_{max}}$. The possible integer values of

K_1 are the integers between $K_{1_{min}}$ and $K_{1_{max}}$. We can solve for the extremal values of K_1 in closed form in the following way.

We can manipulate the solution for $|\vec{K}_1|$ into the form

$$|\vec{K}_1|^2 = a + b\left[b + c\cos(\theta_{g_1} - \theta_{g_0}) - 2|\vec{K}_0| \sin\theta_{g_1}\right], \tag{3.5-12}$$

where

$$a = (c/2)^2 + |\vec{K}_0|^2 + |\vec{K}_0| \, c \sin\theta_{g_0}, \tag{3.5-13a}$$

$$b = \mu D_1 \, g_1 \sin\phi_{g_1}, \tag{3.5-13b}$$

$$c = 2\mu \, D_0 \, g_0 \sin\phi_{g_0}. \tag{3.5-13c}$$

The value of θ_{g_1} at which $|\vec{K}_1|$ achieves an extremum is given by

$$\tan\theta_{g_1} = \frac{c \sin\theta_{g_0} - 2|\vec{K}_0|}{c\cos\theta_{g_0}}. \tag{3.5-14}$$

Equation (3.5-14) has two solutions (which yield a minimum and maximum of $|\vec{K}_1|$), given by

$$\theta_{g_1} = \begin{cases} \theta_e \\ \theta_e + \pi \end{cases}. \tag{3.5-15}$$

The value of θ_e is independent of D_1 and ϕ_{g_1}. Furthermore, D_1 and ϕ_{g_1} appear only in b, so that we can consider b as a single unknown. If we replace θ_{g_1} by θ_e or $\theta_e + \pi$, we can write Equation (3.5-12) as

$$(|\vec{K}_1|^2)_e = a + b^2 + bQ, \tag{3.5-16}$$

where

$$Q = \pm[c \cos(\theta_e - \theta_{g_0}) - 2|\vec{K}_0| \sin \theta_e]. \qquad (3.5\text{-}17)$$

The plus sign goes with $\theta_{g_1} = \theta_e$, and the minus sign with $\theta_{g_1} = \theta_e + \pi$.

The extremal value of $(|\vec{K}_1|^2)_e$ occurs when

$$b = b_e = -Q/2. \qquad (3.5\text{-}18)$$

This extremum is a minimum, and $(|\vec{K}_1|^2)_e$ increases monotonically as b is varied away from b_e. If $|\vec{K}_0|$ is large enough, we will have

$$|b_e| > \mu r_0 g_1, \qquad (3.5\text{-}19)$$

which is impossible because of Equation (3.5-9). Thus, we have the following cases (We use the notation $L = \mu r_0 g_1$.):

Case I: $Q < 0$. (3.5-20)

$$K_1 = K_{1_{max}} \text{ when } b = -L. \qquad (3.5\text{-}21a)$$

$$K_1 = K_{1_{min}} \text{ when} \begin{cases} b = b_e, \text{ if } b_e < L \\ b = L, \text{ if } b_e \geq L \end{cases}. \qquad (3.5\text{-}21b)$$

Case II: $Q > 0$. (3.5-22)

$$K_1 = K_{1_{max}} \text{ when } b = L. \qquad (3.5\text{-}23a)$$

$$K_1 = K_{1_{min}} \text{ when } \left\{ \begin{array}{ll} b = b_e, & \text{if } |b_e| < L \\ b = -L, & \text{if } |b_e| \geq L \end{array} \right\} . \qquad (3.5\text{-}23b)$$

Case III: $Q = 0$. (3.5-24)

In this case, we have

$$\left(|\vec{K}_1|^2 \right)_e = a + b^2, \qquad (3.5\text{-}25)$$

so that we have

$$K_1 = K_{1_{min}} \text{ when } b = 0. \qquad (3.5\text{-}26a)$$

$$K_1 = K_{1_{max}} \text{ when } |b| = L. \qquad (3.5\text{-}26b)$$

Numerical calculations for typical values of the initial collisional parameters indicate that K_1 can take on only one or two possible integer values for each set of initial conditions. This occurs because relatively little rotational excitation can take place for the initial conditions of interest. For example, for an initial rotational quantum number K_0=10, K_1 can range from 8 to 12 for all values of relative velocity $\vec{g}_0$ and impact distance D_0 that occur in the spark (Section 5.5.2). The possible values of K_1 are shown in Table I for several typical cases.

The range of g_0 in Table I is that over which the collision cross section is significant. The range of D_0 corresponds to the radius of the N_2 molecule. The angles ϕ_{g_0} = $\theta_{g_0} = \pi/2$ give the maximum transfer of angular momentum.

TABLE I - POSSIBLE INTEGER VALUES OF K_1

FOR TYPICAL CASES: $K_0 = 10$, $\phi_{g_0} = \pi/2$, $\theta_{g_0} = \pi/2$

g_0(cm/sec x 10^8)	D_0(cm x 10^{-9})	Possible Integer values of K_1
3.0	5.4	11, 12
3.0	3.6	10, 11
3.0	1.8	10, 11
3.0	0	10
3.0	-1.8	9, 10
3.0	-3.6	9, 10
3.0	-5.4	8, 9
2.2	-1.0	10
2.4	-1.0	10
2.6	-1.0	9, 10
2.8	-1.0	9, 10
3.0	-1.0	9, 10

In summary, the possible integer values of K_1 (which are functions of K_0, g_0, D_0, ϕ_{g_0}, and θ_{g_0}) can be found using only the conservation equations and the quantum condition. Neither the interaction potential nor the detail of the electron's trajectory is utilized. The quantum condition makes the system of equations and unknowns determinate by effectively eliminating D_1, ϕ_{g_1}, and θ_{g_1} as unknowns. This approach to the analysis of the collision may be called a "quantized classical model". To our knowledge, this quantum condition has not previously been used to solve a collision problem. The use of this condition is one of the novel aspects of the present analysis.

Since more than one integer value of K_1 is possible for some sets of collision parameters, the quantized classical analysis does not determine K_1 uniquely. In Section 5.5.1, we discuss how we account for this nonuniqueness.

3.6 Validity of the Classical Approach

3.6.1 Uncertainty in the Electron's Trajectory

Although we have exploited the fact that K_1 is quantized, our analysis is partly classical because we have written the free electron's angular momentum as the product of the linear momentum and the impact parameter. A basic assumption of classical mechanics is that an object, such as the free electron in the present problem, is a point mass whose position and momentum are known precisely at

each point on its trajectory. In reality, however, an object has not only a particle nature but a wave nature, which is characterized by its de Broglie wavelength λ_D. In a collision problem, the bombarding object can be assumed to travel on a well-defined trajectory only if λ_D is small compared with the characteristic length of the scattering region. For the present collision, the characteristic length is the internuclear distance of $N_2(X^1\Sigma_g^+)$, which is $2\ r_0 = 1.094 \times 10^{-8}$ cm. The de Broglie wavelength λ_D is given by

$$\lambda_D = h/m\ v_0\ . \qquad (3.6\text{-}1)$$

By using as a typical electron velocity the value $v_0 = 3 \times 10^8$ cm/sec, we obtain

$$\lambda_D/2\ r_0 \approx 2. \qquad (3.6\text{-}2)$$

Hence, the free electron's trajectory is in fact "smeared out" over a distance that is large compared with the internuclear distance.

We see the effect of this smearing from the following consideration. Our classical picture of the collision is the one sketched in Figure 3-1. If, for simplicity, we consider the case $\phi_{g_0} = \theta_{g_0} = \pi/2$, then we assume in our classical analysis that we know D_0 precisely and that the z component of $\vec{g}_0$ is precisely zero. In reality, however, there are uncertainties ΔD_0 in the impact distance and

Δg_{0_z} in the z component of the relative velocity. These uncertainties are related by Heisenberg's uncertainty principle:

$$m \, \Delta g_{0_z} \, \Delta D_0 \geq h. \qquad (3.6\text{-}3)$$

If we have the large (relative to typical values of v_0) uncertainty in g_{0_z} of $\Delta g_{0_z} = 10^8$ cm/sec, then we obtain

$$\Delta D_0 \; / \; 2 \, r_0 \approx 6. \qquad (3.6\text{-}4)$$

With a more precise knowledge of g_0, our knowledge of D_0 would be even less precise. This relatively large uncertainty in D_0 produces a large uncertainty in the amount of rotational excitation that results from the collision. In spite of this, the classical approach has in fact been used successfully to analyze the type of collision of interest here.

3.6.2 Precedents for Analyzing the Collision Classically

Gryzinski, in particular, has developed a classical analysis of atomic collisions. This he applied to, among other collisions, excitation of atoms by electron impact in which electron exchange occurs (see Gryzinski 1965). Bauer and Bartky (1965) extended Gryzinski's method to electron-molecule collisions and used it to predict the cross section for excitation of the second-positive band system of N_2. As we mentioned in Section 3.2, Bauer and Bartky's predicted cross sections agree well with measured

values.

In view of Bauer and Bartky's success in predicting the cross section for excitation of the $C^3\Pi_u$ electronic state by a classical method, we feel it worth a try to predict the accompanying rotational excitation by means of classical mechanics. A full quantum-mechanical analysis would be difficult, if not impossible, to carry out, whereas our quantized classical analysis is relatively simple.

CHAPTER 4

POPULATION OF THE $C^3\Pi_u$ ROTATIONAL LEVELS AS A RESULT OF THE COLLISIONS

4.1 Introduction

In this chapter we derive the formula for the population N_{K_1} of the rotational level K_1 of the ground vibrational level of the $C^3\Pi_u$ electronic state. We obtain this formula by calculating the fractional rates at which the $C^3\Pi_u$ rotational levels are populated by electron-impact electronic excitation of the $X^1\Sigma_g^+$ molecules. We obtain these rates, in turn, by examining the statistics of the electron-molecule collisions, based on our quantized classical analysis (Chapter 3). In Chapter 5, we shall obtain numerical results from this formula.

4.2 Proportionality of the $C^3\Pi_u$ Population to the Excitation Rate

The instantaneous population $N_{K_1}(t)$ is given by

$$N_{K_1}(t) = \int_0^t (r_{ex,K_1} - r_{em,K_1})\, dt', \qquad (4.2\text{-}1)$$

where r_{ex,K_1} is the rate of collisional excitation to the

rotational level K_1 of the ground vibrational level of $N_2(C^3\Pi_u)$ and r_{em,K_1} is the rate of radiative de-excitation from this rotational level. All other population and depopulation processes are negligible (Chapter 2). We assume that the rates are constant with time, so that Equation (4.2-1) reduces to

$$N_{K_1}(t) = (r_{ex,K_1} - r_{em,K_1})\, t. \qquad (4.2\text{-}2)$$

The rate of radiative de-excitation r_{em,K_1} is the number of molecules per unit time that undergo any of the possible downward radiative transitions from the rotational level K_1. From the standard formulas for spontaneous emission (Herzberg 1950), we obtain

$$r_{em,K_1} = A\, N_{K_1}\,, \qquad (4.2\text{-}3)$$

where the proportionality factor A is independent of K_1. By substituting Equation (4.2-3) into Equation (4.2-2), we obtain

$$N_{K_1} = B\, r_{ex,K_1}, \qquad (4.2\text{-}4)$$

where the proportionality factor B(t) is independent of K_1.

Hence the instantaneous population N_{K_1} varies with K_1 in the same way as does the excitation rate r_{ex,K_1}, so that the problem of calculating N_{K_1} reduces to that of calculating r_{ex,K_1}. In Section 4.3, we shall derive the formula for

r_{ex,K_1} as a function of K_1.

4.3 Derivation of the Formula for the Excitation Rate

4.3.1 Relation to the Collision Rate

The excitation rate r_{ex,K_1} is the number of excitation collisions per unit time in which the precollision quantities K_0, $\vec{g}_0$, and D_0 are such as to yield K_1 as the final rotational quantum number. We can separate the dependence on K_0, $\vec{g}_0$, and D_0 in the following way. The rate of excitation collisions in which the initial rotational quantum number is K_0 is proportional to the number N_{K_0} of molecules that are in the rotational level K_0 of the ground vibrational level of $N_2(X^1\Sigma_g^+)$. Since the fraction of molecules that are excited during the spark duration is small (Chapter 2), N_{K_0} is practically constant during the spark. If we let α_{K_0,K_1} be the fraction of molecules in the group N_{K_0} that are excited by electron impact to the K_1 rotational level of the ground vibrational level of $N_2(C^3\Pi_u)$ per unit time, then we have

$$r_{ex,K_1} = \sum_{K_0} N_{K_0} \alpha_{K_0,K_1}. \qquad (4.3\text{-}1)$$

Now consider the phase space in which the coordinates are g_0, ϕ_{g_0}, θ_{g_0}, and D_0 (or equivalently, $\vec{g}_0$ and D_0). For a given value of K_0, each point in this space corresponds to a value K_1' of K_1, i.e., if an excitation collision occurs in which the precollision quantities are K_0, $\vec{g}_0$, and D_0,

then the final rotational quantum number will be K_1'. Because K_1' is discrete-valued, there is a finite volume $\tau_{K_0,K_1'}$ in this space that corresponds to K_1'. There is a set of these volumes for each value of K_0. If we define $\beta(\vec{g}_0,D_0)$ such that $N_{K_0}\ \beta(\vec{g}_0,\ D_0)\ d\vec{g}_0\ dD_0$ is the number of excitation collisions per unit time in which the initial rotational quantum number is K_0, the initial relative velocity is in the range $\vec{g}_0$ to $\vec{g}_0+d\vec{g}_0$, and the impact distance in the range D_0 to D_0+dD_0, then we have

$$\alpha_{K_0,K_1} = \int_{\tau_{K_0,K_1}} \beta(\vec{g}_0,D_0)\ d\vec{g}_0\ dD_0. \qquad (4.3\text{-}2)$$

The relative excitation rate β equals the relative collision rate ν times the probability F that a collision will produce the electronic excitation:

$$\beta(\vec{g}_0,\ D_0) = F(g_0)\ \nu(\vec{g}_0,\ D_0). \qquad (4.3\text{-}3)$$

We write F, which is proportional to the excitation function for the $C^3\Pi_u \leftarrow X^1\Sigma_g^+$ transition, as a function only of g_0 because there is no experimental evidence that F depends on anything else. By substituting Equations (4.3-2) and (4.3-3) into Equation (4.3-1), we obtain finally

$$r_{ex,K_1} = \sum_{K_0} N_{K_0} \int_{\tau_{K_0,K_1}} F(g_0)\ \nu(\vec{g}_0,\ D_0)\ d\vec{g}_0\ dD_0\ . \qquad (4.3\text{-}4)$$

We now derive a formula for $\nu(\vec{g}_0,\ D_0)$.

4.3.2 Derivation of Formula for the Collision Rate

We follow (but modify slightly) the derivation given by Chapman and Cowling (1952), Section 3.5. We begin by counting the number of collisions occurring during the time interval dt and in which the initial molecular rotational quantum number is K_0, the impact parameter between b_0 and b_0+db_0, the electron velocity between $\vec{v}_0$ and $\vec{v}_0+d\vec{v}_0$, and the molecular velocity between $\vec{V}_0$ and $\vec{V}_0+d\vec{V}_0$. Since we are taking the molecular structure into account, we must also specify the orientation of $\vec{K}_0$ and of the internuclear axis. The direction of $\vec{K}_0$ is specified by the polar angles ϕ_{K_0} and θ_{K_0}, and the direction of the internuclear axis is specified by the angle δ between the internuclear axis and an arbitrary line in the plane perpendicular to $\vec{K}_0$. We specify, then, that $\vec{K}_0$ lies within a solid angle $d\Omega$ and that the internuclear axis lies in the range δ to $\delta+d\delta$.

For such a collision to occur, the electron must be in the cylinder sketched in Figure 4-1 at the beginning of the interval dt. Here w is the width of the molecule. The volume of the cylinder is

$$(g_0 dt)(w)(db_0), \qquad (4.3\text{-}5)$$

where wdb_0 replaces the factor $bdbd\varepsilon$ that appears for collisions between point particles. We replace db_0 in terms of dD_0 by

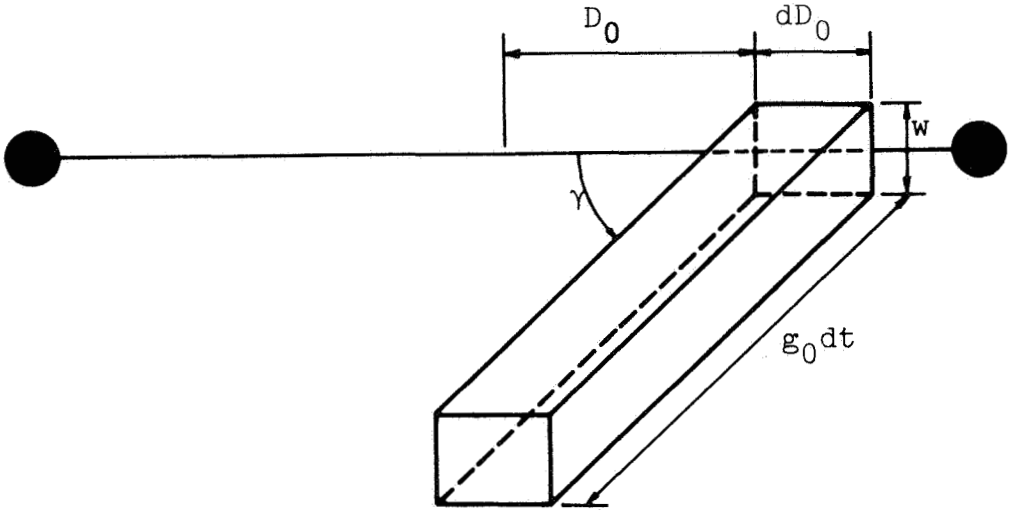

Figure 4-1: Cylinder Used to Calculate the Collision Rate

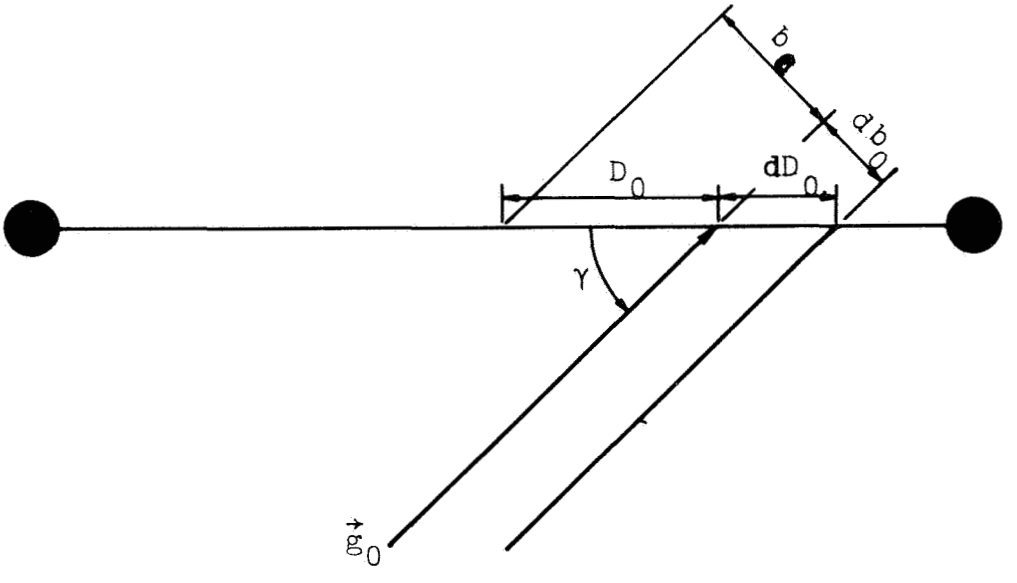

Figure 4-2: Relation between the Impact Parameter and the Distance Along the Internuclear Axis

$$db_0 = dD_0 \sin \gamma, \qquad (4.3\text{-}6)$$

where γ is the angle between $\vec{g}_0$ and the internuclear axis (see Figure 4-2). There is one cylinder of this type for each molecule of the specified type. The fraction of molecules with velocity between $\vec{V}_0$ and $\vec{V}_0+d\vec{V}_0$ is $f_M(\vec{V}_0)d\vec{V}_0$, where f_M is the molecular velocity distribution function. Since all directions of $\vec{K}_0$ and of the internuclear axis are equally likely, the probability that $\vec{K}_0$ is in the solid angle $d\Omega$ is $d\Omega/4\pi$, and the probability that the internuclear axis in the range δ to $\delta+d\delta$ is $d\delta/2\pi$. Hence the number of molecules of the specified type (and hence of cylinders) is

$$N_{K_0} f_M(\vec{V}_0)(d\vec{V}_0\, d\Omega/4\pi)\,(d\delta/2\pi). \qquad (4.3\text{-}7)$$

The total volume of the cylinders is therefore

$$(w\, dt)\, N_{K_0} f_M(\vec{V}_0)\, d\vec{V}_0\, g_0 \sin\gamma\, dD_0\, (d\Omega/4\pi)\,(d\delta/2\pi). \qquad (4.3\text{-}8)$$

Since the number of electrons in the range $\vec{v}_0$ to $\vec{v}_0+d\vec{v}_0$ is $N_e f_e(\vec{v}_0)d\vec{v}_0$ (where N_e is the total electron density and f_e is the electron velocity distribution function), the number of electrons in this total volume is

$$(w\, dt)\, N_{K_0} f_M(\vec{V}_0)\, f_e(\vec{v}_0)\, d\vec{V}_0\, d\vec{v}_0\, g_0 \sin\gamma\, dD_0 \times$$
$$(d\Omega/4\pi)\,(d\delta/2\pi). \qquad (4.3\text{-}9)$$

Since each such electron represents a collision of the

specified type, the number of collisions of the specified type is given by the foregoing expression, and the rate of these collisions is given by the above expression divided by dt:

$$w\, N_{K_0}\, f_M(\vec{V}_0)\, f_e(\vec{v}_0)\, d\vec{V}_0\, d\vec{v}_0\, g_0 \sin\gamma\, dD_0 \times$$

$$(d\Omega/4\pi)\, (d\delta/2\pi). \qquad (4.3\text{-}10)$$

We now transform to relative and center-of-mass velocities, as in Chapter 3. The product of elemental volumes in velocity space becomes

$$d\vec{V}_0\, d\vec{v}_0 = d\vec{g}_0\, d\vec{W}. \qquad (4.3\text{-}11)$$

By substituting Equation (4.3-11) into expression (4.3-10), we obtain

$$w\, N_{K_0}\, g_0 \sin\gamma\, d\vec{g}_0\, f_e(\vec{g}_0,\vec{W})\, f_M(\vec{g}_0,\vec{W})\, d\vec{W}\, dD_0 \times$$

$$(d\Omega/4\pi)\, (d\delta/2\pi). \qquad (4.3\text{-}12)$$

Comparing the foregoing expression with Equation (4.3-4), we obtain

$$\nu(\vec{g}_0, D_0) = w\, g_0 \sin\gamma \int_{\vec{W}} \int_{\Omega} \int_{\delta} f_e(\vec{g}_0, \vec{W})\, f_M(\vec{g}_0, \vec{W}) \times$$

$$d\vec{W}\, (d\Omega/4\pi)\, (d\delta/2\pi), \qquad (4.3\text{-}13)$$

where the integration is taken over all possible values of $\vec{W}$, Ω, and δ.

4.3.3 Integration over the Center-of-Mass Velocity and the Orientation of the Internuclear Axis

To perform the integration over $\vec{W}$, we must know the form of the velocity distribution functions. We are considering only the case in which f_M is Maxwellian. As we show in Appendix B, f_e also is Maxwellian. Hence, f_e and f_M are given by

$$f_e(\vec{v}_0) = C_e \exp(-mv_0^2/2kT_e), \tag{4.3-14a}$$

$$f_M(\vec{V}_0) = C_M \exp(-MV_0^2/2kT_0), \tag{4.3-14b}$$

where C_e and C_M are constants and T_e and T_0 are the electron and molecular temperatures, respectively. In terms of $\vec{g}_0$ and $\vec{W}$, the product $f_e f_M$ becomes

$$f_e\, f_M = C_e\, C_m \exp\left\{ -\frac{1}{2k}\left[\left(\frac{m}{T_e} + \frac{M}{T_0}\right) W^2 + 2\mu\left(\frac{1}{T_e} - \frac{1}{T_0}\right) g_0\, W \cos\Psi\right]\right\} \times \exp\left[-\frac{\mu^2}{2k}\left(\frac{1}{mT_e} + \frac{1}{MT_0}\right) g_0^2\right], \tag{4.3-15}$$

where Ψ is the angle between $\vec{g}_0$ and $\vec{W}$.

We use the coordinate system illustrated in Figure 3-1. The directions of $\vec{W}$ and $\vec{g}_0$ are taken relative to the orientations of $\vec{K}_0$ and the internuclear axis. As we mentioned above, $\vec{K}_0$ and the internuclear axis are randomly oriented

relative to a fixed coordinate system. The integrations over Ω and δ, which we will perform later, will account for all possible collisions. The direction of $\vec{W}$ relative to the coordinate system shown in Figure 3-1 is specified by the polar angles ϕ_W and θ_W as follows:

$$W_x = W \sin \phi_W \cos \theta_W. \tag{4.3-16a}$$

$$W_y = W \sin \phi_W \sin \theta_W. \tag{4.3-16b}$$

$$W_z = W \cos \theta_W. \tag{4.3-16c}$$

The elementary volume in velocity space is

$$d\vec{W} = W^2 \, dW \sin \phi_W \, d\phi_W \, d\theta_W, \tag{4.3-17}$$

and the angle Ψ is given by

$$\cos \Psi = \sin \phi_W \cos \theta_W \sin \phi_{g_0} \cos \theta_{g_0} + \sin \phi_W \sin \theta_W \sin \phi_{g_0} \sin \theta_{g_0} + \cos \phi_W \cos \phi_{g_0}. \tag{4.3-18}$$

The angle γ is given by

$$\gamma = \phi_{g_0}. \tag{4.3-19}$$

The integral I_W over $\vec{W}$ can thus be written

$$I_W = \int_{W=0}^{\infty} \int_{\phi_W=0}^{\pi} \int_{\theta_W=0}^{2\pi} \exp \left\{ - \frac{1}{2k} \left[\left(\frac{m}{T_e} + \frac{M}{T_0} \right) W^2 + 2\mu \left(\frac{1}{T_e} - \frac{1}{T_0} \right) g_0 \, W \cos \Psi \right] \right\} W^2 \, dW \times \sin \phi_W \, d\phi_W \, d\theta_W. \tag{4.3-20}$$

The integrals here can be evaluated in closed form, if we neglect terms that contain the small quantities m/M and T_0/T_e. The result is

$$I_W = \text{(a constant)}. \tag{4.3-21}$$

Hence Equation (4.3-13) becomes

$$\nu(\vec{g}_0, D_0) = C \int_{\Omega} \int_{\delta} g_0 \sin\gamma \exp\left[-\frac{\mu^2}{2k}\left(\frac{1}{mT_e} + \frac{1}{MT_0}\right) g_0^2\right] \times (d\Omega/4\pi)\,(d\delta/2\pi), \tag{4.3-22}$$

where the constant C is given by

$$C = w\, C_e\, C_M\, I_W. \tag{4.3-23}$$

The integrand in Equation (4.3-22) is independent of Ω and δ. Hence the integrations over these angles yield

$$\int_{\Omega=0}^{4\pi} d\Omega/4\pi = 1, \tag{4.3-24a}$$

$$\int_{\delta=0}^{2\pi} d\delta/2\pi = 1. \tag{4.3-24b}$$

By substituting Equations (4.3-24) into Equation (4.3-22), we obtain

$$\nu(\vec{g}_0, D_0) = C\, g_0 \sin\gamma \exp\left[-\frac{\mu^2}{2k}\left(\frac{1}{mT_e} + \frac{1}{mT_0}\right) g_0^2\right]. \tag{4.3-25}$$

With the use of the approximations $\mu \approx m$, $m << M$, and $T_0 << T_e$, the exponential factor in Equation (4.3-25) becomes

$\exp(-mg_0^2/2kT_e)$, so that Equation (4.3-25) becomes

$$\nu(\vec{g}_0, D_0) = C\, g_0 \sin\gamma \exp(-mg_0^2/2kT_e). \qquad (4.3\text{-}26)$$

Substituting this result into Equation (4.3-4), we obtain

$$r_{ex,K_1} = C \sum_{K_0} N_{K_0} \int_{\tau_{K_0,K_1}} F(g_0) \exp(-mg_0^2/2kT_e) \times$$

$$\sin\gamma\, g_0\, d\vec{g}_0\, dD_0. \qquad (4.3\text{-}27)$$

The elementary volume in velocity space is given by

$$d\vec{g}_0 = g_0^2\, dg_0 \sin\phi_{g_0}\, d\phi_{g_0}\, d\theta_{g_0}. \qquad (4.3\text{-}28)$$

By substituting Equations (4.3-19) and (4.3-28) into Equation (4.3-27), we obtain the following expression for the excitation rate in terms of the precollision quantities:

$$r_{ex,K_1} = C \sum_{K_0} N_{K_0} \int_{\tau_{K_0,K_1}} F(g_0) \exp(-mg_0^2/2kT_e) \times$$

$$g_0^3\, dg_0 \sin^2\phi_{g_0}\, d\phi_{g_0}\, d\theta_{g_0}\, dD_0. \qquad (4.3\text{-}29)$$

CHAPTER 5

EVALUATION OF THE PHASE-SPACE INTEGRAL

5.1 Introduction

Although Equation (4.3-29) enables one to compute r_{ex,K_1} in principle, the evaluation of the phase-space integral in Equation (4.3-29) is difficult in practice. In fact, the development of a method for evaluating this integral was a major problem in the present research. The complexity of the integration region τ_{K_0,K_1}, whose geometry is determined by the collision dynamics (Chapter 3), precludes evaluating the integral in closed form. Standard methods of numerical integration are not feasible because the integral is over four variables (g_0, D_0, ϕ_{g_0}, θ_{g_0}) so that a prohibitive amount of computer time is required to obtain any amount of accuracy. Additional difficulties are that τ_{K_0,K_1} is not known explicitly and that K_1 is a discrete-valued, rather than a continuous, function of K_0, g_0, D_0, ϕ_{g_0}, and θ_{g_0}. A Monte-Carlo method, however, proved to be feasible. In the present chapter, we explain the application of this method to the evaluation of the phase-space integral.

5.2 Monte-Carlo Evaluation of the Phase-Space Integral

5.2.1 Description of the Monte-Carlo Method

The Monte-Carlo method (see Brown 1956 for the introductory discussion) has been used by previous workers (Karplus, Porter, and Sharma 1965) to analyze molecular collisions similar to the present one. The Monte-Carlo method simulates the huge number of random collisions occurring in the gas by computing the results of a much smaller number of collisions. These collisions are chosen randomly, except that the collisional parameters are chosen proportionately to how frequently they actually occur in the gas.

5.2.2 Example of the Monte-Carlo Evaluation of an Integral

Consider the quantity I defined by

$$I = \int_a^b f(x)\, dx, \qquad (5.2\text{-}1)$$

where $0 \leq f(x) \leq M$. To evaluate I by the Monte-Carlo Method, we choose a large number of pairs of random numbers X and Y, in the ranges

$$\left.\begin{array}{l} a \leq X \leq b \\ \\ 0 \leq Y \leq M \end{array}\right\} . \qquad (5.2\text{-}2)$$

For each pair of values, we perform the following test: is

$Y \leq f(X)$? This is illustrated in Figure 5-1, which shows two random points - (X_I, Y_I) and (X_{II}, Y_{II}). For point I, the answer is no; for point II, the answer is yes. If n is the number of pairs for which the answer is yes and N is the total number of pairs tested, then I is given by

$$I = (n/N)\ M\ (b-a). \qquad (5.2\text{-}3)$$

The answer becomes exact in the limit as $N \to \infty$, that is,

$$I = M\ (b-a) \lim_{N \to \infty} (n/N). \qquad (5.2\text{-}4)$$

For multiple integrals, the Monte-Carlo method often is superior to ordinary numerical integration (quadrature). The Monte-Carlo method, in fact, may be feasible for integrals for which quadrature is hopelessly impractical. By this we mean that the number of points required to obtain a given error (standard deviation) using the Monte-Carlo method is much less than the number of points required to obtain the same error using quadrature. This results because the Monte-Carlo points are chosen randomly over the integration volume, whereas the quadrature points are chosen in a pre-determined way (usually equally spaced). A given number of randomly chosen points can "fill up" the integration volume in a more representative fashion than the same number of points chosen in a pre-determined manner (Brown 1956).

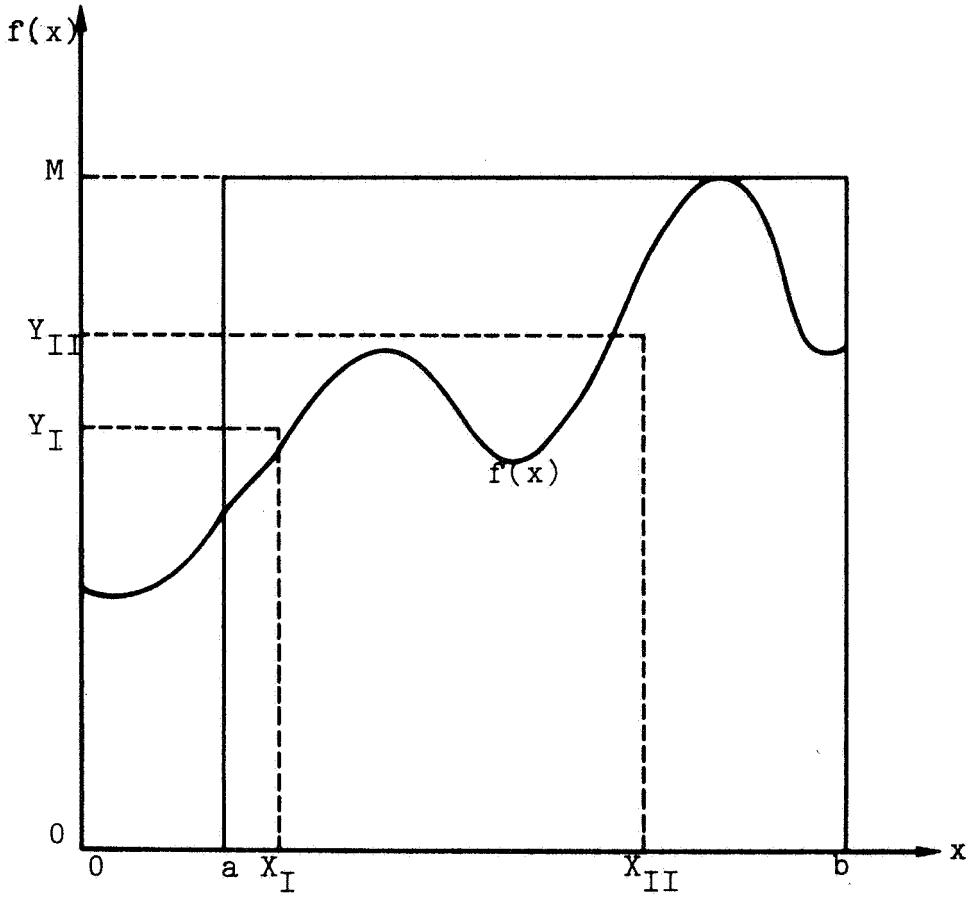

Figure 5-1: Illustration of the Monte-Carlo Evaluation of an Integral

5.2.3 Application of the Method to the Phase-Space Integral

Because of the special nature of the phase-space integral, we use a modified version of the method described in the preceding section. The phase-space integral I_{K_0,K_1} with which we deal is given by

$$I_{K_0,K_1} = \int_{\tau_{K_0,K_1}} F(g_0) \exp(-mg_0^2/2kT_e)\, g_0^3\, dg_0\, \sin^2\phi_{g_0} \times d\phi_{g_0}\, d\theta_{g_0}\, dD_0. \qquad (5.2\text{-}5)$$

From Equation (4.3-29), we see that this integral is proportional to the rate of excitation collisions whose collision parameters lie in the phase-space volume τ_{K_0,K_1}. The situation is shown schematically in Figure 5-2, which shows the g_0-D_0 plane. Hence, the sketch shows a "slice" of phase space with K_0, ϕ_{g_0}, and θ_{g_0} fixed. The rectangle given by

$$\left.\begin{aligned} g_{0_{min}} \le g_0 \le g_{0_{max}} \\ -D_{0_{max}} \le D_0 \le +D_{0_{max}} \end{aligned}\right\} \qquad (5.2\text{-}6)$$

corresponds to the ranges of g_0 and D_0 over which the collisions occur. Each "X" denotes a collision; only a few of the collisions are shown. As shown, the density of X's is independent of D_0 but is a function of g_0. A possible configuration of the τ volumes is shown. In this

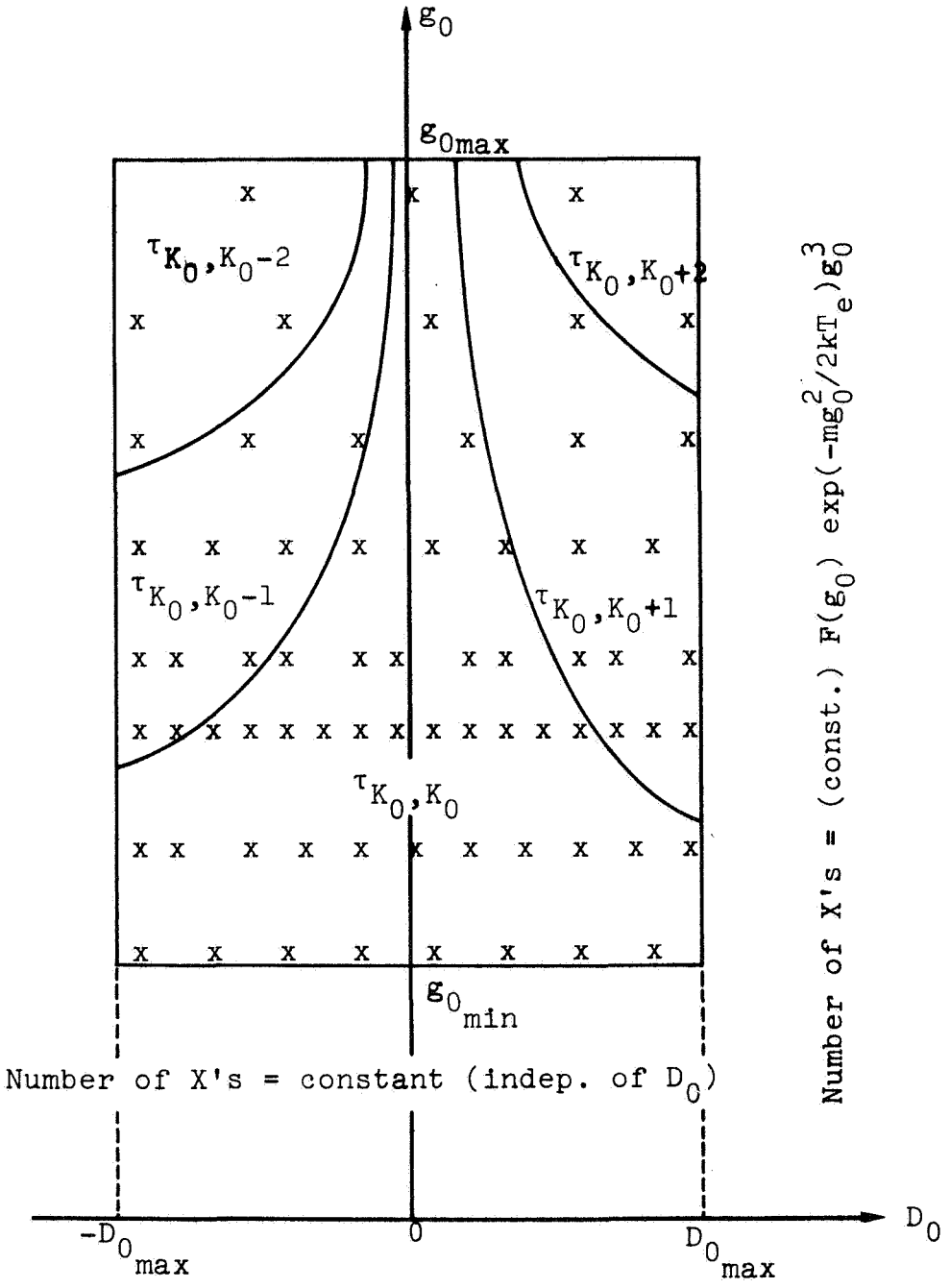

Figure 5-2: Sketch of the g_0-D_0 Plane in Phase Space

hypothetical case, the only possible values of K_1 are

$$K_1 = K_0,\ K_0 \pm 1,\ K_0 \pm 2. \qquad (5.2\text{-}7)$$

The value of any integral I_{K_0,K_1} is proportional to the number of X's within the corresponding region τ_{K_0,K_1}. Figure 5-2 shows qualitatively where the volumes τ are expected to lie in the g_0-D_0 plane. Small values of g_0 or D_0 correspond to $K_1 = K_0$, large positive values of D_0 correspond to $K_1 > K_0$, and large negative values of D_0 correspond to $K_1 < K_0$.

We define the quantity $G(g_0)$ by the relation

$$d[G(g_0)] \equiv F(g_0) \exp(-mg_0^2/2kT_e)\, g_0^3\, dg_0. \qquad (5.2\text{-}8)$$

We also define $P(\phi_{g_0})$ by

$$d[P(\phi_{g_0})] \equiv \sin^2\phi_{g_0}\, d\phi_{g_0} = d[(1/2)\phi_{g_0} - (1/4)\sin 2\phi_{g_0}], \qquad (5.2\text{-}9a)$$

i.e.,
$$P(\phi_{g_0}) = (1/2)\,\phi_{g_0} - (1/4)\sin 2\phi_{g_0}. \qquad (5.2\text{-}9b)$$

By substituting Equations (5.2-8) and (5.2-9) into Equation (5.2-5), we obtain

$$I_{K_0,K_1} = \int_{\tau_{K_0,K_1}} d[G(g_0)]\, dD_0\, d[P(\phi_{g_0})]\, d\theta_{g_0}. \qquad (5.2\text{-}10)$$

Hence, I_{K_0,K_1} is the volume τ_{K_0,K_1} in the phase space in

which the coordinates are $G(g_0)$, D_0, $P(\phi_{g_0})$, and θ_{g_0}. We illustrate this schematically in Figure 5-3, which is the same as Figure 5-2 except that it shows the $[G(g_0)]$-D_0 plane with K_0, $P(\phi_{g_0})$, and θ_{g_0} fixed. This figure shows schematically the situation that was found in most of the numerical computations, that is,

$$I_{K_0,K_0-2} \cong I_{K_0,K_0+2} << I_{K_0,K_0-1} \cong I_{K_0,K_0+1} << I_{K_0,K_0} \,. \tag{5.2-11}$$

Having put I_{K_0,K_1} in the form of Equation (5.2-10), we can apply the Monte-Carlo method in a straightforward manner. For a given value of K_0, we do the following:

(i) Choose random values of $G(g_0)$, D_0, $P(\phi_{g_0})$, and θ_{g_0} distributed uniformly within their respective ranges.

(ii) Compute the value of K_1 that corresponds to each of these sets of values of the collision parameters.

(iii) Repeat steps (i) and (ii) a large number of times [call this number $s(K_0)$], keeping count of the number of times each value of K_1 occurs [call these numbers $q(K_0,K_1)$]. Then, I_{K_0,K_1} is given approximately by

$$I_{K_0,K_1} \cong (\text{const.})\; q(K_0,K_1) \;/\; s(K_0). \tag{5.2-12}$$

Substitution of Equations (5.2-5) and (5.2-12) into Equation (4.3-29) leads to

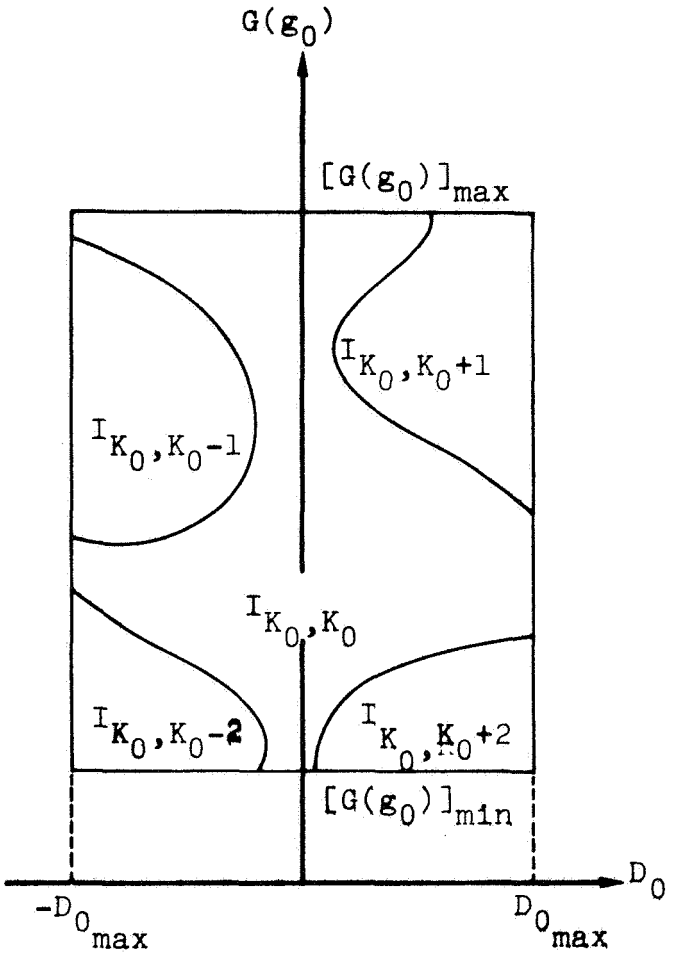

Figure 5-3: Sketch of the $[G(g_0)]$-D_0 Plane in Phase Space

$$r_{ex,K_1} = (\text{const.}) \sum_{K_0} N_{K_0}\, q(K_0,K_1)/\, s(K_0). \qquad (5.2\text{-}13)$$

By putting Equation (5.2-13) into Equation (4.2-4), we then obtain finally

$$N_{K_1} = (\text{const.}) \sum_{K_0} N_{K_0}\, q(K_0,K_1) \,/\, s(K_0). \qquad (5.2\text{-}14)$$

The computations of N_{K_1} as a function of K_1 were performed by means of this equation.

In order to perform the computations of N_{K_1}, we must know the populations N_{K_0} of the $X^1\Sigma_g^+$ rotational levels and the functions of the relative speed contained in $G(g_0)$. In Sections 5.3 and 5.4, we explain how we obtained these values.

5.3 Populations of the $X^1\Sigma_g^+$ Rotational Levels

We consider only the case in which the gas is in equilibrium before the spark is struck, so that it has a rotational temperature T_0 equal to the translational temperature. In this case, the number N_{K_0} of molecules per unit volume in the ground vibrational level of $X^1\Sigma_g^+$ is given by the Boltzmann distribution

$$N_{K_0} = (\text{const.})\ \sigma(K_0)(2K_0+1)\ \exp[(-\hbar^2/2I_0kT_0)\ K_0\ (K_0+1)], \qquad (5.3\text{-}1)$$

where the constant is independent of K_0 and where I_0 is the moment of inertia of the $X^1\Sigma_g^+$ molecule. The subscript is

appended because the moment of inertia is smaller in the $X^1\Sigma_g^+$ state than in the $C^3\Pi_u$ state, the values being

$$I_0 = 1.382 \times 10^{-39} \text{ gm-cm}^2 \quad . \quad (X^1\Sigma_g^+)$$
$$I_1 = 1.523 \times 10^{-39} \text{ gm-cm}^2 \quad . \quad (C^3\Pi_u) \qquad (5.3\text{-}2)$$

The factor σ is a population-alternation factor that appears in the statistical weight of a gas consisting of homonuclear molecules; the alternation is caused by nuclear spin (Herzberg 1950). For $N_2(X^1\Sigma_g^+)$, it is given by

$$\sigma(K_0) = \begin{cases} 6, & K_0 \text{ even} \\ 3, & K_0 \text{ odd} \end{cases} . \qquad (5.3\text{-}3)$$

5.4 Functions of the Relative Speed

5.4.1 Excitation Function

We obtain the excitation function $F(g_0)$ that is contained in $G(g_0)$ from experimental data, the references for which are listed in Section 3.2. We use the data of Kishko and Kuchinka (1959) as plotted by Bauer and Bartky (1965), because these data give the correct result at threshold, viz., $F(g_0) = 0$. This function is plotted in the usual form (F versus $(1/2)\,\mu g_0^2$) in Figure 5-4. We have made the following least squares fit to the data:

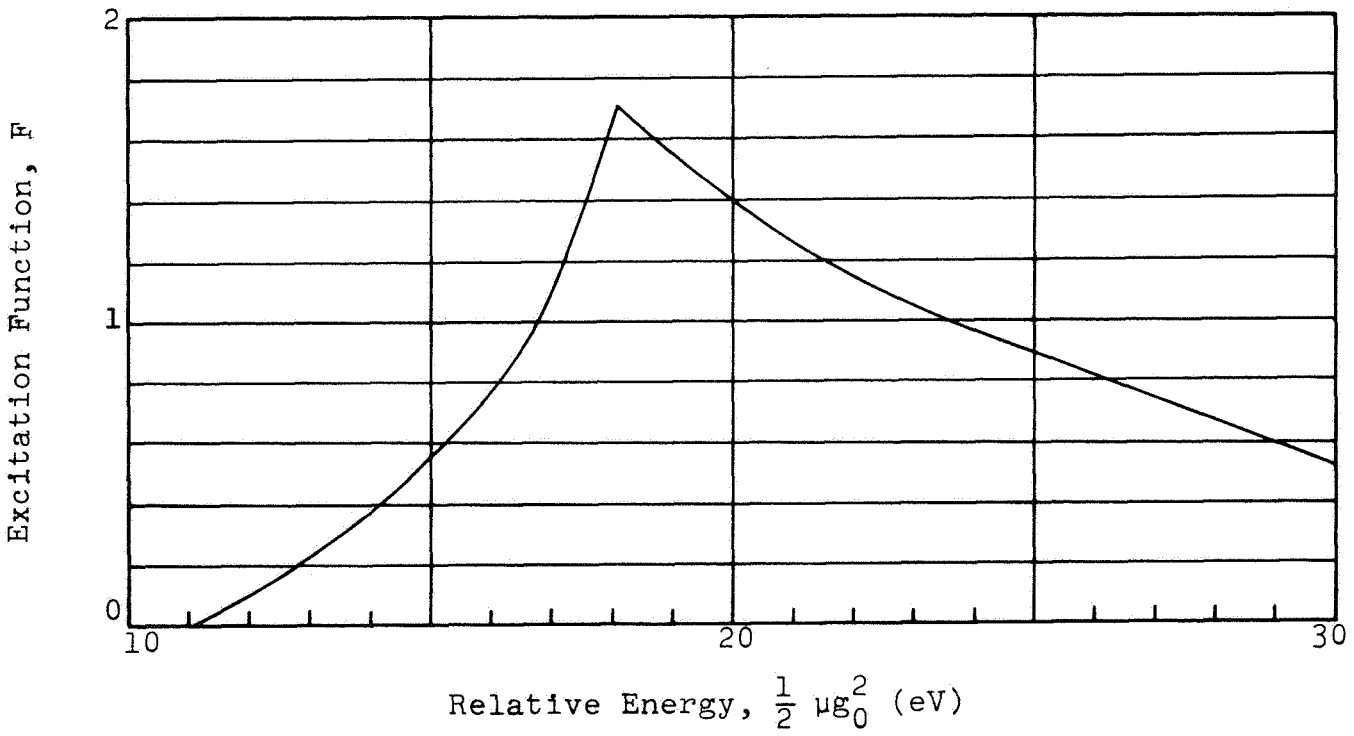

Figure 5-4: Excitation Function of the $C^3\Pi_u \leftarrow X^1\Sigma_g^+$ Transition

$$F(g_0) = 618.8 - 1159\ V + 813.0\ V^2 - 253.4\ V^3 + 29.65\ V^4\ , \qquad (5.4\text{-}1a)$$

for $1.97\ \text{cm/sec} \leq V \leq 2.52\ \text{cm/sec}$,

$$F(g_0) = 17.28 - 9.891\ V + 1.471\ V^2, \qquad (5.4\text{-}1b)$$

for $2.52\ \text{cm/sec} \leq V \leq 3.02\ \text{cm/sec}$,

where

$$V = g_0 \times 10^{-8}\ \text{cm/sec}. \qquad (5.4\text{-}2)$$

The maximum speed for which the least-squares fit is valid ($g_0 = 3.02 \times 10^8$ cm/sec) corresponds to an electron energy of 25 eV.

5.4.2 The Integral Over the Relative Speed

Let $g_{0_{min}}$ be the minimum value of g_0 used in the calculations ($g_{0_{min}} = 1.97 \times 10^8$ cm/sec). Since $F(g_{0_{min}}) = 0$, we have

$$G(g_{0_{min}}) = 0. \qquad (5.4\text{-}3)$$

Then, from Equation (5.2-8), we have

$$G(g_0) = \int_{g_{0_{min}}}^{g_0} F(x)\ \exp(-mx^2/2kT_e)\ x^3\ dx. \qquad (5.4\text{-}4)$$

In view of Equations (5.4-1), a closed form expression for $G(g_0)$ can be obtained by evaluating the integrals

$$I_n = \int_{\ell}^{u} x^{n+2}\ e^{-ax^2}\ dx. \quad (n = 0, 1, \ldots, 5) \qquad (5.4\text{-}5)$$

The results of evaluating this integral are given in

Appendix C. (Although I_0 does not appear explicitly in $G(g_0)$, I_0 must be evaluated because it appears in the formulas for I_2 and I_4.)

It was necessary for this study to know the inverse relation $g_0(G)$, because we chose random values of G rather than g_0 itself. We obtained the inverse relation by making a least-squares polynomial fit to the formula for $G(g_0)$. The result is

$$g_0 = (-2.00 \times 10^{10}\, G^6 + 1.88 \times 10^9\, G^5 - 6.79 \times 10^7\, G^4 + 1.20 \times 10^6\, G^3 - 1.10 \times 10^4\, G^2 + 68.5\, G + 2.00) \times 10^8 \text{ cm/sec}, \quad \text{for } 0 \le G < 2.83 \times 10^{-2} \text{ (cm/sec)}^4. \tag{5.4-6a}$$

$$g_0 = 2.52 \times 10^8 \text{ cm/sec}, \quad \text{for } G = 2.83 \times 10^{-2} \text{(cm/sec)}^4. \tag{5.4-6b}$$

$$g_0 = (6.36 \times 10^9\, G^5 - 1.19 \times 10^9\, G^4 + 8.81 \times 10^7\, G^3 - 3.26 \times 10^6\, G^2 + 5.98 \times 10^4\, G + 4.35 \times 10^2) \times 10^8 \text{ cm/sec}, \quad \text{for } 2.83 \times 10^{-2} < G \le 4.53 \times 10^{-2} \text{ (cm/sec)}^4. \tag{5.4-6c}$$

5.5 Numerical Procedure

5.5.1 Steps in the Procedure

We compute the variation of N_{K_1} as a function of K_1 by the following steps (here we discuss the specific details of the procedure mentioned at the end of Section 5.2.3):

(i) For a fixed value of K_0, we compute 200

pseudorandom sets of collision parameters each chosen as follows. Four pseudorandom numbers - R_I, R_{II}, R_{III}, R_{IV} - are computed by a method described in Appendix D. We then set

$$P(\phi_{g_0}) = (\pi/4)\, R_I, \tag{5.5-1}$$

$$\theta_{g_0} = \pi R_{II}, \tag{5.5-2}$$

$$D_0 = r_0\, (2\, R_{III} - 1), \tag{5.5-3}$$

$$G = 4.53 \times 10^{-2}\, R_{IV}.\ (\text{cm/sec})^4 \tag{5.5-4}$$

This gives uniformly distributed values of $P(\phi_{g_0})$ between 0 and $\pi/4$, θ_{g_0} between 0 and π, D_0 between $-r_0$ and r_0, and G between 0 and $4.53 \times 10^{-2}(\text{cm/sec})^4$. The values of ϕ_{g_0} are distributed between 0 and $\pi/2$, and the values of $(1/2\ g_0^2)$ are distributed between 11 eV and 25 eV. In Section 5.5.2, the sources of the ranges of the collision parameters are explained. We then solve the nonlinear algebraic equation

$$P(\phi_{g_0}) - (\pi/4)R_I = (1/2)\phi_{g_0} - (1/4)\sin 2\phi_{g_0}$$

$$- (\pi/4)R_I = 0 \tag{5.5-5}$$

for the root ϕ_{g_0} by the Newton-Raphson iteration method (Ralston 1965), and we calculate $g_0(G)$ by means of Equations (5.4-6).

(ii) For each set of collision variables, we compute the possible integer values of K_1 by means of the quantized classical model described in Chapter 3. In about 1/3 of the collisions computed, more than one (but never more than

three) integer values of K_1 are possible. For these collisions we arbitrarily assume that

All possible integer values of K_1 are equally probable (5.5-6)

and therefore occur equally frequently in the collisions. We later made a comparison to test the effect of this assumption and found that it does not affect the results significantly (see Section 7.4.2). In about three percent of the collisions, no integer value of K_1 is possible; these collisions are excluded from the computation of N_{K_1}.

(iii) For each value of K_0, the quantity I_{K_0,K_1} is computed from Equation (5.2-12), where

$$s(K_0) = 200 - p(K_0), \tag{5.5-7}$$

in which $p(K_0)$ is the number of collisions in which no integer value of K_1 is possible.

(iv) Steps (i) through (iii) are done for

$$K_0 = 0, 1, 2, \ldots, 25. \tag{5.5-8}$$

(v) N_{K_1} is computed from Equation (5.2-14).

5.5.2 Ranges of the Collision Parameters

We obtain the ranges of the angles ϕ_{g_0} and θ_{g_0} as follows by examining Figure 3-1:

$$0 \leq \phi_{g_0} \leq \pi/2, \tag{5.5-9}$$

$$0 \leq \theta_{g_0} \leq \pi. \tag{5.5-10}$$

When both positive and negative values of the impact dis-

tance D_0 are used, all possible angles of approach and impact point on the molecule are accounted for.

The range of g_0 is

$$1.97 \times 10^8 \text{ cm/sec} \leq g_0 \leq 3.02 \times 10^8 \text{ cm/sec}, \quad (5.5\text{-}11a)$$

or equivalently,

$$11 \text{ eV} \leq (1/2)\mu g_0^2 \leq 25 \text{ eV}. \quad (5.5\text{-}11b)$$

The lower limit of 11 eV is the excitation energy of the $C^3\Pi_u \leftarrow X^1\Sigma_g^+$ transition and is thus the minimum possible value of the electron energy. The upper limit should strictly be infinity, but a finite value must be used in the computations. We choose 25 eV because the product $F(g_0) \times \exp(-mg_0^2/2kT_e)\, g_0^3$ goes to zero as g_0 goes to infinity and is negligible beyond 25 eV. This product is zero at 11 eV because $F(g_0)$ is zero there, rises to a maximum at about 18 eV, then decreases monotonically as g_0 increases further. Hence the majority of the collisions are with electrons of energy near 18 eV, and this shows up in the Monte-Carlo computations (see Table III).

The range of D_0 cannot be determined from physical principles, so that we must make some assumptions. We choose to make the following two:

(1) $$|D_0|_{max} = r_0, \quad (5.5\text{-}12)$$

i.e., the maximum possible impact distance is the molecular radius;

(2) Any value of D_0 within the range

$$- |D_0|_{max} \leq D_0 \leq |D_0|_{max} \qquad (5.5\text{-}13)$$

is equally probable.

Assumption (1) is plausible because the collision involves electron exchange (see Section 3.4), with the result that the incoming electron is "captured" by the molecule. In the context of classical mechanics, this implies that the incoming electron must come within the molecular diameter for the collision to occur. In the same way, assumption (2) is plausible, that is, we expect that impact parameters are randomly distributed in the collisions. The two assumptions have not been checked experimentally, however. We are more confident of the plausibility of assumption (2) than of assumption (1). As explained in Section 7.4.1, however, we found that a modification of assumption (1) does not alter the results very much.

5.5.3 Number of Collisions Computed

For each value of K_0, we compute K_1 for 200 pseudorandom collisions, as mentioned in Section 5.2.1. We do this for 26 values of K_0 (0, 1, 2, ..., 25). Since each collision requires 4 pseudorandom numbers, the entire computation of N_{K_1} requires (200)(4)(26) = 20,800 pseudorandom numbers. We later repeated the computations using a second

set of 20,800 pseudorandom numbers. Hence we used only the first 41,600 numbers of the sequence generated by Equation (D-1) in Appendix D. Since the period of this sequence is 135,000,000, we feel confident that our collisions satisfy the mathematical criteria of randomness.

5.6 Results of the Computations

Using the procedure and assumptions described in Section 5.5, we have computed the variation of N_{K_1} with K_1 for the case tested by Kyser. The important parameters are

$$T_0 = 295^{\circ}K \qquad (5.6\text{-}1)$$

and

$$\frac{3}{2} k T_e = 4.80 \text{ eV}. \qquad (5.6\text{-}2)$$

The value of 4.80 eV comes from Kyser's (1966) semi-empirical analysis of the spark and corresponds to the conditions that he tested. The value of T_0 determines the distribution of N_{K_0} through Equation (5.3-1), and the value of T_e the distribution of electron speeds v_0 through Equation (4.3-14a).

The computed values of I_{K_0,K_1} are presented (rounded off) in Table II for $K_0 = 4, 5, 6, \ldots, 21$. We note the following features:

(1) The great majority (between 63 and 76 percent) of the collisions result in no change in rotational quantum number, i.e., $K_1 = K_0$.

Table II: Computed Values of $p(K_0)$ and I_{K_0,K_1}

For each value of K_0, the two rows of numbers refer to the first and second set of 100 pseudorandom collisions, respectively.

K_0	$p(K_0)$	I_{K_0,K_1} for the value of K_1 given below				
		$K_1=K_0-2$	$K_1=K_0-1$	$K_1=K_0$	$K_1=K_0+1$	$K_1=K_0+2$
4	5	1	12	67	15	0
	3	0	14	67	16	0
5	8	0	9	67	15	0
	4	1	13	65	17	0
6	4	0	11	71	14	0
	2	2	16	72	9	0
7	6	1	16	66	12	0
	5	0	11	66	18	0
8	3	1	15	69	12	0
	4	0	14	63	18	0
9	2	0	12	73	12	0
	1	1	11	73	14	0
10	1	2	13	69	15	1
	3	1	22	64	10	0
11	3	0	16	70	11	0
	3	0	12	74	10	0
12	1	1	12	76	10	0
	2	0	16	68	14	0

Table II (continued)

13	7	0	8	70	14	0
	4	0	9	69	18	0
14	2	1	13	73	11	0
	1	1	12	66	20	0
15	4	0	14	71	12	0
	2	1	15	70	13	0
16	2	1	16	73	8	0
	0	1	13	68	19	0
17	6	1	12	70	12	0
	1	0	16	72	10	0
18	5	0	11	73	11	0
	4	0	12	72	12	0
19	4	0	14	73	9	0
	1	0	15	72	12	0
20	4	0	16	72	8	0
	2	0	18	68	12	0
21	5	0	16	65	14	0
	3	0	15	70	11	0

(2) Very few of the collisions result in $|K_1-K_0| \geq 2$. That is, almost all the remaining 24 to 37 percent of the collisions result in $K_1 = K_0-1$ or $K_1 = K_0+1$.

(3) The number of collisions in which $K_1 = K_0-1$ (between 8 and 22 percent) is roughly equal to the number of collisions in which $K_1 = K_0+1$ (between 8 and 20 percent). The results thus show no consistent trend of favoring either excitation or de-excitation.

(4) The foregoing conclusions apply to each value of K_0. The results show no difference between small and large values of K_0.

The foregoing results are obtained because the electron can transfer very little angular momentum to the molecule in a given collision, even though the electron's energy is much larger than the molecular energy of rotation. As we see from the example given in Table I, the electron can transfer only 2 rotational quanta to the molecule even if the collision variables have the values that yield the maximum angular-momentum transfer, namely,

$$\left.\begin{aligned} g_0 &= 3.0 \times 10^8 \text{ cm/sec} \\ D_0 &= \pm r_0 = \pm 0.547 \times 10^{-8} \text{ cm} \\ \phi_{g_0} &= \theta_{g_0} = \pi/2 \end{aligned}\right\}. \quad (5.6\text{-}3)$$

The Monte-Carlo computations show that most of the collisions have collision variables that would yield less than 1 quantum of angular-momentum transfer, with the result that no angular momentum is transferred. This is shown in Table III, which lists the rounded values of $(1/2)\mu g_0^2$, D_0, ϕ_{g_0}, θ_{g_0}, and the resulting possible integer values of K_1 for the first 100 pseudorandom collisions with $K_0 = 10$. For 52 percent of these collisions, the only possible integer value of K_1 is also 10.

The calculated populations of the $C^3\Pi_u$ rotational levels are plotted in log-slope form (i.e., $N_{K_1}/(2K_1+1)$ versus $K_1(K_1+1)$ on semilog paper) in Figure 5-5. We note the following features:

(1) There are parallel curves for odd and even values of K_1, with the ordinates of the even-K_1 curve approximately 1.4 times larger than those of the odd-K_1 curve.

(2) These curves are approximately straight lines.

(3) The $C^3\Pi_u$ molecules thus have approximately a Boltzmann distribution of rotational states, so that a rotational temperature T_1 can be defined for these molecules.

By the least-squares technique, the best-fit straight lines were found for the odd-K_1 data and for the even-K_1 data. The corresponding rotational temperatures T_1 were found from the slope of these lines by the standard log-slope method

Table III: Values of K_1 for 100 Pseudorandom Collisions

(K_0 = 10)

$\frac{1}{2}\mu g_0^2$ (eV)	$D_0 \times 10^9$ (cm)	ϕ_{g_0} (°)	θ_{g_0} (°)	K_1
20	-0.02	67	179	10
17	5.3	42	131	10,11
23	4.1	81	96	11
19	4.9	53	14	10,11
17	1.7	61	37	10
17	0.8	67	89	10
19	1.1	65	25	10
16	-0.02	80	145	10
21	-3.5	33	156	9,10
16	-2.5	81	97	9,10
16	-0.3	58	76	10
16	-3.6	56	176	10
18	4.4	29	65	10,11
16	-5.4	68	41	9,10
14	-4.3	72	154	10
19	4.4	55	50	10,11
23	2.2	74	132	10,11
13	-3.4	69	14	10
14	-4.1	47	101	9,10
14	-3.9	66	102	9
16	-0.4	89.9	123	10

Table III (2nd of 5 pages)

18	3.5	89	138	10,11
17	-3.2	83	56	9,10
20	4.1	83	150	10,11
21	-4.1	88	102	8,9,10
17	-1.3	44	23	10
20	-5.0	37	99	9,10
14	1.4	73	46	10
19	1.8	44	72	10,11
17	4.6	82	27	10,11
13	-1.5	51	64	10
20	-0.7	64	24	10
21	-4.9	37	151	9,10
14	5.4	84	176	10
13	4.7	60	87	11
15	4.2	42	172	10
15	-1.8	89	40	10
12	2.1	69	164	10
15	0.4	58	60	10
13	-4.5	81	61	9
19	0.6	81	94	10
15	1.7	60	74	10
16	5.4	82	174	10
16	2.1	84	13	10
22	3.4	59	69	10,11

Table III (3rd of 5 pages)

16	-5.0	45	16	10
19	-3.6	49	17	10
17	4.1	89.6	19	10
18	-3.1	51	17	10
15	0.3	89	128	10
17	4.8	79	17	10,11
17	-1.9	43	95	10
15	4.7	80	108	11
16	-1.7	44	39	10
15	-3.0	61	177	10
17	-2.3	72	107	9,10
16	-4.1	35	93	9,10
16	-2.7	59	121	9,10
12	5.2	88	82	11
16	0.5	85	129	10
15	-5.3	37	18	10
16	0.2	67	58	10
20	-3.6	88	153	9,10
14	-1.4	81	84	10
14	3.9	67	49	No Integer Possible
23	5.1	81	102	11,12
20	3.4	77	29	10,11
16	1.3	63	101	10

Table III (4th of 5 pages)

16	4.5	80	109	11
14	4.9	77	172	10
17	4.9	61	74	10
20	1.5	43	159	10
21	-0.1	44	59	10
15	-1.9	22	34	10
21	1.7	84	144	10,11
23	-1.9	73	84	9,10
19	4.8	78	60	11
13	0.2	79	25	10
19	-5.2	82	73	8,9
17	-4.3	81	91	9
19	1.3	52	29	10
19	-0.4	51	148	10
17	-3.2	76	85	9,10
17	4.7	85	62	11
18	4.7	60	2	10
21	1.5	39	74	10,11
20	-1.6	78	52	9,10
17	-2.3	58	88	9,10
15	-2.1	65	133	10
17	-5.1	50	44	9,10
23	1.9	89.8	140	10,11

Table III (5th of 5 pages)

17	-3.3	17	109	10
15	-3.1	76	155	10
23	-3.4	81	146	9,10
16	-1.2	50	97	10
20	-3.1	86	90	9,10
25	-3.8	88	97	8,9,10
13	-3.6	48	135	10
13	3.0	33	146	10
15	-1.0	60	28	10

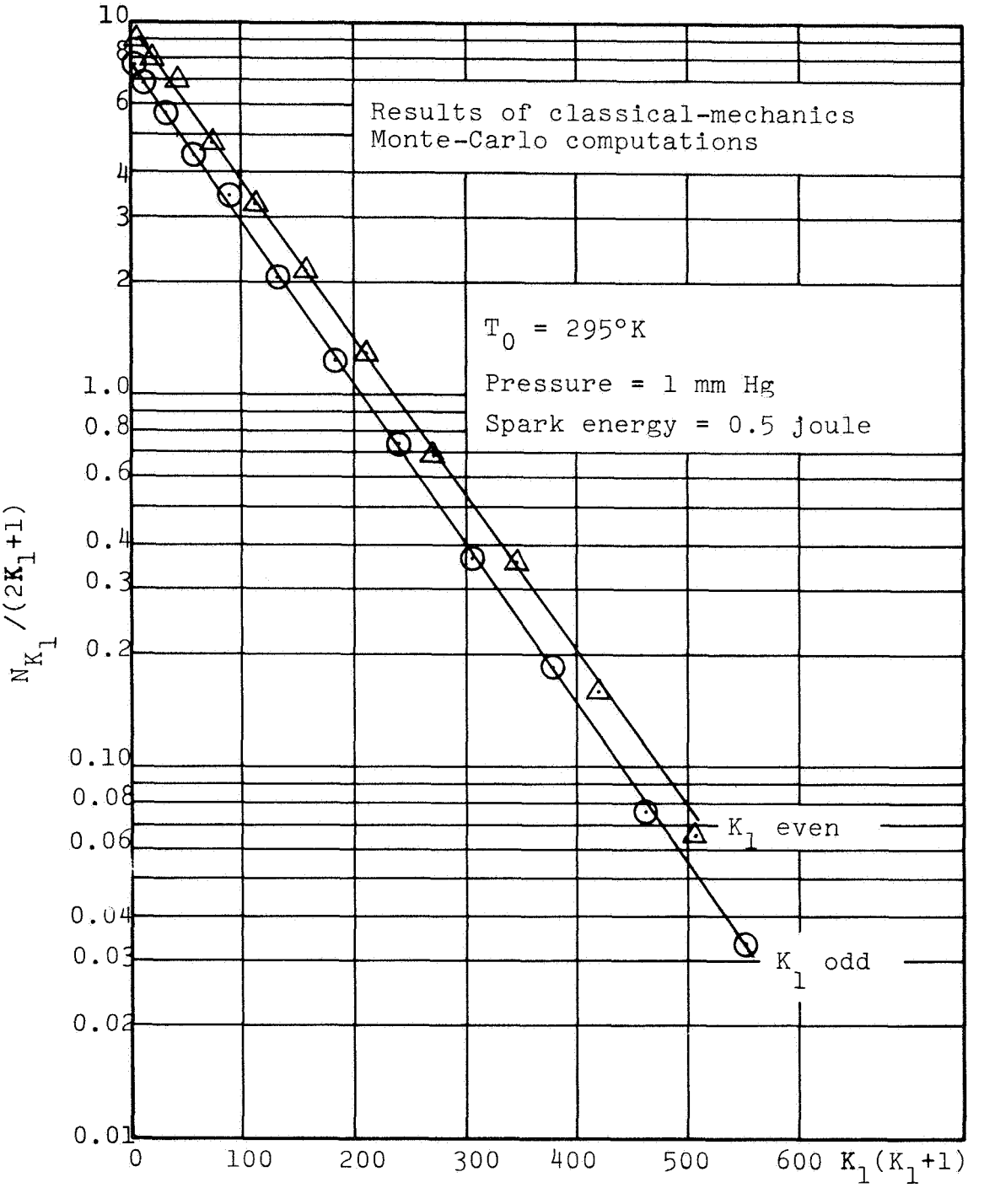

Figure 5-5: Computed Populations of the $C^3\Pi_u$ Rotational Levels

described in Section 1.3. The results are as follows:

$$\left.\begin{aligned} T_1 &= 268^{\circ}K, \text{ for even } K_1 \\ T_1 &= 267^{\circ}K, \text{ for odd } K_1 \end{aligned}\right\}. \qquad (5.6\text{-}4)$$

Our analysis thus predicts the surprising result that

$$T_1 < T_0. \qquad (5.6\text{-}5)$$

Kyser (1966) used a modification of the standard log-slope method that we have used in this chapter. To compare our predictions with Kyser's measurements, we must compute the quantity that he measured in the laboratory. We shall do this in Chapter 6.

5.7 Physical Explanation for the Temperature Decrease.

The predicted decrease in rotational temperature results from the fact that most of the electron-molecule collisions that cause electronic excitation do not change the rotational quantum number of the molecules very much. (There is no evidence that this effect is typical of exchange collisions.) Herzberg (1950), page 207, explains the situation succinctly as follows:

"If there were strictly no change of angular momentum upon excitation of a molecule by electron collisions and if no redistribution through collisions occurs in the upper state one would expect the rotational distribution to be determined by the B value of the ground state (from which the excitation takes place) rather than that of the initial

state of the emission. In other words, if B'_v is used ... the temperature obtained would be too small by a factor B'_v/B''_v."*

For the second positive band system of N_2, this factor is 0.907. We note that

$$0.907\ T_0 = (0.907)(295^\circ K) = 268^\circ K, \qquad (5.7\text{-}1)$$

which is within $1^\circ K$ of our predicted values of T_1 [Equation (5.6-4)].

The only effect of the collisions is to reduce the amount of population alternation. The $X^1\Sigma_g^+$ rotational levels alternate in the ration 2:1, whereas the $C^3\Pi_u$ rotational levels alternate in the ratio 1.4:1.

As Herzberg (1950) points out, Ginsburg and Dieke (1941) observed a decrease in rotational temperature for H_2 spectra excited in an electrical discharge. At low pressures, they found the apparent rotational temperature deduced using the log-slope method to be appreciably less than room temperature. At higher pressures and current densities, the apparent rotational temperature became higher than room temperature.

---

*In terms of the present notation, the rotational constant is given by $B'_v = h/8\pi^2 cI_1$, $B''_v = h/8\pi^2 cI_0$, where c is the speed of light.

5.8 Adequacy of the Number of Collisions Computed

One might question how adequately we have simulated the tremendous number of collisions occuring in the spark by using 200 collisions for each of 26 values of K_0. We have made one check on this by splitting each set of 200 collisions into 2 sets of 100 collisions each. The result is shown in Table II. We see that the 2 sets of values of I_{K_0,K_1} agree with each other very well. For $K_1 = K_0$, the maximum difference is 8 percent (which occurs for $K_0 = 12$). For $K_1 = K_0-1$, it is 11 percent (for $K_0 = 10$). For $K_1 = K_0+1$, it is 11 percent (for $K_0 = 16$).

To make a more conclusive check, we repeated the entire computation of N_{K_1} versus K_1 using the second set of 20,800 pseudorandom numbers generated by Equation (D-1). Proceeding as described in Section 5-6, we computed the following values of T_1:

$$\left.\begin{aligned} T_1 &= 267^{\circ}K, \text{ for even } K_1 \\ T_1 &= 272^{\circ}K, \text{ for odd } K_1 \end{aligned}\right\}. \qquad (5.8\text{-}1)$$

These temperatures agree closely with those obtained using the first set of pseudorandom numbers (Equation 5.6-4). We conclude that we have used a sufficiently large number of collisions.

CHAPTER 6

ROTATIONAL TEMPERATURE AS A FUNCTION OF MEASURED INTENSITY RATIO

6.1 Kyser's Derivation

In the usual log-slope method described in Section 1.3, one measures the intensity I of the individual rotational lines within a vibrational band. If population of the rotational levels of the emitting molecules follows a Boltzmann distribution, then the function $\ln(I_{K_B}/I_{K_A})$ versus $1/T_1$ is a straight line, where K_B and K_A are any values of rotational quantum number.

In Kyser's (1966) experiments, however, the close line spacing made it impossible to measure the intensity of the individual lines. Kyser's spectrometer responded to the input from a wavelength interval significantly larger than the interval between lines, with the result that his intensity readings "at a given wavelength" included contributions from several lines. To account for this, he arbitrarily assumed that the rotational levels of the emitting molecules are distributed <u>continuously</u> as a function of K_1 according to the Boltzmann formula

$$N_{K_1} = (\text{const.})(2K_1+1)\exp[-(\hbar^2/2I_1kT_1)K_1(K_1+1)], \quad (6.1\text{-}1)$$

where K_1 is a continuous variable. Kyser then obtained his

predicted intensities at a given wavelength by integrating the product of the "continuum" intensity and the relative instrument response over the instrument profile. He found that the ratio of two of these integrated intensities centered about given wavelengths is still a unique function of T_1 and used this relationship to deduce T_1 from his measured intensity ratios.

6.2 Modification of Kyser's Derivation

6.2.1 Reason for Modifying Kyser's Derivation

Kyser's assumption that the $C^3\Pi_u$ rotational levels are distributed continuously as a function of K_1 ignores the possibility that population alternation may occur in the $C^3\Pi_u$ state. Since the populations of the $X^1\Sigma_g^+$ rotational levels alternate in the ratio

$$\sigma(K_0 \text{ even})/\sigma(K_0 \text{ odd}) = 6/3 = 2 \qquad (6.2\text{-}1)$$

(see equation (5.3-3)), the populations of the $C^3\Pi_u$ rotational levels also may alternate. As discussed in Section 5.6, the present analysis predicts that

$$\sigma(K_1 \text{ even})/\sigma(K_1 \text{ odd}) = 1.4. \qquad (6.2\text{-}2)$$

We have modified Kyser's derivation of the equations for measured intensity ratio as a function of rotational temperature to take account of the discreteness of the rotational

lines and of possible population alternation in the $C^3\Pi_u$ state. This derivation is presented below.

6.2.2 Notation

The appropriate formulas are given in Herzberg (1950). We will use Herzberg's notation throughout the rest of this section. A schematic energy-level diagram is given in Figure 6-1. The vibrational quantum number of the upper state is denoted by v', that of the lower state by v". The corresponding rotational constants are B_v' and B_v'', respectively, and the rotational quantum numbers are K' and K". The arrow in the figure shows one of the many possible transitions of the (0,2) vibrational band, namely, that corresponding to K'=4, K"=3. According to the selection rules for $^3\Pi \rightarrow {}^3\Pi$ transitions, only the following transitions (or branches) are allowed:

$$\left.\begin{array}{l} \text{P-branch: } K' - K'' = -1 \\ \text{Q-branch: } K' - K'' = 0 \\ \text{R-branch: } K' - K'' = +1 \end{array}\right\} . \qquad (6.2\text{-}3)$$

The transition shown in Figure 6-1 belongs to the R-branch.

6.2.3 Wavelengths of the Rotational Lines

Herzberg's formulas are given in terms of wave number ν, which is related to wavelength λ by

$$\nu = 1/\lambda . \qquad (6.2\text{-}4)$$

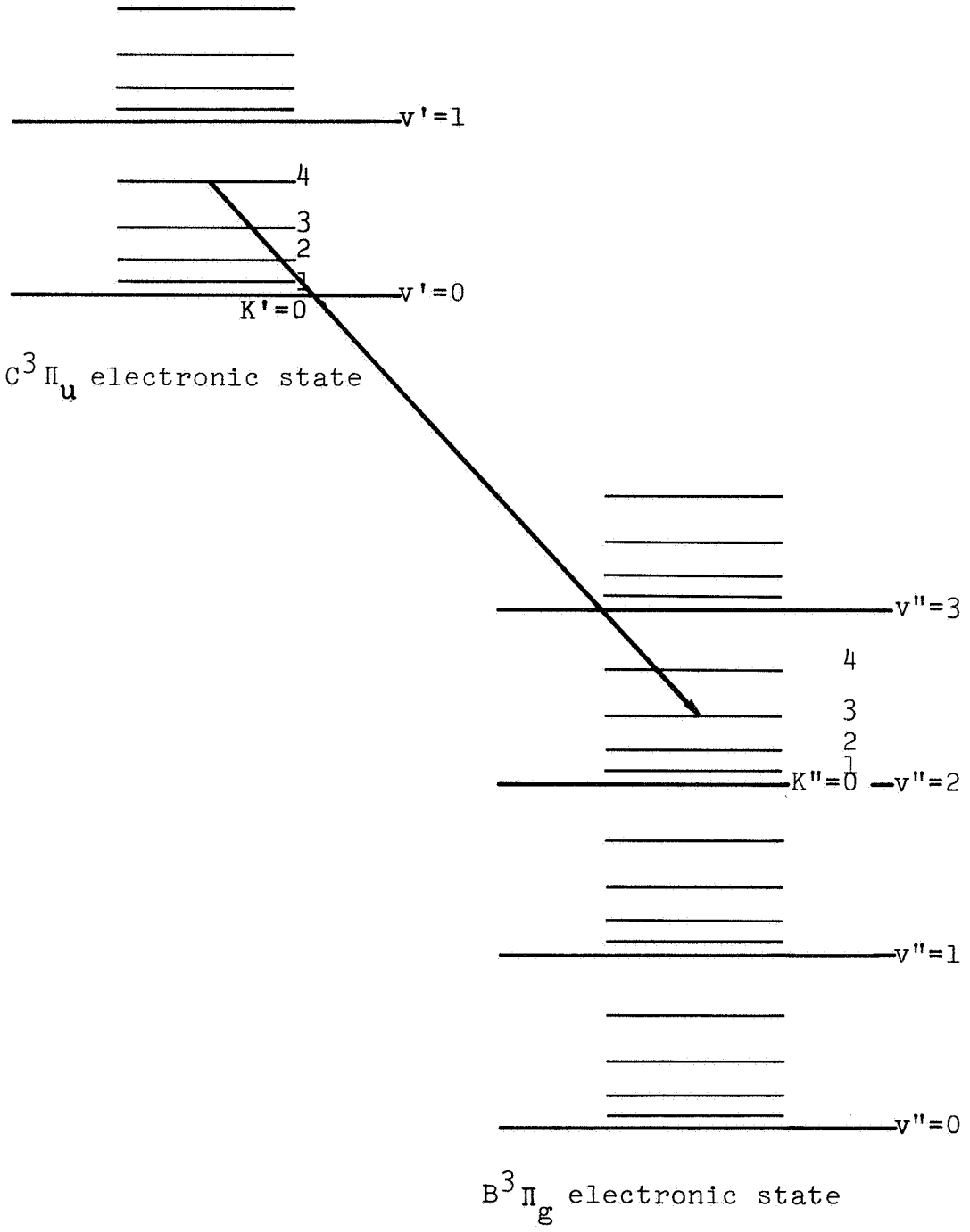

Figure 6-1: Schematic Energy-Level Diagram of the Second-Positive Band System of N_2

The wave number of a given line corresponding to the transition $K' \rightarrow K''$ is given by the formula

$$\nu = \nu_0 + B'_v K' (K'+1) - B''_v K'' (K''+1), \qquad (6.2\text{-}5)$$

where ν_0 is the wave number of the transition $K' = K'' = 0$.

From the Table 8, page 29, of Dieke and Heath (1959), we find that for the (0,2) band

$$\begin{aligned} \nu_0 &= 88{,}941.24 \text{ cm}^{-1} - 62{,}648.06 \text{ cm}^{-1} \\ &= 26{,}293.18 \text{ cm}^{-1}. \end{aligned} \qquad (6.2\text{-}6)$$

The rotational constant B_v is given in terms of the molecular constants B_e and α_e by the formula

$$B_v = B_e - \alpha_e \left(v + \tfrac{1}{2}\right) . \qquad (6.2\text{-}7)$$

From Table 39, page 552, of Herzberg, we obtain

$$\left.\begin{aligned} B'_e &= 1.8259 \text{ cm}^{-1}, \ \alpha'_e = 0.0197 \text{ cm}^{-1} \\ B''_e &= 1.6380 \text{ cm}^{-1}, \ \alpha''_e = 0.0184 \text{ cm}^{-1} \end{aligned}\right\} . \qquad (6.2\text{-}8)$$

Hence, for the (0,2) band we have

$$\left.\begin{aligned} B'_v &= 1.8259 \text{ cm}^{-1} - (0.0197 \text{ cm}^{-1})(0+\tfrac{1}{2}) = 1.8161 \text{ cm}^{-1} \\ B''_v &= 1.6380 \text{ cm}^{-1} - (0.0184 \text{ cm}^{-1})(2+\tfrac{1}{2}) = 1.5920 \text{ cm}^{-1} \end{aligned}\right\} . \qquad (6.2\text{-}9)$$

By substituting Equations (6.2-6) and (6.2-9) into Equation (6.2-5), we obtain

$$\nu = 26{,}293.18 + 1.8161\ K'\ (K'+1) - 1.5920\ K''\ (K''+1). \quad (cm^{-1}) \qquad (6.2\text{-}10)$$

Now consider the R-branch. By replacing K" in Equation (6.2-10) in terms of K' by means of the last of Equations (6.2-3), we obtain after rearrangement

$$\nu = 26{,}293.18 + 3.6322\ K' + 0.2241\ K'\ (K'-1). \quad (cm^{-1}) \qquad (6.2\text{-}11)$$

Finally, by putting the result into Equation (6.2-4) and using the binomial theorem, we obtain the following relation between the wavelength λ of a line of the R-branch and the upper-state rotational quantum number K':

$$\lambda = 3803.3 - 0.525\ K' - 0.0324\ K'\ (K'-1). \quad (\text{Å}) \qquad (6.2\text{-}12)$$

We wish to solve explicitly for K' as a function of λ. Equation (6.2-12) is a quadratic equation for K', with the solution

$$K' = -\left\{0.4926 \pm [0.24265 + (0.1296)(3803.3-\lambda)]^{1/2}\right\} / 0.0648. \qquad (6.2\text{-}13)$$

Only the minus sign in front of the radical gives a positive

value. The equations for the P- and Q-branches are similar to those for the R-branch.

6.2.4 Relative Order of Magnitude of the Line Intensities of the Three Branches

The intensity I of a line is given by the formula

$$I_{K'} = (\text{const.})\ S_{K'}\ N_{K'}/(2K'+1), \qquad (6.2\text{-}14a)$$

where $S_{K'}$ is the line strength. For a Boltzmann distribution of rotational states, this equation becomes

$$I_{K'} = (\text{const.})\ S_{K'}\ \exp[-(\hbar^2/2I'kT')K'(K'+1)]. \qquad (6.2\text{-}14b)$$

For a $^3\Pi \rightarrow {}^3\Pi$ transition, the Honl-London formulas for the line strengths are

$$\left.\begin{aligned} \text{P-branch:}\quad & S_{K'} = \frac{(K'+2)\ K'}{K'+1} \\ \text{Q-branch:}\quad & S_{K'} = \frac{2K'+1}{K'\ (K'+1)} \\ \text{R-branch:}\quad & S_{K'} = \frac{(K'+1)(K'-1)}{K'} \end{aligned}\right\}. \qquad (6.2\text{-}15)$$

Kyser measured I at the two wavelengths

$$\left.\begin{aligned} \lambda &= 3785\ \text{Å} \\ \lambda &= 3795\ \text{Å} \end{aligned}\right\}. \qquad (6.2\text{-}16)$$

From Equation (6.2-13) and the corresponding equations for

the other branches, we have computed the values of K' for these two wavelengths. The results are given (rounded to the nearest integer) in Table IV. For these large values of K', the Honl-London formulas (6.2-15) become approximately

$$\left.\begin{array}{ll} \text{P-branch:} & S_{K'} \approx K' \\ \text{Q-branch:} & S_{K'} \approx 2/K' \\ \text{R-branch:} & S_{K'} \approx K' \end{array}\right\} . \qquad (6.2\text{-}17)$$

The intensity of the Q-branch is therefore negligible compared with that of the P- and R-branches. Furthermore, the exponential factor in Equation (6.2-14b) dominates the factor $S_{K'}$ at these large values of K', with the result that the intensity of the P-branch is negligible compared with that of the R-branch. Hence, only the R-branch contributes significantly to the emitted intensity. We will therefore neglect the P- and Q-branches from now on.

6.2.5 Formula for the Intensity Ratio

Using Equation (6.2-12), we have computed the wavelength of each of the lines of the R-branch. The results are displayed in Figure 6-2, superposed on a graph of Kyser's instrument profile plotted as relative response Q versus wavelength λ. With the spectrometer set at 3785 Å, all the lines between K' = 14 and K' = 20 contribute to the measured intensity $I(\lambda=3785\ \text{Å})$. At 3795 Å, the lines between K'=4

Table IV: Upper-State Rotational Quantum Number

	$\lambda = 3785$ Å	$\lambda = 3795$ Å
P-branch	31	24
Q-branch	23	15
R-branch	17	10

⊙ Experimentally determined instrument profile (Kyser 1966)
K' = 20, 19, ..., 4 denotes wavelength of line with upper-state rotational quantum number K'

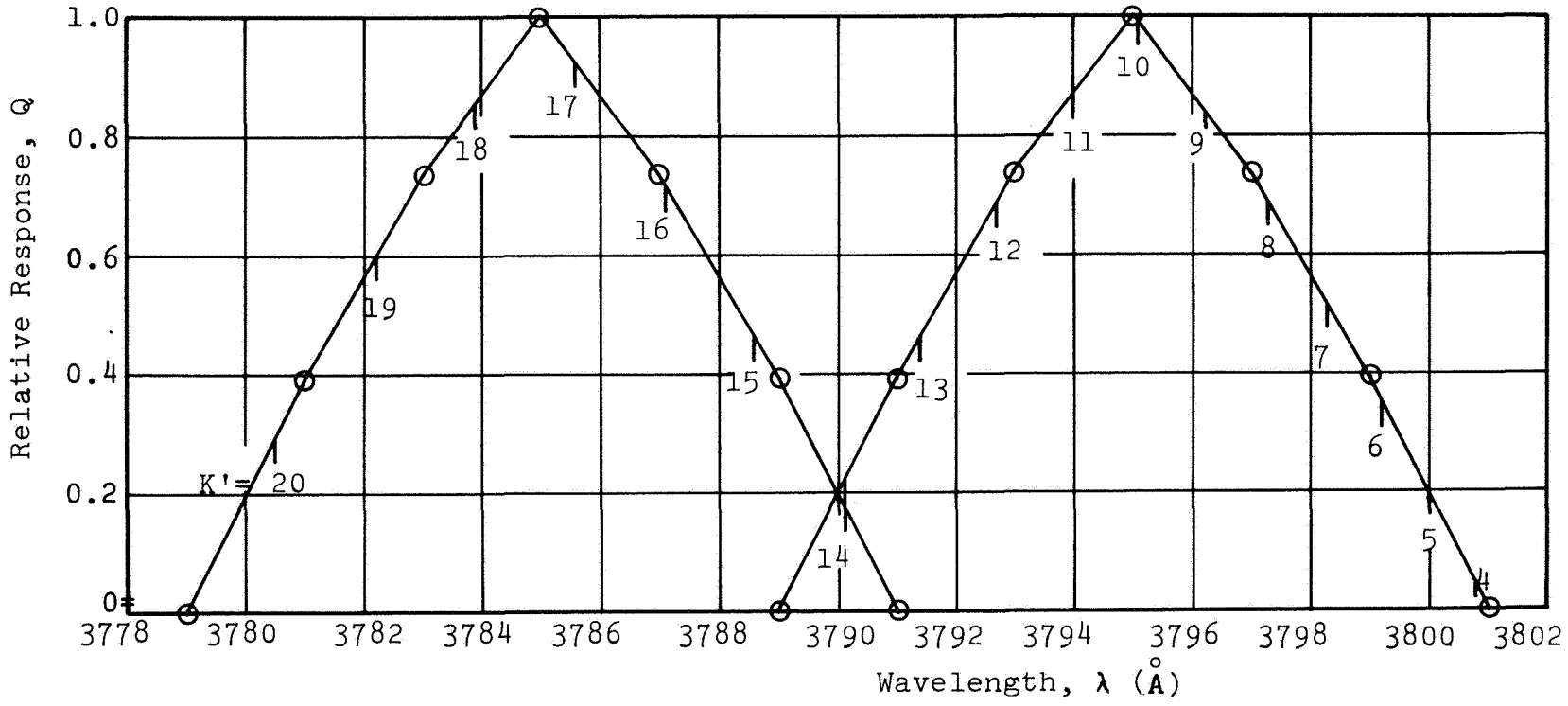

Figure 6-2: Position of the Rotational Lines on the Instrument Profile.

and K'=14 contribute to the intensity I(λ=3795 Å). The ratio r of these intensities is hence given by the formula

$$r = \frac{I(\lambda=3785\ \text{Å})}{I(\lambda=3795\ \text{Å})} = \frac{\sum_{K'=14}^{20} Q(K')\ I_{K'}}{\sum_{K'=4}^{14} Q(K')\ I_{K'}} \cdot \qquad (6.2\text{-}18)$$

By substitution from Equation (6.2-14a), we obtain

$$r = \frac{\sum_{K'=14}^{20} Q(K')\ S(K')\ N_{K'}/(2K'+1)}{\sum_{K'=4}^{14} Q(K')\ S(K')\ N_{K'}/(2K'+1)} \cdot \qquad (6.2\text{-}19)$$

The quantity r is what Kyser actually measured in his experiments.

The quantities Q and S are functions only of K'. We obtain Q from Figure 6-2 and S from Equation (6.2-15). The values are given in Table V. The ratio r is then a function only of the populations $N_{K'}$ of the upper-state rotational levels.

6.3 Numerical Results

To compare with Kyser's result, we have computed r as a function of upper-state rotational temperature T_1 for a Boltzmann distribution of $C^3\Pi_u$ rotational levels. We considered two extreme cases of population alternation in the $C^3\Pi_u$ state:

Table V: Relative Instrument Response and Line Strength

K'	Q(K')	S(K')	Q(K') S(K')
4	0.04	3.750	0.150
5	0.19	4.800	0.912
6	0.35	5.833	2.042
7	0.51	6.857	3.497
8	0.69	7.875	5.434
9	0.85	8.889	7.556
10	0.99	9.900	9.801
11	0.87	10.909	9.491
12	0.68	11.917	8.104
13	0.46	12.923	5.945
14 (3795 Å)	0.21	13.929	2.925
14 (3785 Å)	0.17	13.929	2.368
15	0.46	14.933	6.869
16	0.72	15.938	11.475
17	0.92	16.941	15.586
18	0.86	17.944	15.432
19	0.60	18.947	11.368
20	0.29	19.950	5.786

Case 1: $\sigma(K' \text{ even})/\sigma(K' \text{ odd}) = 1$

(no population alternation).

Case 2: $\sigma(K' \text{ even})/\sigma(K' \text{ odd}) = 2$.

In Figure 6-3, we plot the results as r versus $1/T_1$ on semi-log paper. To our surprise, we found that population alternation has an insignificant effect on r, the values of r with population alternation differing from those without alternation only in the third decimal place. This is why only one curve, instead of two curves, appears in Figure 6-3.

If we were to measure the intensity of one line at each wavelength (rather than the resultant intensity of several lines), ln r versus $1/T_1$ would plot exactly as a single straight line. The actual plot is very nearly a straight line in three distinct regions. There is one line for $100^{\circ}K \leq T_1 \leq 200^{\circ}K$ (which does not appear on the figure), a slightly steeper line for $200^{\circ}K \leq T_1 \leq 500^{\circ}K$, and a line for $500^{\circ}K \leq T_1 \leq 1000^{\circ}K$ that is slightly steeper yet.

Figure 6-3 supersedes Figure 10 of Kyser's (1966) report. Our numerical values differ slightly from his. For example, in Kyser's curve, r=0.274 corresponds to $T_1=355^{\circ}K$; in our curve, r=0.274 corresponds to $T_1=342^{\circ}K$.

The present numerical results differ from Kyser's not because population alternation is taken into account or because some details of the present computation are different. They differ because the basic approaches are different.

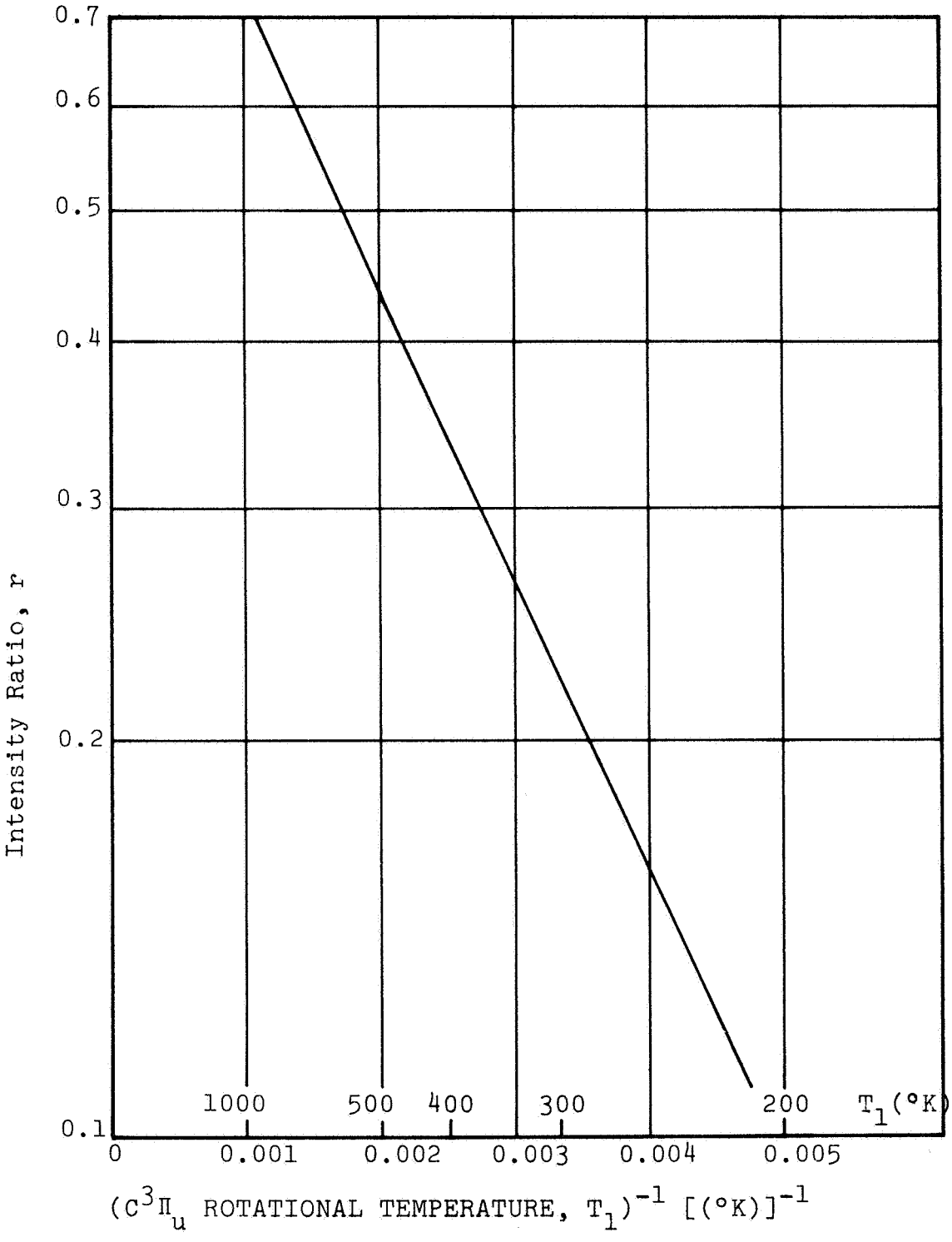

Figure 6-3: Rotational Temperature vs. Measured Intensity Ratio

Whereas Kyser integrated over an assumed continuous distribution of intensity versus wavelength, we sum over the individual spectral lines.

From these results, we come to the following conclusions:

(1) The quantity r that Kyser measured in his experiments is indeed a single-valued function of the $C^3\Pi_u$ rotational temperature T_1. Hence T_1 can be deduced from a measurement of r.

(2) Kyser's method is actually a better way of measuring T_1 than the usual log-slope method, because the function r versus T_1 does not depend on the population alternation in the $C^3\Pi_u$ state. If one line instead of several were used at each wavelength, the measured intensity would be directly proportional to the $C^3\Pi_u$ population-alternation factor. This factor must be obtained from an analysis of the $C^3\Pi_u \rightarrow X^1\Sigma_g^+$ excitation process, e.g., the analysis reported in the present report. The use of several lines at each wavelength makes this factor cancel approximately in the numerator and denominator of the equation for r, so that an analysis of the excitation process is unnecessary for the deduction of T_1 as a function of r.

We can now substitute our predicted values of N_K, as a function of K' (discussed in Section 5.6) into Equation (6.2-19), compute our predicted value of r, and compare it

with Kyser's measured value. We do this in the next chapter.

CHAPTER 7

COMPARISON BETWEEN PREDICTED AND MEASURED ROTATIONAL TEMPERATURES

7.1 Prediction of the Present Analysis

By substituting our predicted values of $N_{K'}$ as a function of K' (Section 5.6) into Equation (6.2-19), we obtain the predicted value of the intensity ratio r as

$$r = 0.181. \qquad (7.1\text{-}1)$$

From Figure 6-3, we see that the corresponding value for the $C^3\Pi_u$ rotational temperature is

$$T_1 = 266^{\circ}K. \qquad (7.1\text{-}2)$$

This value agrees closely with those obtained by using the usual log-slope method on the basis of our predicted values of $N_{K'}$ (Equation 5.6-4). We also obtain the same value of r when we use the second set of 20,800 pseudorandom numbers in the Monte-Carlo computations (Section 5.8), thus verifying that we have computed enough collisions to obtain statistical trends.

7.2 Comparison with Kyser's Measurements

Kyser's measured value for the intensity ratio is

$$r = 0.274. \qquad (7.2\text{-}1)$$

From Figure 6-3, we see that the corresponding value of T_1 is

$$T_1 = 342^{\circ}K. \qquad (7.2\text{-}2)$$

[If Kyser's (1966) curve of r versus T_1 is used, r = 0.274 corresponds to $T_1 = 355^{\circ}K$.] Our prediction disagrees with Kyser's measurement. We predict a temperature $29^{\circ}K$ lower than the ambient temperature $T_0 = 295^{\circ}K$, whereas Kyser's measured value is $47^{\circ}K$ higher.

As pointed out in Section 5.7, our predicted temperature is equal to T_0 times the ratio of the B-values of the $C^3\Pi_u$ and $X^1\Sigma_g^+$ states. Our theory thus predicts that the collisions produce essentially no change in the distribution over the rotational states, whereas Kyser's measurements indicate that the collisions cause considerable change in this distribution.

The discrepancy between theory and experiment suggests that something is in error with our analysis. We have made a thorough reappraisal of the assumptions of the analysis in an attempt to discover the source of the discrepancy. We discuss these matters in the next section.

7.3 Assumptions of the Analysis

We have been able to show by various means (e.g., order-of-magnitude calculations) that many of the assumptions are valid. The most important remaining assumption

whose validity we could not verify is that classical mechanics is adequate for the analysis of the electron-molecule collisions (Chapter 3). Within the context of the classical analysis, the most important assumption is that the maximum possible impact parameter is the molecular radius (Section 5.5). An additional assumption is that, if two or more integer values of K_1 are possible for a given set of collision parameters, each value is equally probable.

One cannot estimate quantitatively the error produced by the use of classical mechanics. One can only anticipate that the predictions may be in error. We have, on the other hand, been able to make quantitative checks of the effect of modifying the other two assumptions. These checks consisted simply of redoing the calculations of N_{K_1} versus K_1, and thence of T_1, a number of times with one of the assumptions modified each time.

We examined the effect of the assumption concerning $|D_0|_{max}$ by repeating the computations of T_1 twice, each time using the first set of 20,800 pseudorandom numbers to obtain the collision parameters. In doing this, we modified the pseudorandom values of D_0 as described below. The values of g_0, ϕ_{g_0}, and θ_{g_0} for each collision were the same as for the basic computations (Section 5.6).

In the first modification, the maximum impact distance was tripled to obtain

$$|D_0|_{max} = 3\ r_0, \tag{7.3-1}$$

and the values of D_0 were assumed to be distributed uniformly between $-3r_0$ and $3r_0$. We thus tripled each pseudo-random value of D_0. The resulting predictions are

$$\left.\begin{aligned} r &= 0.196 \\ T_1 &= 279^{\circ}K \end{aligned}\right\} . \tag{7.3-2}$$

The second modification was similar to the first in that the maximum impact distance was multiplied by six to obtain

$$|D_0|_{max} = 6\ r_0. \tag{7.3-3}$$

The resulting predictions are

$$\left.\begin{aligned} r &= 0.216 \\ T_1 &= 295^{\circ}K \end{aligned}\right\} \tag{7.3-4}$$

These results show that it would take a huge value of $|D_0|_{max}$ to obtain Kyser's measured temperature of $342^{\circ}K$. There is no evidence, however, as to what value of $|D_0|_{max}$ other than r_0 is most nearly correct.

This matter was investigated further by calculating some trajectories of electrons passing molecules. These calculations, which are described in Appendix E, lead to the following conclusions:

(1) The molecule does not "capture" the electron if $|D_0|$ is much larger than r_0.

(2) Very little angular momentum is exchanged between the electron and the molecule during the electron's flight past the molecule except at the instant of impact.

These results corroborate the validity of Equation (5.5-12).

We conclude that the assumption concerning $|D_0|_{max}$ cannot account for the disagreement between the predicted and measured values of T_1.

Our assumption that all integer values of K_1 for a given set of collision parameters are equally probable is arbitrary. If a different assumption is used, a different value of T_1 might be predicted. A higher temperature will result, for example, if the higher integer values of K_1 are more probable than the lower ones.

We have investigated the magnitude of this effect by modifying the calculations of Section 5.6, using the same pseudorandom collision parameters as in Section 5.6. For each collision in which more than one integer value of K_1 is possible, however, we assumed that

Only the highest possible integer value of K_1 occurs. (7.3-5)

The resulting predictions are

$$\left.\begin{aligned} r &= 0.186 \\ T_1 &= 270^{\circ}K \end{aligned}\right\} \qquad (7.3\text{-}6)$$

This is only $4^{\circ}K$ higher than the temperature in Equation (7.1-2). This modification causes such a small increase in T_1 because, for most of the collisions, the only possible value of K_1 is K_0 (e.g., see Table III).

7.4 The Use of Classical Mechanics

Within the context of classical mechanics, subsidiary assumptions either are demonstrably valid or do not affect the predicted value of T_1 very much. We therefore conclude that the use of classical mechanics must be the cause of the disagreement between theory and experiment. Unfortunately, the current state of knowledge in collision theory precludes a full quantum-mechanical analysis.

In the work mentioned earlier, Muntz (1962) analyzed electron-impact excitation by applying the standard formulas for absorption of light by molecules. This is valid in his situation because the high-energy (50,000 eV) electrons in Muntz's beam act like photons when they strike a molecule. Such an analysis is not valid, however, for the low-energy (18 eV) electrons in Kyser's spark. In spite of this, we

did perform a calculation of the excitation using Muntz's model, to obtain at least some quantum-mechanical results. Interestingly, this model predicts the following values:

$$\left.\begin{aligned} r &= 0.181 \\ T_1 &= 266^{\circ}K \end{aligned}\right\} , \qquad (7.4\text{-}1)$$

which agree with the classical-mechanics Monte-Carlo prediction. The details of the calculation are given in Appendix F.

CHAPTER 8

CONCLUDING REMARKS

In view of the discrepancy between the present analysis and Kyser's (1966) experiments (Section 7.2), the tracer-spark technique cannot yet be considered a reliable means for deducing static temperature in nitrogen. Measurements of the deduced rotational temperature at combinations of ambient temperature, ambient pressure, and spark energy other than those tested by Kyser (Section 1.2) would be desirable. Even if these measurements continued to disagree with the present analysis, they would provide an empirical relation between the ambient temperature and the deduced temperature.

The present analysis is, in any event, the first of its kind and gives new understanding of the excitation of the nitrogen second-positive band system. Of the several facets of the analysis discussed in Chapters 2 through 6, only the dynamics of the individual collisions (Chapter 3) is of questionable validity (because we have tried to apply classical mechanics to an electron-molecule collision). The other facets of the analysis may be useful to future investigators of the excitation of band systems by a discharge. Many of these ideas are applicable to band systems

other than the second-positive, as well as to other gases. They may also be applicable to excitation phenomena in related devices, such as lasers (Gerry 1965). It is also hoped that our critical examination of the assumptions in the analysis will expedite the work of future analysts in this kind of problem.

APPENDIX A

Derivation of the Angular-Momentum Equation

In this appendix, we derive Equation (3.3-1c).

We use the notation shown in the following sketch:

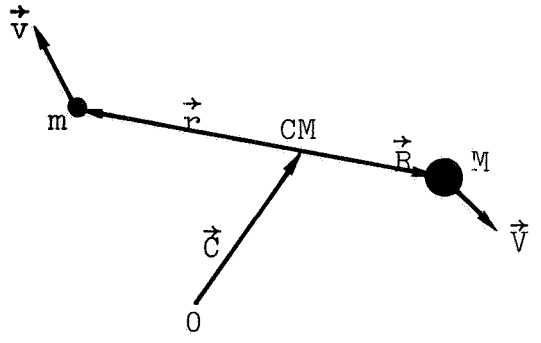

The vector $\vec{C}$ is the distance between the origin O of an inertial coordinate system and the center of mass CM of the system (electron plus molecule), $\vec{r}$ is the distance between CM and the electron, and $\vec{R}$ is the distance between CM and the molecular center of mass. The angular-momentum equation is

$$(\vec{C}_0+\vec{r}_0) \times m\vec{v}_0 + (\vec{C}_0 +\vec{R}_0) \times M\vec{V}_0 + \vec{K}_0 =$$

$$(\vec{C}_1+\vec{r}_1) \times m\vec{v}_1 + (\vec{C}_1 +\vec{R}_1) \times M\vec{V}_1 + \vec{K}_1,$$

or equivalently,

$$\vec{C}_0 \times (m\vec{v}_0+M\vec{V}_0) + m\vec{r}_0 \times \vec{v}_0 + M\vec{R}_0 \times \vec{V}_0 + \vec{K}_0 =$$
$$\vec{C}_1 \times (m\vec{v}_1+M\vec{V}_1) + m\vec{r}_1 \times \vec{v}_1 + M\vec{R}_1 \times \vec{V}_1 + \vec{K}_1. \qquad (A\text{-}1)$$

From the linear-momentum equation (3.4-3b), it follows that

$$\vec{W}_0 = \vec{W}_1 , \tag{A-2}$$

where $\vec{W}$ is the center-of-mass velocity, given by

$$\vec{W} = \frac{m\vec{v} + M\vec{V}}{m+M} . \tag{A-3}$$

(The constancy of $\vec{W}$ results because there are no external forces acting on the system.) Hence $\vec{C}_1$ is related to $\vec{C}_0$ by

$$\vec{C}_1 = \vec{C}_0 + \vec{W}t, \tag{A-4}$$

where t is the time interval between the $(\ )_0$ situation and the $(\ )_1$ situation.

Since $\vec{W}$ is parallel to $m\vec{v}+M\vec{V}$, we have

$$\vec{W} \times (m\vec{v}+M\vec{V}) = 0, \tag{A-5}$$

so that we obtain

$$\vec{C}_1 \times (m\vec{v}_1+M\vec{V}_1) = \vec{C}_0 \times (m\vec{v}_0+M\vec{V}_0). \tag{A-6}$$

(The constacy of the portion of the angular momentum that is due to the center-of-mass motion results because there are no external torques acting on the system.)

Hence Equation (A-1) reduces to

$$m\vec{r}_0 \times \vec{v}_0 + M\vec{R}_0 \times \vec{V}_0 + \vec{K}_0 = m\vec{r}_1 \times \vec{v}_1 + M\vec{R}_1 \times \vec{V}_1 + \vec{K}_1 . \tag{A-7}$$

By definition of the center of mass, we have

$$m\vec{r} = -M\vec{R}, \qquad \text{(A-8)}$$

and substitution of this into Equation (A-7) gives

$$m\vec{r}_0 \times (\vec{v}_0 - \vec{V}_0) + \vec{K}_0 = m\vec{r}_1 \times (\vec{v}_1 - \vec{V}_1) + \vec{K}_1. \qquad \text{(A-9)}$$

The distance $\vec{D}$ between the electron and the molecule is

$$\vec{D} = \vec{r} - \vec{R}. \qquad \text{(A-10)}$$

By substituting Equation (A-8) into this relation, we obtain

$$m\vec{r} = \mu\vec{D}, \qquad \text{(A-11)}$$

where μ is the reduced mass defined by

$$\mu = \frac{mM}{m+M} \cdot \qquad \text{(A-12)}$$

Putting Equation (A-11) into Equation (A-9), we obtain finally

$$\mu\vec{D}_0 \times (\vec{v}_0 - \vec{V}_0) + \vec{K}_0 = \mu\vec{D}_1 \times (\vec{v}_1 - \vec{V}_1) + \vec{K}_1. \qquad \text{(A-13)}$$

APPENDIX B

Verification that the Electron Velocity Distribution Function is Maxwellian

In this appendix, we verify the validity of Equation (4.3-14a).

Kruger and Mitchner (1967) show that, if electron-electron collisions are dominant, the electron velocity distribution function is a Maxwellian at the electron temperature. This will be true if the following inequality is satisfied:

$$\nu_{ee} >> \nu_{eM} \quad m/M, \tag{B-1}$$

where ν_{ee} is the electron-electron collision frequency and ν_{eM} is the electron-molecule collision frequency.

We now compute the orders of magnitude of ν_{ee} and ν_{eM} for typical spark conditions. If we assume that an electron-molecule collision occurs only when the electron and molecule touch each other, then we have

$$\nu_{eM} \approx N_M \, v_e \, \pi \, r_0^2 , \tag{B-2}$$

where N_M is the molecular number density, v_e is the mean electron speed, r_0 ($= 0.547 \times 10^{-8}$ cm) is the molecular radius, and ν_{eM} includes both elastic and inelastic collisions. Similarly, an electron-electron collision occurs when one electron passes within the other electron's Debye sphere, so that we have

$$\nu_{ee} \approx N_e \, v_e \, \pi \, \lambda^2, \qquad \text{(B-3)}$$

where λ is the Debye length. From these equations, we obtain

$$\frac{\nu_{ee}}{\nu_{eM} \, m/M} \approx \frac{M}{m} \, \frac{N_e}{N_M} \, \frac{\lambda^2}{r_0^2} \quad . \qquad \text{(B-4)}$$

From Spitzer (1962), page 22, we find

$$\lambda = 6.90 \, (T_e \, / \, N_e)^{1/2}, \qquad \text{(B-5)}$$

where λ is in cm, T_e is the electron temperature in ^{o}K, and N_e is the electron density in cm^{-3}. The values of v_e, N_e, and N_M are given in Section 2.2. From them we compute for the electron temperature

$$T_e = O(10^4 \ ^{o}K). \qquad \text{(B-6)}$$

The numerical value of the Debye length is

$$\lambda = O(10^{-4} \text{ cm}). \qquad \text{(B-7)}$$

The ratio in Equation (B-4) is thus found to have the numerical value

$$\frac{\nu_{ee}}{\nu_{eM} \, m/M} = O(10^9), \qquad \text{(B-8)}$$

so that the criterion expressed by inequality (B-1) is satisfied. The number 10^9 is so large that any errors due to the crudeness of the calculation should not change this conclusion.

APPENDIX C

Results of Evaluating the Integral

$$I_n = \int_{\ell}^{u} x^{n+2} e^{-ax^2} dx. \quad (n = 0, 1, \ldots, 5)$$

In this appendix, we list the integrals used in the evaluation of $G(g_0)$ in Section 5.4.2.

$$I_0 = \left\{ \left[\ell \exp(-L^2) - u \exp(-U^2) \right] + A_1 \right\} / 2a, \qquad (C\text{-}1)$$

$$I_1 = \left[\exp(-L^2)\ (L^2+1) - \exp(-U^2)(U^2+1) \right] / 2a^2, \qquad (C\text{-}2)$$

$$I_2 = -\left\{ u \exp(-U^2)\ (U^2+1) - \ell \exp(-L^2)\ (L^2+1) - aI_0 - A_1 \right\} / 2a^2, \qquad (C\text{-}3)$$

$$I_3 = -\left[\exp(-U^2)\ (U^4 + 2U^2 + 2) - \exp(-L^2)\ (L^4 + 2L^2 + 2) \right] / 2a^3, \qquad (C\text{-}4)$$

$$I_4 = \left[\ell \exp(-L^2)\ (L^4 + 2L^2 + 2) - u \exp(-U^2)\ (U^4 + 2U^2 + 2) + a^2 I_2 + 2a I_0 + 2A_1 \right] / 2a^3, \qquad (C\text{-}5)$$

$$I_5 = \left[\exp(-L^2)(L^6 + 3L^4 + 6L^2 + 6) \right.$$

$$\left. - \exp(-U^2)(U^6 + 3U^4 + 6U^2 + 6) \right] / 2a^4, \qquad \text{(C-6)}$$

where

$$L = a^{1/2} \ell, \qquad \text{(C-7)}$$

$$U = a^{1/2} u, \text{ and} \qquad \text{(C-8)}$$

$$A_1 = \tfrac{1}{2}(\pi/a)^{1/2} [\operatorname{erf}(U) - \operatorname{erf}(L)]. \qquad \text{(C-9)}$$

APPENDIX D

Generation of Pseudorandom Numbers.

In this appendix, we describe the method by which the pseudorandom numbers used in the Monte-Carlo calculations of Chapter 5 were generated.

The random numbers were generated with a digital-computer program. This program generates what are called "pseudorandom" numbers. The same sequence of numbers is generated each time the program is run, but the numbers satisfy statistical tests for randomness. The program used was a mixed congruential method, as programmed by the Stanford Computation Center. The n'th number R_n (n=0,1,2,...) is given by

$$R_n = [(2^{11}-3)\ R_{n-1} + 211,527,139](\text{mod } 2^{27}), \quad \text{(D-1)}$$

where

$$R_0 = 0. \quad \text{(D-2)}$$

This formula generates a sequence of pseudorandom numbers that are uniformly distributed in the interval

$$0 \leq R_n < 1. \quad \text{(D-3)}$$

The period of the sequence is 2^{27} (= 135,000,000). One does not have to take the entire sequence of 135,000,000 numbers, however, to obtain a random set. The members of any sufficiently large subset - e.g., R_1, R_2, R_3, ... , R_{100} or R_4,

R_8, R_{12}, ... , R_{400} - also are distributed uniformly in [0,1).

The first 100 numbers in the sequence are listed in Table D-1. Their mean is 0.48, so that the numbers are distributed evenly about 0.5, as random numbers between 0 and 1 should be. We illustrate the randomness of the numbers by plotting them in pairs as 50 points on a grid in Figure D-1. Point 1 uses R_1 as absicissa and R_2 as ordinate, point 2 uses R_3 as absicissa and R_4 as ordinate, etc. The points fill the grid fairly well. If we use these points to compute the quantity

$$I = \int_0^1 x \, dx \qquad \text{(D-4)}$$

using equation (5.2-3), we obtain

$$I \approx (23/50)\ (1)\ (1) = 0.46, \qquad \text{(D-5)}$$

as compared with the exact value of 0.50.

For the computations of N_{K_1} versus K_1, we use the numbers R_n in groups of 4, rather than in pairs.

Table D-1: The First 100 Pseudorandom Numbers

The numbers are rounded to 2 decimal places.

n	R_n	n	R_n	n	R_n	n	R_n	n	R_n	n	R_n
1	.58	19	.998	37	.11	55	.92	73	.66	91	.86
2	.50	20	.43	38	.86	56	.52	74	.74	92	.09
3	.89	21	.53	39	.56	57	.32	75	.95	93	.10
4	.99	22	.52	40	.77	58	.11	76	.66	94	.46
5	.72	23	.32	41	.52	59	.27	77	.37	95	.80
6	.88	24	.82	42	.14	60	.90	78	.12	96	.74
7	.91	25	.91	43	.81	61	.50	79	.81	97	.35
8	.51	26	.84	44	.92	62	.77	80	.15	98	.18
9	.95	27	.53	45	.09	63	.35	81	.27	99	.82
10	.88	28	.76	46	.51	64	.62	82	.50	100	.25
11	.46	29	.07	47	.06	65	.06	83	.09		
12	.34	30	.62	48	.25	66	.97	84	.21		
13	.61	31	.09	49	.48	67	.63	85	.06		
14	.54	32	.52	50	.35	68	.23	86	.30		
15	.16	33	.03	51	.14	69	.53	87	.78		
16	.34	34	.07	52	.24	70	.78	88	.02		
17	.04	35	.35	53	.37	71	.21	89	.64		
18	.20	36	.06	54	.15	72	.61	90	.70		

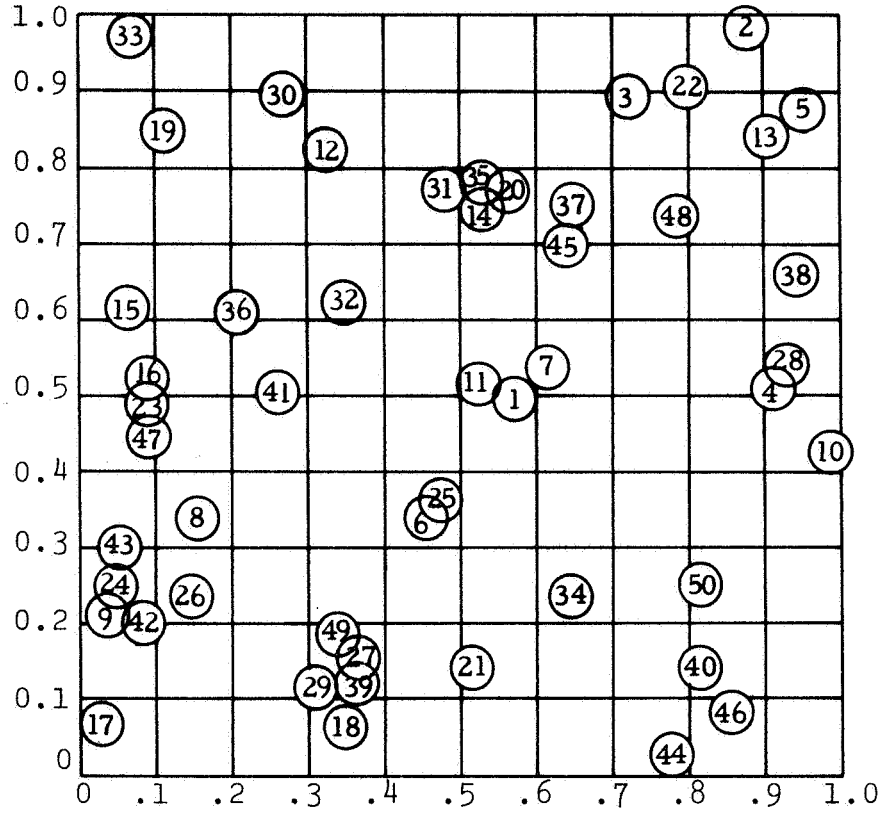

Figure D-1: The First 100 Pseudorandom Numbers, Taken in Pairs

APPENDIX E

Trajectory Calculations

E.1 Introduction

In this appendix, we calculate the following quantities:

(1) Trajectories followed by electrons during their encounters with the molecular interaction potential.

(2) The angular momentum transferred between the electron and molecule during these encounters.

The purpose of these calculations, as we mentioned in Section 7.4, is to investigate the validity of the assumption that the maximum impact distance is the molecular radius.

As in our Monte-Carlo calculations, g_0, D_0 (or b_0), ϕ_{g_0}, and θ_{g_0} are parameters.

E.2 Units

We use atomic units in these computations. The units of the basic quantities are as follows:

Length: Bohr radius = 0.529167×10^{-8} cm. (E.2-1a)

Mass: Proton mass = 1.67252×10^{-24} gm. (E.2-1b)

Energy: Twice the energy of the first Bohr orbit = 27.2 eV. (E.2-1c)

The unit of velocity is therefore

$$\text{Velocity} = (\text{energy/mass})\ 1/2 = (27.2\ \text{eV}/1.67252 \times 10^{-24}\ \text{gm})^{1/2} = 5.09401 \times 10^{6}\ \text{cm/sec.} \qquad \text{(E.2-2)}$$

E.3 Dynamics of a Particle in a Noncentral Force Field

E.3.1 Equivalence to the Actual Collision

Any binary collision can be recast as an encounter between a ficticious particle and a ficticious point potential. The ficticious particle's mass and velocity are the reduced mass of and the relative velocity between the collision partners, respectively. The ficticious potential is the interaction potential between the collision partners, and the distance between the ficticious particle and the ficticious potential is the distance between the collision partners.

For the electron-molecule collision that we are analyzing, the reduced mass is nearly equal to the electron mass. Hence, the trajectory of the ficticious particle is nearly the same as the trajectory of the electron.

E.3.2 Orbit Equation

The coordinate system for the collision is shown in Figure E-1.

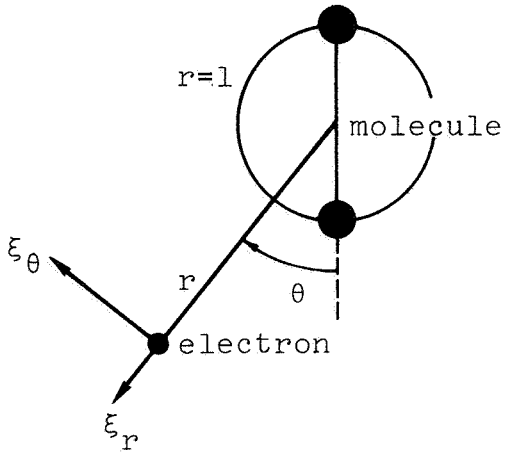

Figure E-1: Coordinate System

The location of the particle is specified by polar coordinates r and θ relative to the origin, where a noncentral potential ϕ is located. The r and θ components of the relative velocity are ξ_r and ξ_θ, respectively.

The differential equation describing the orbit of a particle in a noncentral force field has been derived by Prager and Rasmussen (1967) and is

$$\frac{d}{d\theta}\left[\frac{\frac{2r^2}{\mu}(E-\phi)+\frac{r_\theta^2}{r}-\frac{L_z^2}{\mu^2 r^2\sin^2\theta}}{\frac{r_\theta^2}{r^2}+1}\right]+\frac{2r^2}{\mu}\frac{\partial\phi}{\partial\theta}=0, \qquad \text{(E.3-1)}$$

where μ is the reduced mass, $r_\theta = dr/d\theta$, L_z is the x component of the angular momentum about the origin, and

$$E = \frac{\mu}{2}\left[\xi_r^2\ (1+r^2\theta_r^2) + \frac{L_z^2}{\mu^2 r^2 \sin^2\theta}\right] + \phi \qquad \text{(E.3-2)}$$

is the energy of the electron-molecule system.

Far from the origin, the relative speed is g_0; hence, by conservation of energy, we have

$$E = \frac{1}{2}\,\mu\ g_0^2 = \text{constant.} \qquad \text{(E.3-3)}$$

We note that, since ϕ is a function of $r(\theta)$ and θ, $d\phi/d\theta$ is given by the formula

$$\frac{d\phi}{d\theta} = \frac{dr}{d\theta}\frac{\partial\phi}{\partial r} + \frac{\partial\phi}{\partial\theta} = r_\theta \frac{\partial\phi}{\partial r} + \frac{\partial\phi}{\partial\theta}\ . \qquad \text{(E.3-4)}$$

For the interaction between an electron and a diatomic molecule, we can write

$$\phi = \phi(r,\theta)\ . \qquad \text{(E.3-5)}$$

Therefore, the trajectory is planar, so that

$$L_z = 0\ . \qquad \text{(E.3-6)}$$

Using Equation (E.3-6) to simplify (E.3-1) and carrying out the differentiation, we obtain the following second-order ordinary differential equation for the trajectory $r(\theta)$:

$$\frac{d^2r}{d\theta^2} = \frac{2}{r}\left(\frac{dr}{d\theta}\right)^2 + r + \frac{\left(\frac{dr}{d\theta}\frac{\partial\phi}{\partial\theta} - r^2\frac{\partial\phi}{\partial r}\right)\left[\left(\frac{dr}{d\theta}\right)^2 + r^2\right]}{2r^2(E-\phi)}\ . \qquad \text{(E.3-7)}$$

For a central potential, we have $\partial\phi/\partial\theta = 0$. In this case, Equation (E.3-7) reduces to the equation given in Section 3-5 of Goldstein (1950). This is a check on Equation (E.3-7).

E.3.3 Initial Conditions

To integrate Equation (E.3-7), we must know $r(\theta_0)$ and $r_\theta(\theta_0)$ at some angle θ_0.* Physically, we must have

$$\left.\begin{array}{l} r(\theta) \to \infty \\ \\ r_\theta(\theta) \to -\infty \end{array}\right\} \quad \text{as } \theta \to 90^\circ \ . \tag{E.3-8}$$

The impact parameter b_0 is given by

$$b_0 = \lim_{\theta \to 90^\circ} [r(\theta) \cos \theta] \ . \tag{E.3-9}$$

E.3.4 Angular Momentum

The angular momentum L of the relative motion is given by

$$L = \mu \, r \, \xi_\theta \ . \tag{E.3-10}$$

The initial angular momentum L is given by

$$L_0 = \mu \, b_0 \, g_0 \ . \tag{E.3-11}$$

We express L in terms of the orbit variables r and r_θ by means of the formulas

$$\xi_\theta = r \, \xi_r / r_\theta \ , \tag{E.3-12a}$$

*The notation $r_\theta(\theta_0)$ means $(dr/d\theta)_{\theta=\theta_0}$.

$$\xi_r = r_\theta \left[\frac{\frac{2}{\mu}(E-\phi)}{r_\theta^2 + r^2} \right]^{1/2} \qquad \text{(E.3-12b)}$$

Since the interaction potential is noncentral, the electron can exert a torque on the molecule and thus change its angular momentum. By conservation of angular momentum, the change in angular momentum of the molecule (i.e., the rotational excitation or de-excitation) is equal and opposite to the change in angular momentum of the electron.

E.4 Potential Used

If the potential $\phi(r,\theta)$ is known, Equation (E.3-7) can be solved for $r(\theta)$, at least numerically. As we pointed out in Section 3.4, however, the potential is known only for large values of r. From Takayanagi and Geltman (1965), the asympototic potential is, in atomic units,

$$\phi(r,\theta) \underset{r\to\infty}{\longrightarrow} -\frac{\alpha}{2r^4} - \left(\frac{\alpha'}{2r^4} + \frac{Q}{r^3}\right)\left(\frac{3}{4}\cos 2\theta + \frac{1}{4}\right), \qquad \text{(E.4-1)}$$

where α and α' are related to the polarizability of the molecule and Q is the electric-quadrupole moment of the molecule. For N_2, we have

$$\alpha = 12.00 , \qquad \text{(E.4-2a)}$$

$$\alpha' = 4.20 , \qquad \text{(E.4-2b)}$$

$$Q = -1.10 . \qquad \text{(E.4-2c)}$$

For lack of anything better, we applied the asymptotic potential at small, as well as large, values of r. The strongly attractive r^{-4} terms, however, pull the particle into the origin for small r. To prevent this, we assumed that the potential can be represented by an impenetrable sphere with a radius equal to the molecular radius (0.547×10^{-8} cm). This is nearly equal to 1 atomic unit of length (0.529167×10^{-8} cm). Thus, the potential used in the computations was

$$\phi(r,\theta) = -\frac{\alpha}{2r^4} - \left(\frac{\alpha'}{2r^4} + \frac{Q}{r^3}\right)\left(\frac{3}{4}\cos 2\theta + \frac{1}{4}\right), \quad r > 1, \tag{E.4-3a}$$

$$\phi(r,\theta) = +\infty, \quad r \leq 1. \tag{E.4-3b}$$

Since the computations are based on a potential of questionable validity and are not quantum-mechanical, the results should be valid only for showing trends.

E.5 Integration of the Orbit Equation

E.5.1 Numerical Method

The complicated potential (E.4-3) makes the orbit equation (E.3-7) nonlinear and complicated, and precludes obtaining a closed-form solution for $r(\theta)$. Instead, we obtained numerical solutions by means of the Kutta-Merson

method (Fox 1962), as programmed by the Stanford Computation Center. To apply this method, we first wrote Equation (E.3-7) as two simultaneous, first-order, ordinary differential equations as follows:

$$\frac{dr}{d\theta} = r_\theta \cdot \qquad \text{(E.5-1a)}$$

$$\frac{dr_\theta}{d\theta} = \frac{2r_\theta^2}{r} + r + \frac{\left(r_\theta \frac{\partial\phi}{\partial\theta} - r^2 \frac{\partial\phi}{\partial r} \; r_\theta^2 + r^2\right)}{2r^2 \; (E-\phi)} \cdot \qquad \text{(E.5-1b)}$$

The simultaneous numerical solution of these equations yields $r(\theta)$ and $r_\theta(\theta)$.

E.5.2 Approximate Initial Conditions

The initial conditions, which are imposed at infinity (Section E.3.3), must be approximated by finite values of r and r_θ for the numerical solution. For a given impact parameter b_0, we used the approximate initial conditions shown in Figure E-2, namely,

$$\begin{aligned} r(89.5^\circ) &= |b_0| \; / \cos 89.5^\circ \\ &= |b_0| \; / \; 0.0087265354984, \end{aligned} \qquad \text{(E.5-2a)}$$

$$\begin{aligned} r_\theta(89.5^\circ) &= -|b_0| \sec 89.5^\circ \tan 89.5^\circ \\ &= -r(89.5^\circ) \tan 89.5^\circ \\ &= -r(89.5^\circ) \; (114.58865013). \end{aligned} \qquad \text{(E.5-2b)}$$

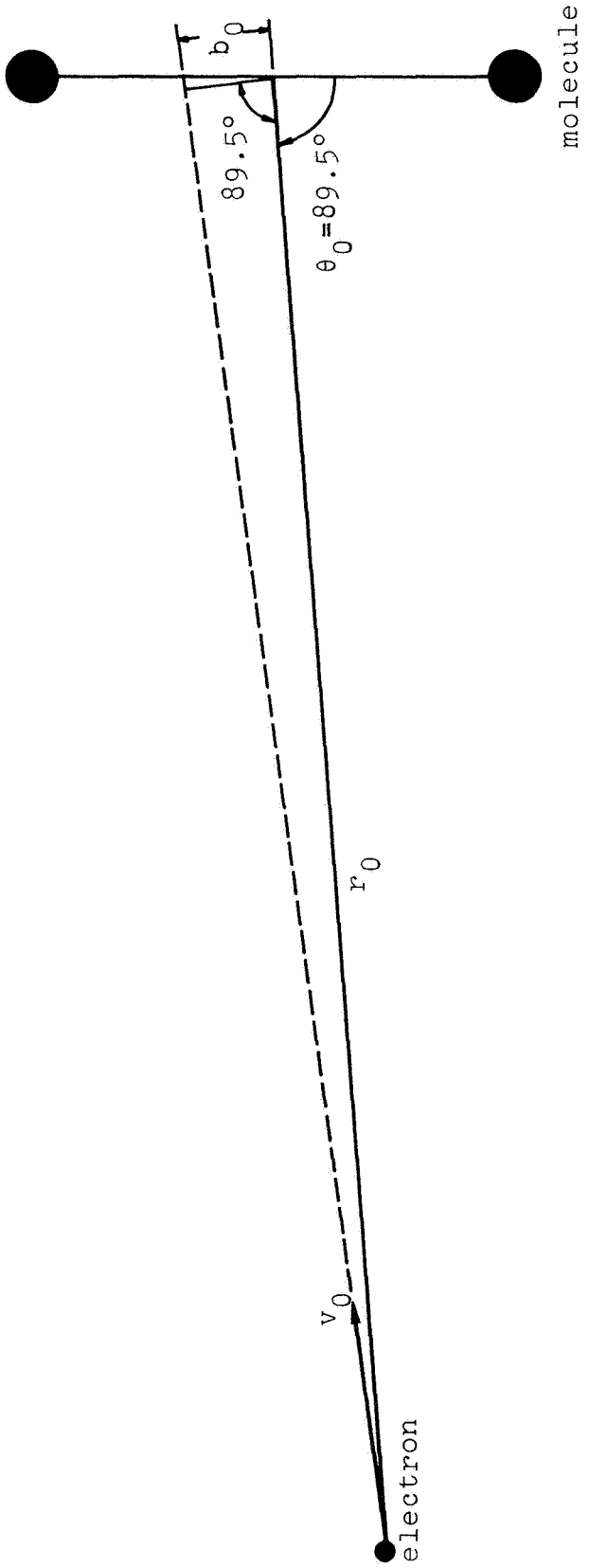

Figure E-2: Approximate Initial Conditions

E.5.3 Angular-Momentum Transfer

From the equations in Section E.3.4, we have computed the variation of L along the trajectory. The final angular momentum L_1 was found by carrying the computation far enough that the particle had passed the origin and L was approaching an asymptotic value. The final molecular angular momentum $|\vec{K}_1|$ was then obtained from the formula

$$|\vec{K}_1| = |\vec{K}_0| - (L_1 - L_0)\ \text{sign}(b_0), \qquad \text{(E.5-3)}$$

where

$$|\vec{K}_0| = \hbar[K_0(K_0+1)]^{1/2} . \qquad \text{(E.5-4)}$$

The sign (b_0) factor enters because, relative to the sign of L_0,

$$\text{sign}\ (\vec{K}_0) = \text{sign}\ (b_0). \qquad \text{(E.5-5)}$$

The final rotational quantum number K_1 was computed by means of Equation (3.5-6).

E.5.4 Verification of the Correctness of the Method

The equations and the digital-computer program were verified by computing the trajectory for the Coulomb potential

$$\phi = -K/r. \qquad \text{(E.5-6)}$$

For this potential, a closed-form solution for the orbit exists (Goldstein 1950, page 77). Computations were

performed for the four cases K = 1, 10, 100, 1000. We checked that our numerical solution agrees with the closed-form solution. We also checked that $L = L_0$ throughout the orbit, as is the case for any central potential $\phi(r)$.

In addition to the foregoing, we computed trajectories for the potential

$$\phi = -K/r^4, \qquad \text{(E.5-7)}$$

with K = 1, 10, 100, 1000, and checked that L remained constant throughout each orbit. To prevent the particle from being attracted into the origin by the potential of Equation (E.5-8), we used for some cases the cutoff potential

$$\phi = -K/r^4, \; r > r_c. \qquad \text{(E.5-8a)}$$

$$\phi = -K/r_c^4, \; r \leq r_c. \qquad \text{(E.5-8b)}$$

E.5.5 Treatment of the Conditions at the Hard Sphere

For a given set of collision parameters, the orbit equations (E.5-1) were integrated in the direction of increasing θ, starting from the initial conditions (E.5-2). For the collisions in which the radius became unity at some angle θ_I, we had to account for the impenetrability of the sphere at r=1.

The boundary conditions at the hard sphere for the

incoming particle can be expressed as

$$(r, r_\theta, \theta)_{in} = (1, (r_\theta)_I, \theta_I), \qquad \text{(E.5-9)}$$

where

$$(r_\theta)_I < 0. \qquad \text{(E.5-10)}$$

Computations were performed on the basis of two different initial conditions for the outgoing particle as follows:

(1) Elastic, specular reflection:

$$(r, r_\theta, \theta)_{out} = (1, -(r_\theta)_I, \theta_I). \qquad \text{(E.5-11)}$$

In this case, the energy E of the outgoing particle is the same as that of the incoming particle.

(2) Inelastic impact:

$$(r, r_\theta, \theta)_{out} = (1, (r_\theta)_D, 180^\circ). \qquad \text{(E.5-12)}$$

In this case, the energy of the outgoing particle is taken to be lower than that of the incoming particle by the amount of the excitation energy of the $C\,^3\Pi_u \leftarrow X\,^1\Sigma_g^+$ transition. This case corresponds to our analysis described in Chapter 3; the angle $\theta = 180^\circ$ for the outgoing particle means that the magnitude of the impact parameter b_1 has its maximum value, namely, r_0. The effect of varying the initial slope $(r_\theta)_D$ is discussed in Section E.6.2.

On the basis of one of the two sets of initial conditions at the hard sphere, the integration was continued in

the direction of increasing θ. The integration was ended when the particle was far from the origin and L was approaching an asymptotic value.

E.6 Results

E.6.1 Elastic Reflection from the Hard Sphere

Trajectories were calculated for the following sets of collision parameters:

(1) $$\left\{ \begin{array}{l} g_0 = 3 \times 10^8 \text{ cm/sec} \\ |b_0| \text{ ranging from } 1 \times 10^{-9} \text{ cm to } 20 \times 10^{-9} \text{ cm} \end{array} \right\}. \quad \text{(E.6-1)}$$

(2) $$\left\{ \begin{array}{l} g_0 \text{ ranging from } 2.2 \times 10^8 \text{ cm/sec to } 3 \times 10^8 \text{ cm/sec} \\ |b_0| = 10^{-9} \text{ cm} \end{array} \right\}. \quad \text{(E.6-2)}$$

For all collisions, we set

$$\phi_{g_0} = \theta_{g_0} = \pi/2, \quad \text{(E.6-3)}$$

so that the initial relative velocity $\vec{g}_0$ is in the initial plane of rotation of the molecule and is perpendicular to the internuclear axis.

(The angles ϕ_{g_0} and θ_{g_0} refer to the notation of Chapter 3 and should not be confused with the ϕ and θ of this chapter.)

Since $\phi_{g_0} = \theta_{g_0} = \pi/2$, a single trajectory is valid for both $+b_0$ and $-b_0$. The sign of b_0 appears only in Equation (E.5-3). These trajectories are valid for any value of K_0;

the value of K_0 enters only in the computation of K_1 (Equation E.5-3).

In Figure E-3, we show trajectories for various values of $|b_0|$, with g_0 fixed. For $|b_0| = 1.0 \times 10^{-9}$ cm, the trajectories for g_0 ranging from 2.2×10^8 cm/sec to 3.0×10^8 cm/sec are nearly coincident with each other. The potential does not "capture" the particle (i.e., the radius remains greater than unity) for $|b_0| \geq 12.0 \times 10^{-9}$ cm, which is 2.2 times the molecular radius.

In each of the computed collisions, very little rotational excitation occurs. In no collision does $|K_1-K_0|$ exceed 0.2, which occurs for the case $K_0=10$. Furthermore, $|K_1-K_0|$ is less than 0.001 for $|b_0| \geq 14.0 \times 10^{-9}$ cm, and decreases as $|b_0|$ increases beyond this value.

E.6.2 Inelastic Impact at the Hard Sphere

We discuss only the outgoing part of the trajectory here, because the incoming part is the same as with elastic reflection at the hard sphere. In Figure E-4, we show the effect of varying $(r_\theta)_D$ on the outgoing part of the trajectory for the collision parameters

$$\left.\begin{aligned} g_0 &= 3.0 \times 10^8 \text{ cm/sec} \\ |b_0| &= 5.4 \times 10^{-9} \text{ cm} \\ \phi_{g_0} &= \theta_{g_0} = \pi/2 \end{aligned}\right\}. \qquad \text{(E.6-4)}$$

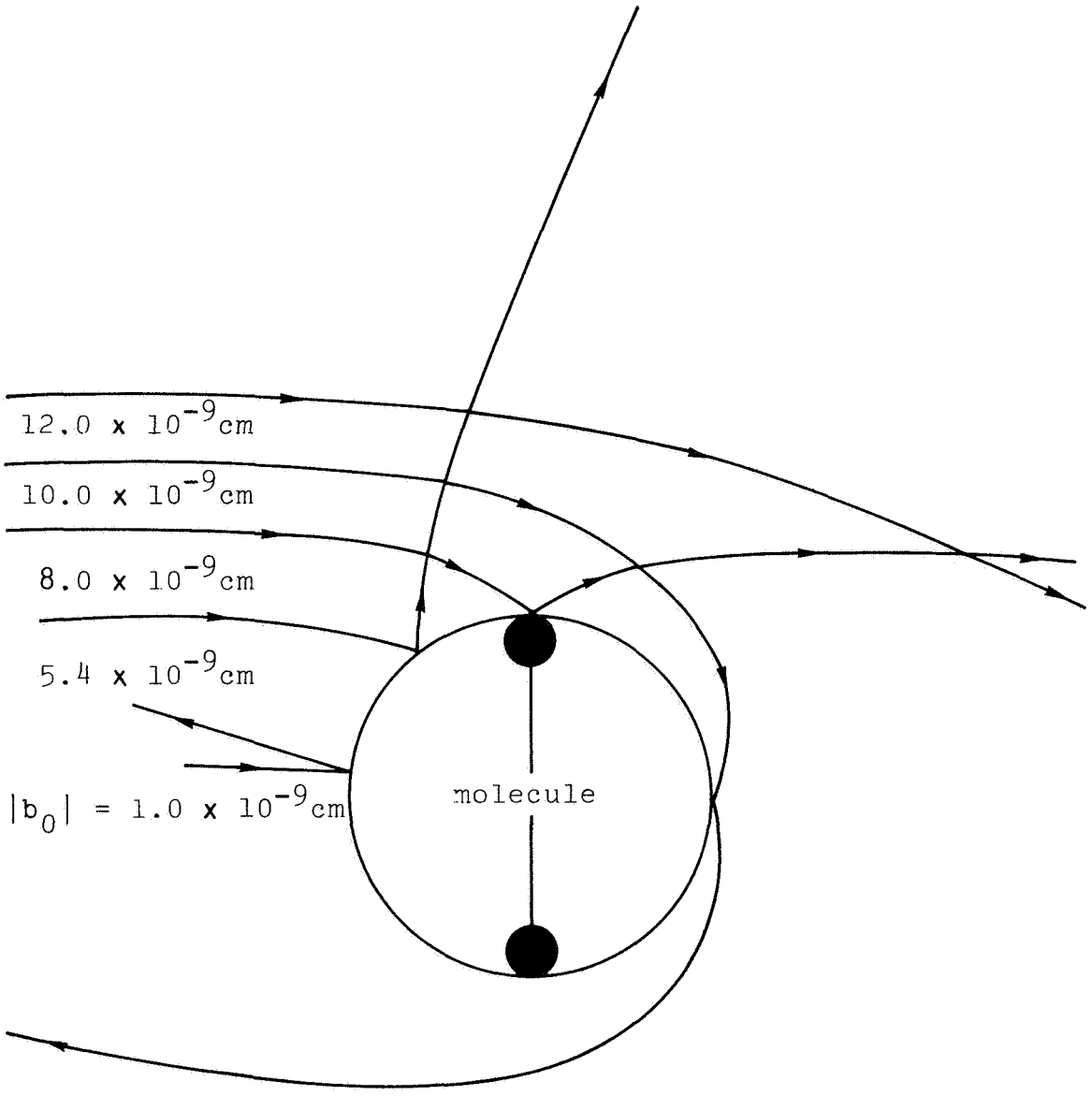

Figure E-3: Trajectories with Elastic Reflection at the Hard Sphere

$g_0 = 3.0 \times 10^8$ cm/sec

$\phi_{g_0} = \theta_{g_0} = \pi/2$

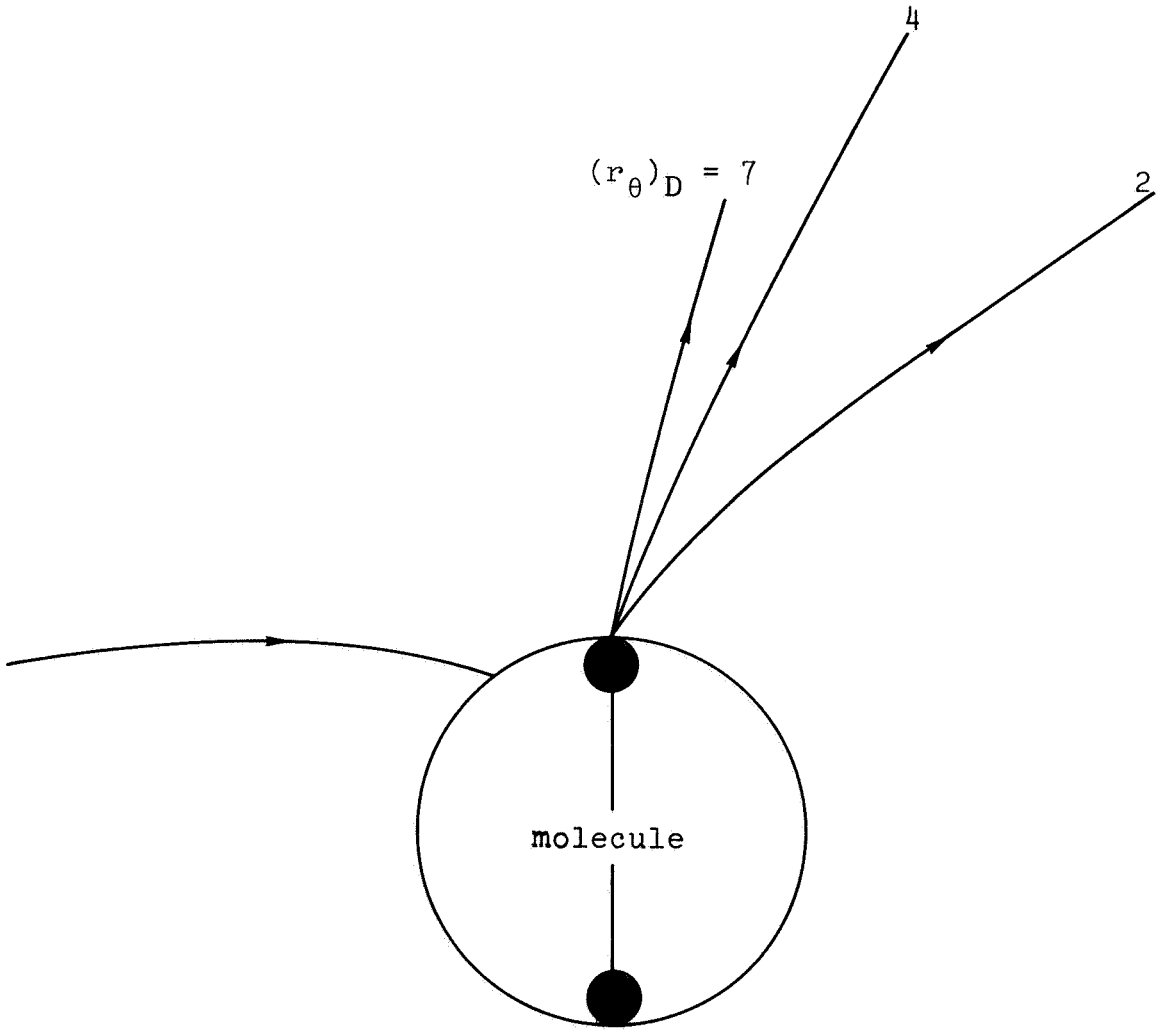

Figure E-4: Trajectories with Inelastic Impact at the Hard Sphere

$g_0 = 3.0 \times 10^8$ cm/sec

$|b_0| = 5.4 \times 10^{-9}$cm

$\phi_{g_0} = \theta_{g_0} = \pi/2$

In Figure E-5, we plot K_1 versus $(r_\theta)_D$ for the subcase

$$\left.\begin{aligned} b_0 &= 5.4 \times 10^{-9} \text{ cm} \\ K_0 &= 10 \end{aligned}\right\} . \qquad \text{(E.6-5)}$$

We see that K_1 is a rather strong function of $(r_\theta)_D$. As in Section 3.5.2, we note that only certain values of $(r_\theta)_D$ yield integer values of K_1; these integer values agree reasonably well with the values for the corresponding cases listed in Table I. In all the results shown in Figures E-4 and E-5, we have considered only the case in which the departing particle travels in the same plane as the incoming particle (i.e., in the notation of Chapter 3, $\phi_{g_1} = \phi_{g_0}$).

Our trajectory computations show that the angular momentum L changes very little during the outgoing part of the trajectory. Almost all the change in L takes place at the instant of impact with the hard sphere.

E.7 Conclusions

Our trajectory computations indicate that

(1) The molecule does not "capture" the electron if $|b_0|$ is larger than about 2 r_0.

(2) Almost all the angular-momentum transfer occurs when the particle impacts the hard sphere.

(3) The rotational excitation can be calculated by applying the conservation laws immediately before and after the impact at the hard sphere, along with the quantum

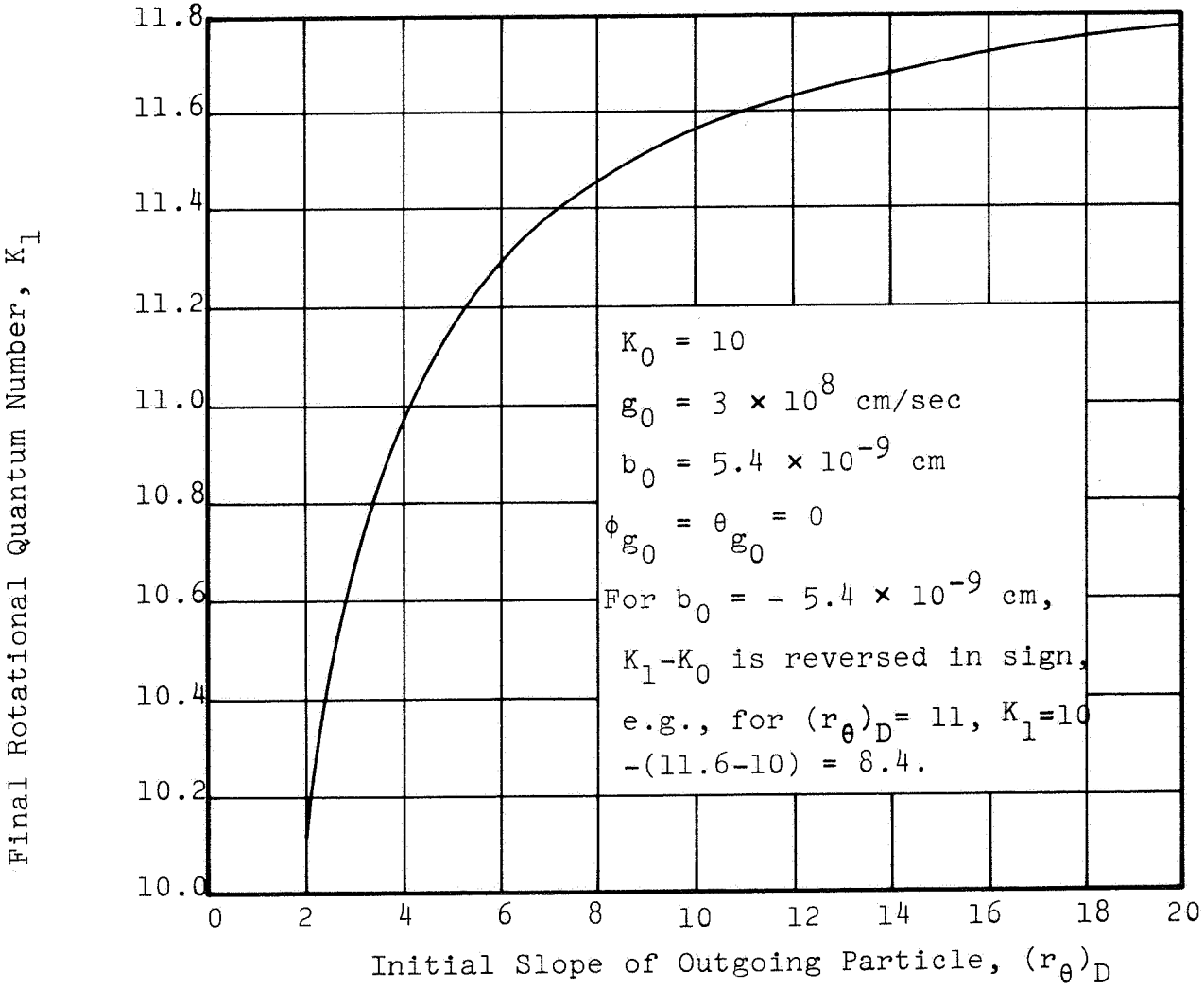

Figure E-5: Final Rotational Quantum Number versus Initial Slope of Outgoing Particle

condition to fix the initial direction of the outgoing particle. The trajectory calculations thus reduce, for the purpose of computing K_1, to the analysis described in Chapter 3.

APPENDIX F

Excitation by Photon Absorption

F.1 Analysis

In this appendix, we perform the calculation (referred to in Section 7.4) of the excitation using Muntz's (1962) model.

As in Chapter 6, we use Herzberg's (1950) notation. Let $(\ )'''$ denote values in the $X^1\Sigma_g^+$ state and $(\ )'$ denote values in the $C^3\Pi_u$ state.

According to the selection rules for $^3\Pi \leftarrow {}^1\Sigma$ transitions, only the following branches are allowed:

$$\left.\begin{aligned} &\text{P-branch: } K'-K''' = -1 \\ &\text{Q-branch: } K'-K''' = 0 \\ &\text{R-branch: } K'-K''' = +1 \end{aligned}\right\} . \qquad \text{(F.1-1)}$$

Hence the number $N_{K'}$ of $C^3\Pi_u$ molecules that have rotational quantum number K' and a given vibrational quantum number v' is given by the relation

$$\begin{aligned} N_{K'} = &\text{(number of molecules in the } K''' = K'-1 \\ &\text{level of } X^1\Sigma_g^+ \text{ that are excited to the } v' \\ &\text{level of } C^3\Pi_u \text{ with an upward rotational} \\ &\text{transition of +1) + (similar terms for} \\ &K'''=K'+1 \text{ and } K'''=K'). \end{aligned} \qquad \text{(F.1-2)}$$

By use of Equation (III, 173), page 127, of Herzberg (1950), we put Equation (F.1-2) into mathematical form as follows:

$$N_{K'} = (\text{const.}) \left\{ [S^{R}_{K',,,} N_{K',,,}/(2K'''+1)]_{K'''=K'-1} + [S^{Q}_{K',,,} N_{K',,,}/(2K'''+1)]_{K'''=K'} + [S^{P}_{K',,,} N_{K',,,}/(2K'''+1)]_{K'''=K'+1} \right\}, \tag{F.1-3}$$

where $S^{P}_{K',,,}$, $S^{Q}_{K',,,}$, $S^{R}_{K',,,}$ are the line strengths. We have used the result (Section 4.2) that the population of each $C^{3}\Pi_{u}$ rotational level is proportional to the excitation rate to that level.

For a $\Pi \leftarrow \Sigma$ transition, the Honl-London formulas for the line strengths are as follows (Herzberg 1950, page 208):

$$\left.\begin{aligned} (S^{R}_{K',,,})_{K'''=K'-1} &= (\text{const.})\ (K'+1) \\ (S^{Q}_{K',,,})_{K'''=K'} &= (\text{const.})\ (2K'+1) \\ (S^{P}_{K',,,})_{K'''=K'+1} &= (\text{const.})\ K' \end{aligned}\right\} . \tag{F.1-4}$$

For a Boltzmann distribution, we have

$$N_{K',,,} = (\text{const.})\ o(K''')\ (2K'''+1) \times \exp[-C'''K'''(K'''+1)], \tag{F.1-5}$$

where

$$\sigma(K''') = \begin{cases} 6, & K''' \text{ even} \\ 3, & K''' \text{ odd} \end{cases} \qquad \text{(F.1-6)}$$

and

$$C''' = \hbar^2/2I'''kT'''. \qquad \text{(F.1-7)}$$

By substitution of Equations (F.1-4) through (F.1-6) into Equation (F.1-3), we obtain an equation for $N_{K'}$ as follows:

$$N_{K'} = (\text{const.}) \Big\{ (K'+1)\exp[-C'''(K'-1)K'] + 2(2K'+1)\exp[-C'''K'(K'+1)] + K'\exp[-C'''(K'+1)(K'+2)] \Big\}, \quad K' \text{ even}, \qquad \text{(F.1-8a)}$$

$$N_{K'} = (\text{const.}) \Big\{ 2(K'+1)\exp[-C'''(K'-1)K'] + (2K'+1)\exp[-C'''K'(K'+1)] + 2K'\exp[-C'''(K'+1)(K'+2)] \Big\}, \quad K' \text{ odd}. \qquad \text{(F.1-8b)}$$

This equation agrees with the one derived by Muntz (1962) when the same case is considered.

F.2 Numerical Results

The important parameter that affects $N_{K'}$ is the ground-state temperature T''' (Equation F.1-7). By means of Equations (F.1-8), we have computed $N_{K'}$ for $T'''=295^{\circ}K$, which is the temperature used in Kyser's (1966) experiments. The results are plotted in Figure F-1. We see that

(1) The values of $\ln[N_{K'}/(2K'+1)]$ versus $K'(K'+1)$

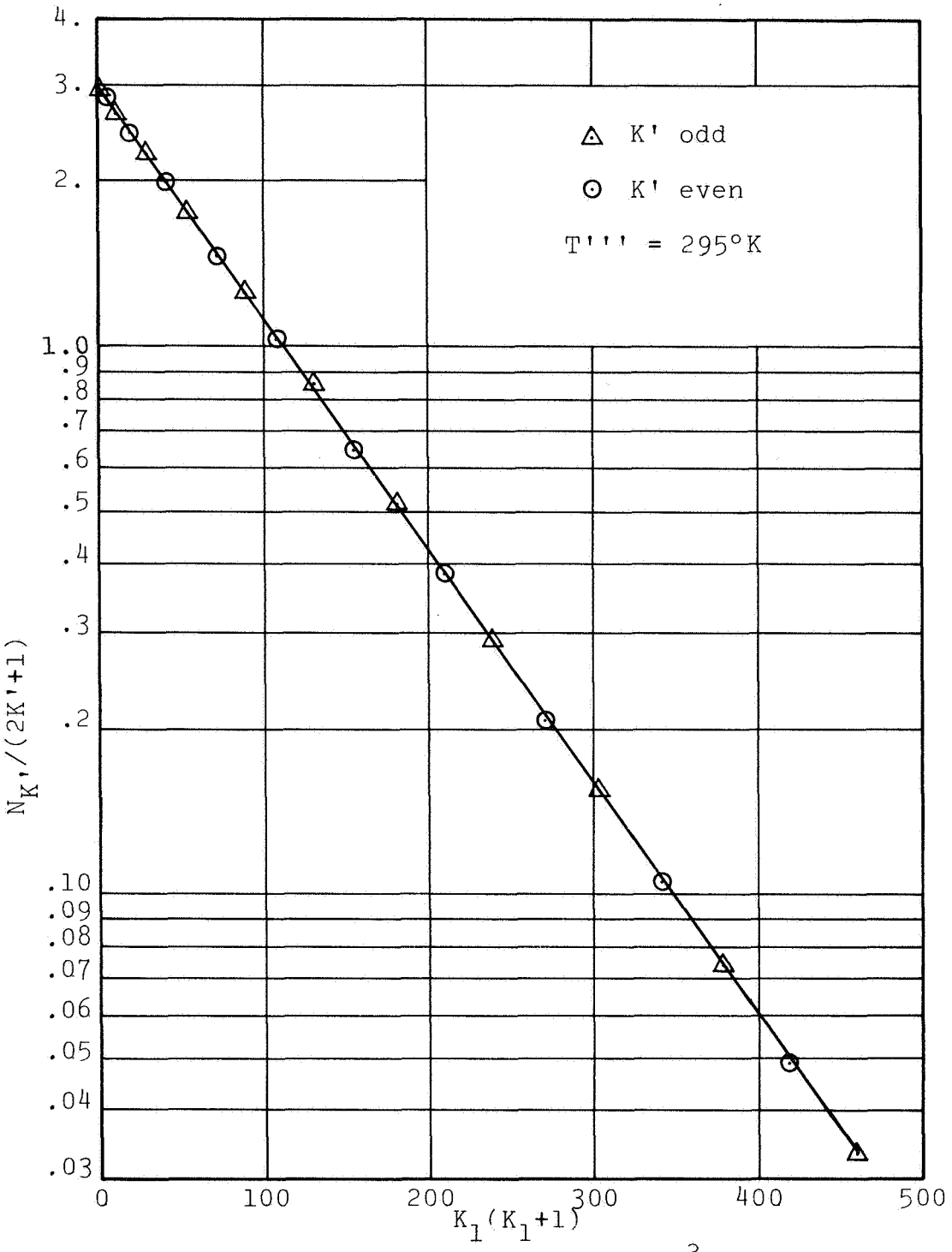

Figure F-1: Computed Populations of the $C^3\Pi_u$ Rotational Levels, for Excitation by Photon Absorption

fall on a straight line.

(2) There is no population alternation in the $C^3\Pi_u$ state.

By substituting the computed values of N_K, into Equation (6.2-19), we find the intensity ratio r to be

$$r = 0.181. \qquad \text{(F.2-1)}$$

From Figure (6-3), we see that the corresponding $C^3\Pi$ rotational temperature is

$$T' = 266^{\circ}K. \qquad \text{(F.2-2)}$$

This temperature agrees with that predicted by the classical-mechanics Monte-Carlo analysis.

REFERENCES

Bates, D. R. (1949): "The Intensity Distribution in the Nitrogen Band Systems Emitted from the Earth's Upper Atmosphere", Proc. Roy. Soc. (London) A196, 217-250.

Bauer, E., and Bartky, C. D. (1965): "Calculation of Inelastic Electron-Molecule Collision Cross Sections by Classical Methods", J. Chem. Phys. 43, 2466-2476.

Brown, G. W. (1956): "Monte Carlo Methods", in Modern Mathematics for the Engineer, edited by E. F. Beckenbach, McGraw-Hill Book Company, Inc., New York, 279-303.

Chapman, S., and Cowling, T. G. (1952): The Mathematical Theory of Non-Uniform Gases, Second Edition, Cambridge University Press.

Dieke, G. H., and Heath, D. F. (1959): "The First and Second Positive Bands of N_2", Johns Hopkins Spectroscopic Report No. 17, The Johns Hopkins University, Department of Physics.

Fox, L. (1962): Numerical Solution of Ordinary and Partial Differential Equations, Addison-Wesley Publishing Company, Inc., Reading, Massachusetts.

Gerjuoy, E., and Stein, S. (1955): "Rotational Excitation by Slow Electrons", Phys. Rev. 97, 1671-1679.

Gerry, E. T. (1965): "Pulsed-Molecular-Nitrogen Laser Theory", Appl. Phys. Letters 7, 6-8.

Ginsburg, N., and Dieke, G. H. (1941): "Intensity Measurements in the Molecular Spectrum of Hydrogen", Phys. Rev. 59, 632-644.

Goldstein, H. (1950): Classical Mechanics, Addison-Wesley Publishing Company, Inc., Reading, Massachusetts.

Gryzinski, M. (1965): "Classical Theory of Atomic Collisions. I. Theory of Inelastic Collisions", Phys. Rev. 138A, 336-358.

Herzberg, G. (1950): Spectra of Diatomic Molecules, Second Edition, D. Van Nostrand, Inc., Princeton, New Jersey.

Jobe, J. D., Sharpton, F. A., and St. John, R. M. (1967): "Apparent Cross Sections of N_2 for Electron Excitation of the Second Positive System", J. Opt. Soc. Am. 57, 106-107.

Karplus, M., Porter, R. N., and Sharma, R. D. (1965): "Exchange Reactions with Activation Energy. I. Simple Barrier Potential for (H, H_2)", J. Chem. Phys. 43, 3259-3287.

Khare, S. P. (1966): "Excitation of Hydrogen Molecules by Electron Impact", Phys. Rev. 149, 33-37.

Kishko, S. M., and Kuchinka, M. Iu. (1959): "Excitation Functions of Certain Bands of the Second Positive System of N_2", Opt. Spectrosc. 6, 378-379.

Kruger, C. H., and Mitchner, M. (1967): "Kinetic Theory of Two-Temperature Plasmas", Phys. Fluids 10, 1953-1961.

Kyser, J. B. (1964): "Development of a Tracer-Spark Technique for the Study of Hypervelocity Flow Fields",

Stanford University, Department of Aeronautics and Astronautics, Report SUDAER No. 190; summarized in Proc. Third Hypervelocity Techniques Symposium, Denver, and in AIAA J. 2, 393.

Kyser, J. B. (1966): "A Study of the Structure of Spark Columns for Velocity Measurement in a Hypersonic Stream", Stanford University, Department of Aeronautics and Astronautics, Report SUDAAR No. 272; also available as NASA CR-760, May 1967.

Langstroth, G. O. (1934): "The Excitation of Band Systems by Electron Impact", Proc. Roy. Soc. (London) A146, 166-177.

Leonard, D. A. (1965): "Saturation of the Molecular Nitrogen Second Positive Laser Transition", Appl. Phys. Letters, 7, 4-6.

Marrone, P. L. (1967): "Temperature and Density Measurements in Free Jets and Shock Waves", Phys. Fluids 10, 521-538.

Muntz, E. P. (1962): "Static Temperature Measurements in a Flowing Gas", Phys. Fluids 5, 80-90.

Oksyuk, Yu. D. (1966): "Excitation of the Rotational Levels of Diatomic Molecules by Electron Impact in the Adiabatic Approximation", Soviet Physics JETP 22, 873-881.

Prager, D. J., and Rasmussen, M. L. (1967): "The Flow of a Rarefied Plasma Past a Sphere", Stanford University,

Department of Aeronautics and Astronautics, Report SUDAAR No. 299; also issued by Institute for Plasma Research, Stanford University, as SU-IPR Report No. 132.

Ralston, A. (1965): A First Course in Numerical Analysis, McGraw-Hill Book Company, Inc., New York.

Sampson, D. H., and Mjolsness, R. C. (1965): "Theory of Rotational Excitation of Homonuclear Diatomic Molecules by Slow Electrons: Application to N_2 and H_2", Phys. Rev. 140, 1466-1476.

Spitzer, L., Jr. (1962): Physics of Fully Ionized Gases, Second Edition, Interscience Publishers, New York.

Stewart, D. T., and Gabathuler, E. (1958): "Some Electron Collision Cross Sections for Nitrogen and Oxygen", Proc. Phys. Soc. (London) A72, 287-289.

Takayanagi, K., and Geltman, S. (1965): "Excitation of Molecular Rotation by Slow Electrons", Phys. Rev. 138, 1003-1010.

Tilford, S. G., Vanderslice, J. T., and Wilkinson, P.G. (1965): "The High-Resolution Absorption Spectrum of Nitrogen from 1060 to 1520 Å. V. The $C^3\Pi_u \leftarrow X^1\Sigma_g^+$ System", Astrophys. J. 142, 1203-1226.

Tyte, D. C. (1962): "Intensity Measurements on the Nitrogen Second Positive System in a Low Temperature Discharge", Proc. Phys. Soc. (London) 80, 1347-1353.